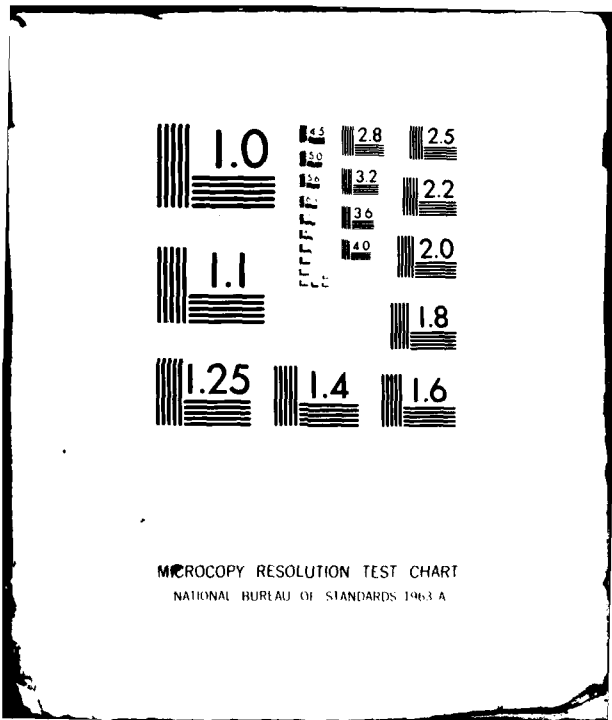| | 1.0 | | 2.8 | 2.5 |
			3.2	2.2
			36	
			40	2.0
	1.1			
				1.8
	1.25	1.4		1.6

MICROCOPY RESOLUTION TEST CHART

NATIONAL BUREAU OF STANDARDS 1963 A

AFWAL-TR-80-3012

LEVEL II

CONDUCTION HEAT TRANSFER ANALYSIS IN COMPOSITE MATERIALS

LIT S. HAN
ANDREW A. COSNER

THE OHIO STATE UNIVERSITY
RESEARCH FOUNDATION
1314 KINNEAR ROAD
COLUMBUS, OH 43212

MARCH 1980

FLIGHT DYNAMICS LABORATORY
AIR FORCE WRIGHT AERONAUTICAL LABORATORIES
AIR FORCE SYSTEMS COMMAND
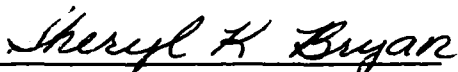WRIGHT-PATTERSON AIR FORCE BASE, OHIO 45433
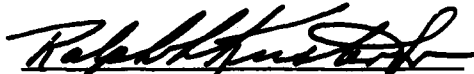
DTIC

SEP 5 1980

A

80 9 4 023

NOTICE

When Government drawings, specifications, or other data are used for any purpose other than in connection with a definitely related Government procurement operation, the United States Government thereby incurs no responsibility nor any obligation whatsoever; and the fact that the government may have formulated, furnished, or in any way supplied the said drawings, specifications, or other data, is not to be regarded by implication or otherwise as in any manner licensing the holder or any other person or corporation, or conveying any rights or permission to manufacture, use, or sell any patented invention that may in any way be related thereto.

This report has been reviewed by the Information Office (OI) and is releasable to the National Technical Information Service (NTIS). At NTIS, it will be available to the general public, including foreign nations.

This technical report has been reviewed and is approved for publication.

SHERYL K. BRYAN, 2Lt, USAF
Design & Analysis Methods Group
Analysis & Optimization Branch
FOR THE COMMANDER

FREDERICK A. PICCHIONI, Lt Col, USAF
Ch, Analysis & Optimization Branch
Structures & Dynamics Division

RALPH L. KUSTER, JR., Col, USAF
Chief, Structures & Dynamics Div.

"If your address has changed, if you wish to be removed from our mailing list, or if the addressee is no longer employed by your organization please notify AFWAL/FIBR   , W-PAFB, OH 45433 to help us maintain a current mailing list".

Copies of this report should not be returned unless return is required by security considerations, contractual obligations, or notice on a specific document.

AIR FORCE/56780/26 August 1980 — 250

Final rept. 1 Jul 78 - 30 Jun 79.

REPORT DOCUMENTATION PAGE		READ INSTRUCTIONS BEFORE COMPLETING FORM
1. REPORT NUMBER AFWAL-TR-80-3012	2. GOVT ACCESSION NO. AD-A088 741	3. RECIPIENT'S CATALOG NUMBER
4. TITLE (and Subtitle) CONDUCTION HEAT TRANSFER ANALYSIS IN COMPOSITE MATERIALS		5. TYPE OF REPORT & PERIOD COVERED Final Report 7/1/78 - 6/30/79
		6. PERFORMING ORG. REPORT NUMBER 761108/711129
7. AUTHOR(s) Lit S. Han Andrew A. Cosner		8. CONTRACT OR GRANT NUMBER(s) Grant No. AFOSR-78-3649
9. PERFORMING ORGANIZATION NAME AND ADDRESS The Ohio State University Research Foundation, 1314 Kinnear Road Columbus, Ohio 43212		10. PROGRAM ELEMENT, PROJECT, TASK AREA & WORK UNIT NUMBERS Proj. No. 2307 Task 230701 Work Unit 230701-12
11. CONTROLLING OFFICE NAME AND ADDRESS Air Force Office of Scientific Research Bolling Air Force Base, D.C. 20332		12. REPORT DATE Mar 80
		13. NUMBER OF PAGES 154
14. MONITORING AGENCY NAME & ADDRESS(if different from Controlling Office) Flight Dynamics Laboratory (AFWAL/FIB) Airforce Wright Aeronautical Laboratories (AFSC) Wright Patterson Air Force Base, Ohio 45433		15. SECURITY CLASS. (of this report) Unclassified
		15a. DECLASSIFICATION/DOWNGRADING SCHEDULE

16. DISTRIBUTION STATEMENT (of this Report)

Approved for public release; distribution unlimited.

17. DISTRIBUTION STATEMENT (of the abstract entered in Block 20, if different from Report)

18. SUPPLEMENTARY NOTES

19. KEY WORDS (Continue on reverse side if necessary and identify by block number)

Heat conduction, composites, fiber-matrix, equivalent conductivity

20. ABSTRACT (Continue on reverse side if necessary and identify by block number)

With anticipated increased use of composite materials in aerospace structures and other applications, thermal properties of composites are needed as essential design information. There has been, in the past, only scanty amount of research effort in thermal analysis of composites, as most of the work has been concerned with their mechanical properties. This report contains

The work contained herein results from a rigorous analysis to determine steady-state effective thermal conductivities of fiber-matrix type of composites. The fibers bundled into tows are considered dispersed in a matrix of resin.

DD FORM 1 JAN 73 1473

20. (cont.)

The dispersion patterns of configurations considered are: (1) uni-directional fibers in a matrix, as the simplest geometry, and (2) 0/90 configuration in which two uni-directional tapes are overlaid at 90 degrees to each other.

The method of analysis is to solve a two-region steady-state heat conduction equation either analytically or numerically. The analysis assumes a prior knowledge of the geometry of a composite and the constituents thermal conductivities.

FOREWORD

The content of this report presents results of the first twelve month period, July 1, 1978 through June 30, 1979, of studies on the thermal property research on composite materials.

Under the sponsorship of the Air Force Office of Scientific Research, grant no. 78-3640, the technical monitor was initially Lt. Steve Lamberson and was subsequently changed to Mr. Donald Russell of The Flight Dynamics Laboratory, Wright-Patterson Air Force Base, Dayton, Ohio.

Steady-state-conduction analyses were performed on composites made of fibers in resins. Orientations of fibers considered are (1) uni-directional arrangements in which all fibers are aligned in one direction and (2) 0° - 90° arrangements in which fibers are arrayed alternately in mutually perpendicular directions. The method of analysis is either an exact solution of the conduction heat equation by boundary collocation or a numerical relaxation of the three-dimensional heat conduction. The results expressed by an effective thermal conductivity in three principal directions supersedes the so-called model equations established by previous investigators.

The report was submitted 24 September 1979 through the contractor, The Ohio State University Research Foundation, 1314 Kinnear Road, Columbus, Ohio 43212.

iii

TABLE OF CONTENTS

LIST OF ILLUSTRATIONS

LIST OF ILLUSTRATIONS (concluded)

LIST OF SYMBOLS

A	integration constant, area
a	horizontal length of unit cell
B	integration constant
b	vertical length of unit cell
C	integration constant
c	specific heat
D	distance between finite-difference nodes
K	thermal conductivity
M	number of matching points per side of unit cell
n	power series index, normal direction
n_{xy}	cosine of angle between x and y axes
q	heat flow per unit area
Q	total heat flow
r	radial direction, principal axis
s	principal axis
t	principal axis
T	temperature
V	volume ratio (fiber volume/total volume)
x	arbitrary axis
y	arbitrary axis
z	one-half the diagonal distance of the unit cell, arbitrary axis
α	fiber angle that defines packing geometry
β	conductivity ratio (fiber conductivity/matrix conductivity)
λ	relaxation factor
ρ	density

Subscripts

B	back
D	down
eff	effective value
f	fiber value

x

LIST OF SYMBOLS (concluded)

F	front
	for staggered array, a point in the upper left region
G	for staggered array, a point in the lower right region
i	finite-difference direction subscript
j	finite-difference direction subscript
k	finite-difference direction subscript
L	left
m	matrix value
R	right
U	up

SECTION I

INTRODUCTION

1.1 COMPOSITE MATERIALS

The idea of a composite material is a very broad one indeed. Generally speaking, a composite material is any material having more than one distinct phase which exist together on a macroscopic scale. This broad definition covers materials as diverse as concrete, fiberglass, and even the skeletal structures of animals. In these examples, two or more components exist together to create a "higher performance" structure than could be made of one of the components alone. In this context, higher performance signifies a higher strength-to-weight or strength-to-volume ratio of the material.

An important class of composite materials today are those in which high strength fibers are molded into a general matrix material. This category is still quite broad in that it includes such varied materials as steel reinforced concrete and fiberglass. This report is concerned with that general type of engineering material in which continuous nonwoven fibers are oriented in a matrix in a very specific arrangement so as to produce a high structural efficiency. The fibers used are typically extremely strong and possess a high modulus of elasticity. Some common fiber materials are carbon and boron, for example. The matrix material ranges from organic materials to those of a ceramic or metallic nature depending on the purpose of the overall composite.

Typically, the fibers are the load carrying component of the structure, while the matrix serves to hold the fibers in place and provide a means of transmitting the load to other parts of the material. As one example, graphite, which is among the most common fiber materials in use today, has an ultimate strength on the order of 500,000 psi [1].* When it is then noted that its density is one-fifth that of steel, it is evident that a material made from it can have extremely good strength-to-weight characteristics. In addition, graphite has a modulus of elasticity two to three times that of steel, and so these composite materials are extremely stiff.

It is because of the good strength-to-weight and stiffness characteristics that some of the first applications of fibrous composite materials and the bulk of the research took place, and still do, in the aerospace industry. Aircraft radomes were made of laminated fiberglass because of the high strength needed and the desirable characteristics with respect to electromagnetic wave propagation. In some applications, solid rocket motor casings were made out of glass fibers. Similar casings are now being designed with much stronger carbon fibers. In short, composite materials are being used extensively today throughout

---

* Number in brackets refers to reference number.

1

the aerospace industries and are being chosen more and more for the primary structural components.

These materials can technically be described as nonhomogeneous because of the distinct phases present and nonisotropic because the overall properties are dependent on the direction being considered. However, on the macroscopic scale where the dimensions of the material are large compared to those of the fibers and the spacings, they can be considered as homogeneous. Here, this means that properties are essentially uniform on a macroscopic scale and thus do not vary with position, although they may still vary with direction.

The properties within each component--fiber or matrix--may vary with direction although typically they do not, except for a few of the fiber mechanical properties. The thermal properties of the two components typically do not vary with direction, and none of the properties varies with position within the component. Thus, taken seperately, they can be considered as homogeneous and isotropic.

Typical composite materials of the type being considered for current use are constructed of many layers, or laminae. Each lamina is formed individually with the fibers being laid down in a parallel fashion and then being covered by the matrix material. These lamina which are one fiber thick are then stacked together to form a laminate, or composite. The stacking is done so as to have all the fibers parallel and thus have very pronounced directional characteristics, or the layers can be rotated with respect to each other to give more isotropic characteristics. The term quasi-isotropic is often used when an attempt has been made to arrange the laminae to give a laminate whose properties are nearly directional-independent.

The simplest composite from the geometrical standpoint is one in which all the fibers are parallel and are stacked in a square array as shown below.
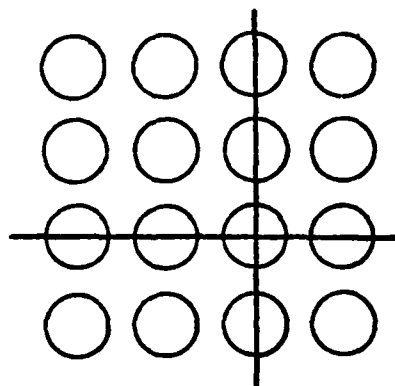
Figure 1. Square array cross-section.

2

For the arrangement of Figure 1, it can be seen that there are three mutually perpendicular planes of geometrical symmetry in the material. In the figure, two planes are shown on edge with the third laying parallel to the paper. These planes are referred to as the principal planes with a set of coordinate axes overlayed on them referred to as the principal axes.

A material which has these three planes of symmetry is said to be orthotropic on the macroscopic level--a subset of all nonisotropic materials. It should be noted that a material can be homogeneous, or of uniform structure, and still have these directionally dependent properties.

In the simple composite structure shown, the properties such as strength, elasticity, and conductivity will be different along the three mutually perpendicular directions since the two components will typically have quite different properties. For example, for the strong fiber and weak matrix combination, the strength will be much higher along the direction parallel to the fibers than the other two directions. When the fibers are isotropic, the overall composite will be orthotropic, having the principal axes with respect to the properties the same as the principal axes with respect to geometry. The vast majority of composites in use today are orthotropic in this manner. The major exception is when the fibers are randomly placed such that there are no planes of symmetry, and consequently it is not orthotropic.

A great deal of effort has been extended toward studying the mechanical properties of composite materials. This is due to the fact that it is the mechanical properties which are so outstanding and which brought composites into widespread use. Studies of thermal properties, and specifically studies of heat conduction, are lagging in the literature. However, because of the critical applications for which composites are being used there is a definite need for studies of heat conduction. This report will present detailed numerical studies of heat conduction in the steady state in fibrous composite materials.

1.2 HEAT CONDUCTION IN COMPOSITE MATERIALS

In general, the amount of heat conducted through an orthotropic material per unit area when in steady state is given by the following equations [3]:

$$-q_x = K_{xx} \frac{\partial T}{\partial x} + K_{xy} \frac{\partial T}{\partial T} + K_{xz} \frac{\partial T}{\partial x}$$

$$-q_y = K_{yx} \frac{\partial T}{\partial x} + K_{yy} \frac{\partial T}{\partial y} + K_{yz} \frac{\partial T}{\partial z}$$

$$-q_z = K_{zx} \frac{\partial T}{\partial x} + K_{zy} \frac{\partial T}{\partial y} + K_{zz} \frac{\partial T}{\partial z} \tag{1}$$

3

In these equations x, y, and z are any arbitrary orthogonal axes, and the constant K_{ij} gives the heat conducted in the i direction due to a temperature gradient in the j direction. For an isotropic material, only the values of K_{xx}, K_{yy}, and K_{zz} would be non-zero. The nine values of K are not found in the literature, however, because of the infinite number of orientations of the x-y-z coordinate system that can be used.

Let the principal axes of conductivity be denoted by r, s, and t so that the principal conductivities are denoted as K_{rr}, K_{ss}, and K_{tt}. Also, let the cosines of the angles between the principal and the general sets of axes be denoted by n_{ij} where i is the name of the general axis and j is the name of the principal axis. In this manner, the heat flow per unit area can be described by the following equations:

$$q_x = n_{xr}q_r + n_{xs}q_s + n_{xt}q_t$$

$$q_y = n_{yr}q_r + n_{ys}q_s + n_{yt}q_t$$

$$q_z = n_{zr}q_r + n_{zs}q_s + n_{zt}q_t \qquad (2)$$

The principal axes have the unique characteristic that a temperature gradient along one axis will cause a heat flow only along that axis. In other words, the values of K_{rs}, K_{rt}, K_{sr}, K_{tr}, and K_{ts} are zero. This means that heat flow along the principal axes is described in the much simpler manner as shown below.

$$q_r = -K_{rr}\frac{\partial T}{\partial r}$$

$$q_s = -K_{ss}\frac{\partial T}{\partial s}$$

$$q_t = -K_{tt}\frac{\partial T}{\partial t} \qquad (3)$$

4

Because temperature is a scalar, the temperature gradients expressed in these two coordinate systems are related by:

$$\frac{\partial T}{\partial r} = n_{xr} \frac{\partial T}{\partial x} + n_{yr} \frac{\partial T}{\partial y} + n_{zr} \frac{\partial T}{\partial z}$$

$$\frac{\partial T}{\partial s} = n_{xs} \frac{\partial T}{\partial x} + n_{ys} \frac{\partial T}{\partial y} + n_{zs} \frac{\partial T}{\partial z}$$

$$\frac{\partial T}{\partial t} = n_{xt} \frac{\partial T}{\partial x} + n_{yt} \frac{\partial T}{\partial y} + n_{zt} \frac{\partial T}{\partial z} \tag{4}$$

Now, by combining Equations 2, 3, and 4, the following relationship is obtained:

$$-q_x = (K_{rr} n_{xr}^2 + K_{ss} n_{xs}^2 + K_{tt} n_{xt}^2) \frac{\partial T}{\partial x}$$

$$+ (K_{rr} n_{xr} n_{yr} + K_{ss} n_{xs} n_{ys} + K_{tt} n_{xt} n_{yt}) \frac{\partial T}{\partial y}$$

$$+ (K_{rr} n_{xr} n_{zr} + K_{ss} n_{xs} n_{zs} + K_{tt} n_{xt} n_{zt}) \frac{\partial T}{\partial z} \tag{5}$$

Equations for q_y and q_z are similar but are omitted here.

It is clear that Equation 5 is of the same form as Equation 1. Consider the first term of the equation for q_x. Then the following relationship holds:

$$K_{xx} = K_{rr} n_{xr}^2 + K_{ss} n_{xs}^2 + K_{tt} n_{xt}^2 \tag{6}$$

From this and similar reasoning for the other eight conductivities, an important conclusion can be drawn: when calculating heat flow in any direction in an orthotropic material, the only conductivities which are needed are the three principal conductivities.

By knowing the three principal conductivities and the temperature field, the total heat flux is found by the following integration:

$$Q = \int_{Area} q(n) dA = \int_{Area} \overline{q} \cdot \overline{dA} \qquad (7)$$

Here, q is the magnitude of the heat flux vector, $\overline{q}$, and n is the cosine of the angle between $\overline{q}$ and the normal to the area, $\overline{dA}$. Consider the x direction to be perpendicular to a plane of integration. Since the x-y-z coordinate system is arbitrary anyway, this is no special restriction. Then, Equation 7 can be rewritten as follows:

$$Q_x = \int_{Area} q_x n \, dA \qquad \text{for } n = 1$$

$$= \int_{Area} q_x dA$$

$$= \int_{Area} (K_{xx} \frac{\partial T}{\partial x} + K_{xy} \frac{\partial T}{\partial y} + K_{xz} \frac{\partial T}{\partial z}) dA \qquad (8)$$

Now consider the restrictions that the material be homogeneous (properties independent of position) and that the temperature gradients be constant over the area, A. Then the following equation is obtained:

$$Q_x = (-K_{xx} \frac{\partial T}{\partial x} - K_{xy} \frac{\partial T}{\partial y} - K_{xz} \frac{\partial T}{\partial z})(A) \qquad (9)$$

Therefore, since these three conductivities are dependent solely on the three principal conductivities and the geometry, the total heat flux can be easily found if the material is homogeneous and if the temperature field is uniform.

A composite material can very often be considered homogeneous when the dimension of temperature resolution is much larger than that of the fibers or spacings. Then from that practical viewpoint, the material could be analyzed with proper representation of an effective conductivity. If a uniform temperature gradient were then imposed across a large section of composite material, the effective conductivities could be used with Equation 9 to determine the heat flux.

When nonhomogeneities with a conductivity different from the matrix material exist in the material, the temperature field will be very complex as it curves around the nonhomogeneities. However when the nonhomogeneities are very abundant, the minute details of the heat flux in the vicinity of each will be repetitious and predictable. An effective conductivity for the material would then take into account the net effect that the nonhomogeneities have on the overall heat flux without having to consider the details of the temperature field in the vicinity of each inclusion.

Only the principal effective conductivities are necessary since by using them the effective conductivity in any direction can be determined. The procedure for calculating these principal effective conductivities for fibrous composite materials will be discussed in detail in the following sections.

1.3 STUDIES OF CONDUCTION IN COMPOSITE MATERIALS

The problem of heat conduction in general composite materials can be divided into three basic groups. The first of these groups includes layered composites in which continuous layers exist whose properties are different from adjacent layers. The second group includes those materials where various shaped particles are dispersed randomly throughout a matrix material. The last group includes fibrous composites with specific orientations which is the subject of this report.

Because of the simplicity of layered composites, exact methods can be employed to solve for effective conductivities. Their solutions are in the form of relatively simple expressions and can be used as simplified problems for more complex geometries. There has been a great deal of work concerned with the effects of thin films and interface resistances. This is not considered in this effort.

Materials in which particles are distributed randomly through a matrix are by their nature not suitable to exact studies, and a statistical approach is much more productive. Hashin and Shtrikman [9] developed bounds for cases where only the volume ratio and component conductivities are known and where the geometry is quite arbitrary. These bounds are quite close for low volume ratios but diverge very rapidly for higher values. Other bounds in which the particles are specified to be spheres or in which a well dispersed random mixture is specified are discussed by Hale [10]. For dilute suspensions of a powder within a matrix, he has presented equations to predict the thermal conductivity. All of the work in this area points to the fact that with large volume ratios the geometry of the material is critical, and accurate predictions of effective conductivity cannot be made without that information.

For fiber-reinforced materials, the Hashin [9] bounds are of course applicable since they allow for any fiber and packing geometries. Beran and Silnutzer [11] developed improved bounds for parallel fiber composites where the fiber geometry was specified although no attempt was made to consider the packing geometry. Elsayed and McCoy [12] then developed better bounds for cases when the packing geometry is completely defined. These bounds showed that packing geometry is absolutely critical for volume ratios greater than 10 percent.

Tsou, Chou, and Singh [8] approximated a fibrous material by averaging the properties for each layer and then treating them as continuous homogeneous regions with heat flow transverse and parallel to

7

them. This approximation is satisfactory for volume ratios of less than 20 percent, but it deteriorates rapidly for higher values.

Springer and Tsai [13] refined this approach by assuming one-dimensional heat flow through the material. They were then able to integrate across a layer of the material and arrive at an expression for the effective thermal conductivity. For a cylindrical fiber and a square packing array with heat flow transverse to all fibers, the equation is as follows:

$$\frac{K_{eff}}{K_{matrix}} = 1 - 2\sqrt{\frac{V}{\pi}} + \frac{1}{B}[\pi - \frac{4}{\sqrt{1-\frac{B^2 V}{\pi}}} \tan^{-1}(\frac{\sqrt{1-B^2 V/\pi}}{1+\sqrt{B^2 V/\pi}})] \qquad (10)$$

$$B = 2(\frac{K_{matrix}}{K_{fiber}} - 1) \qquad (11)$$

As with other methods, these equations are good for low volume ratios but are inaccurate for high volume ratios.

Behrens [14] developed a simpler expression (Equation 12) which incorporates volume ratio and fiber geometry information but says nothing of the packing geometry. For circular fibers his equation is as follows:

$$\frac{K_{eff}}{K_{matrix}} = \frac{1 + V(\frac{\beta-1}{\beta+1})}{1 - V(\frac{\beta-1}{\beta+1})} \qquad (12)$$

This equation is also developed by analogy to the equations for effective shear modulus [1]. A comparison of these two equations is shown below for a square array, (Figure 2).

Springer and Tsai's equation gives a somewhat lower thermal conductivity than that of Behrens. They do however agree with each other within 5 percent up to volume ratios of 50 percent.

Because the effective shear modulus in a composite is governed by equations analogous to those for heat conduction, any results obtained for the shear modulus are directly applicable to those for heat conduction. Adams and Donner [16] used a finite-difference approach to determine the effective shear modulus for the square array. Fiber-to-matrix shear modulus ratios and volume ratios were varied considerably. The results they obtained compare well with those presented in the appendix to this report. They were however restricted to the square packing array.

8
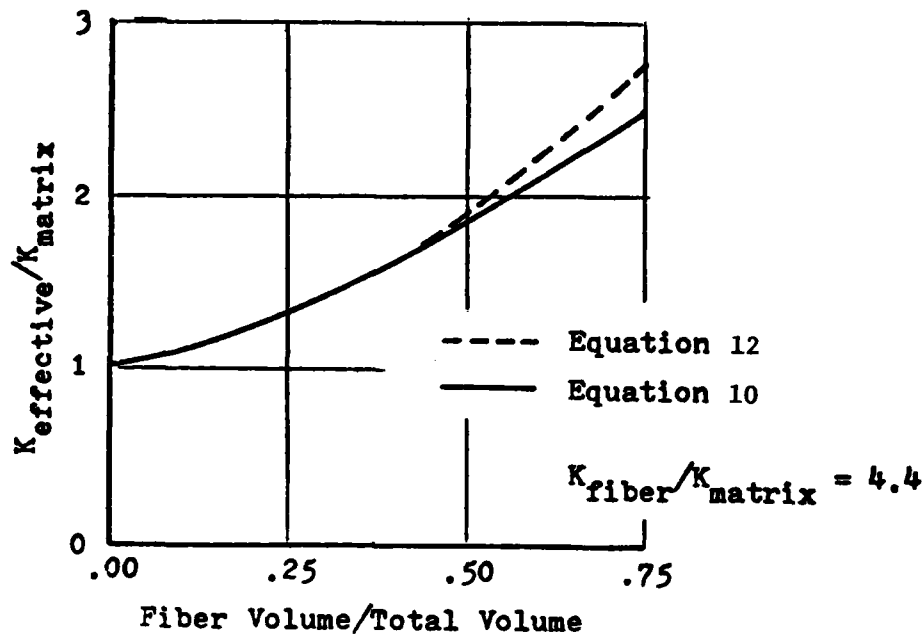
Figure 2. Comparison of equations for square array.

Thus, a number of methods have been used to predict the effective conductivity of a parallel fiber composite material. However, most were restricted to the simplest packing geometry and made broad simplifying assumptions. Reference 1 contains a good review of these various methods. No attempt has been made to study the $0°$ -$90°$ case in which adjacent layers of fibers lie at right angles to each other. The present report will present complete parametric studies in each of these areas without the use of broad simplifying assumptions.

1.4 SCOPE OF THE PROJECT

It is the purpose of this study to analyze the principal effective conductivities for various geometrical arrangements of fiber reinforced composite materials. The following basic types of geometries will be analyzed:

1.) Unidirectional fibers with all regular packing patterns.
2.) Layers of fibers perpendicular to adjacent layers with selected values of layer separation-to-fiber separation to be studied.

For these cases the following quantities will be varied in these parametric studies:

i.) Ratio of fiber to matrix conductivity.
ii.) Ratio of fiber to total volume.

9

SECTION II

PARALLEL FIBER MATERIALS

2.1 PROBLEM DEFINITION

The simplest class of composite materials is that in which all the fibers are parallel to each other and which behaves according to the assumptions discussed in section 1.3. The geometry for these materials can be described in two dimensions, and when a uniform temperature gradient exists across the fibers, the temperature field that exists is two-dimensional.

The configurations of this class fall into two basic categories. Cross-sections of each are shown in Figure 3. The first category is referred to as the rectangular array. The second is referred to as the staggered array because every other layer is staggered horizontally by one-half of the distance between fibers. For both, the independent variables from the geometric point of view are the vertical distance between layers, the horizontal distance between fibers in each layer, and the volume ratio which is the ratio of fiber volume to total volume.

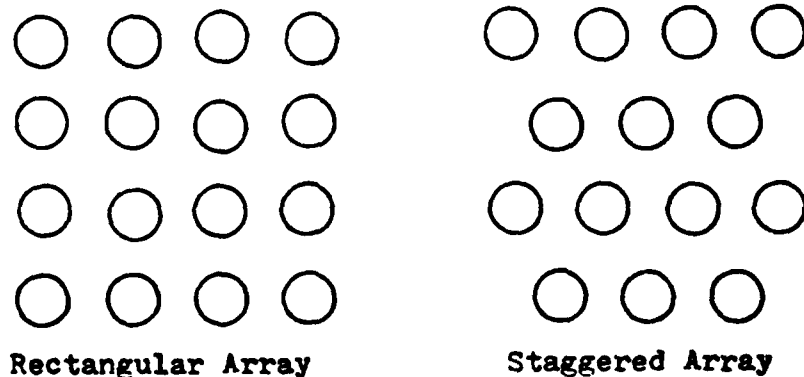**Rectangular Array**   **Staggered Array**

Figure 3. Parallel fiber arrays

It is desired to find the heat flux across a plane within a particular composite material. As discussed in Section I, the heat flux for an isotropic material is given by the following equation:

$$Q = -\int \left(K \frac{\partial T}{\partial n} \right) dA \tag{13}$$

11

Here, n is the direction normal to the plane of integration. On a macro scale a composite is definitely not isotropic. However, each component is so this equation is valid when integrating across a particular component.

To find the effective conductivity for a composite, a uniform (one-dimensional) temperature gradient on the macro scale must be imposed across a section of uniform thickness. The heat flux across a plane in the material must then be determined according to Equation 13. The effective conductivity is then given by Equation 14. Here, $\Delta T/\Delta n$ is the uniform temperature gradient across the section on the macro scale.

$$K_{eff} = Q/(A\frac{\Delta T}{\Delta n}) \tag{14}$$

It is therefore necessary to find the temperature field in the material on the scale of the fiber and spacing size so as to perform the integration of Equation 13.

The rectangular array will be considered first as it is the simplest arrangement for a composite material. Consider a uniform temperature gradient (from the top to the bottom) to be imposed over a section of this material. To do this, let the top face and the bottom face be at constant temperature so that in general heat flows from top to bottom. Then, on horizontal lines of symmetry the temperature will be constant. This can be seen to be true because on lines of symmetry where the general temperature gradient is perpendicular to the line, effects of changing conductivity above exactly cancel the effects of changing conductivity below. Then the temperature along the line becomes uniform as the overall temperature gradient is uniform.

On vertical lines of symmetry, lines which trace the heat flow through the material will be vertical. In other words, the temperature gradient in the horizontal direction along vertical lines of symmetry will be constant at zero. This is the case because the effects of changing conductivity to the left exactly cancel the effects to the right, and so there is no net effect to cause the flow of heat to deviate from a vertical path. This of course assumes that the material has large numbers of fibers. Lines of symmetry are superimposed on a section of rectangular array below.

Based on the one-dimensional vertical temperature gradient, a repeating pattern can be identified as that inside the heavy lines. It is repeated below with the previously discussed temperature boundary conditions along the edges indicated. The obvious restrictions at the fiber-matrix interface are that the temperature is the same in each region and the heat flux normal to the interface is the same in each region.

12
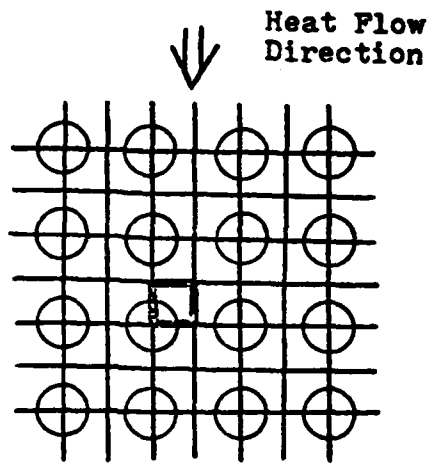
Figure 4. Rectangular array repeating cell.
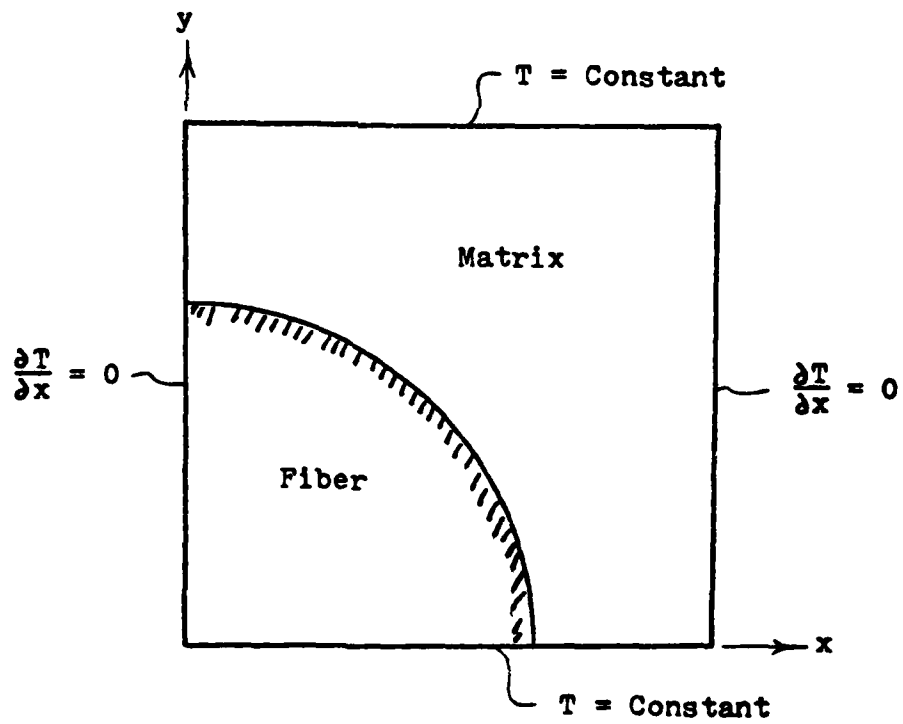
Figure 5. Rectangular array boundary conditions.

Therefore, the temperature field needs to be found in this area so that the heat flux can be obtained by integrating across some plane. The heat flux will be the same as that for all the other repeating cells in the material and so the effective conductivity found for this area is the same as that for the material as a whole. The rest of this section is devoted to finding the temperature field given these boundary conditions and performing the subsequent integration. Figure 6 shows a typical set of constant temperature lines for a rectangular array with the particular constants given.
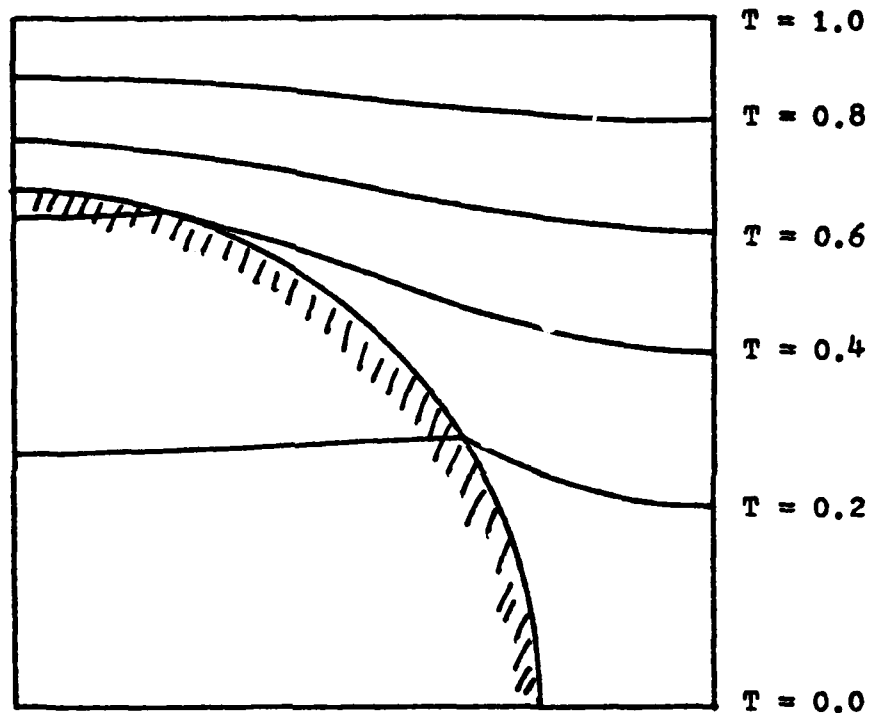
$$K_{fiber}/K_{matrix} = 4 \qquad \text{Volume Ratio} = .442$$

Figure 6. Rectangular array constant temperature lines.

The staggered array is considered next and is assumed to have the same one-dimensional vertical temperature gradient imposed on it. The lines of symmetry then appear as shown in Figure 7.

As with the rectangular array, a repeating pattern appears as outlined by the heavy line. The temperature field behaves along these lines of symmetry as it did with those of the rectangular array and so these conditions are shown in the sketch of the repeating area in Figure 8.

14
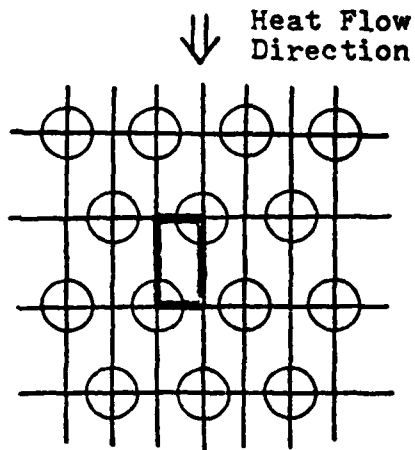
Figure 7. Staggered array repeating cell.
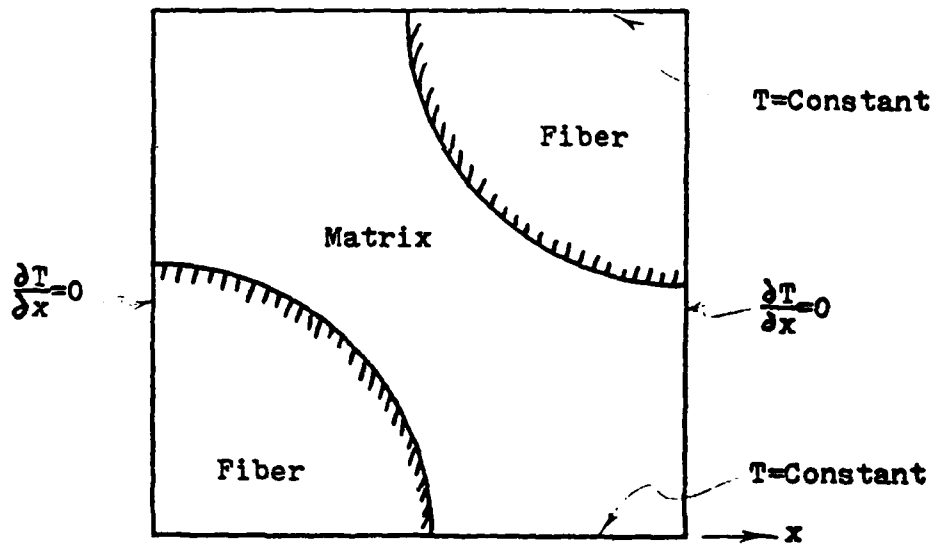
Figure 8. Staggered array boundary conditions.

As in the case of the rectangular array, the temperature field must now be found so that the heat flux can be found across a plane. Figure 9 shows a typical set of constant temperature lines for a staggered array having the indicated constants.
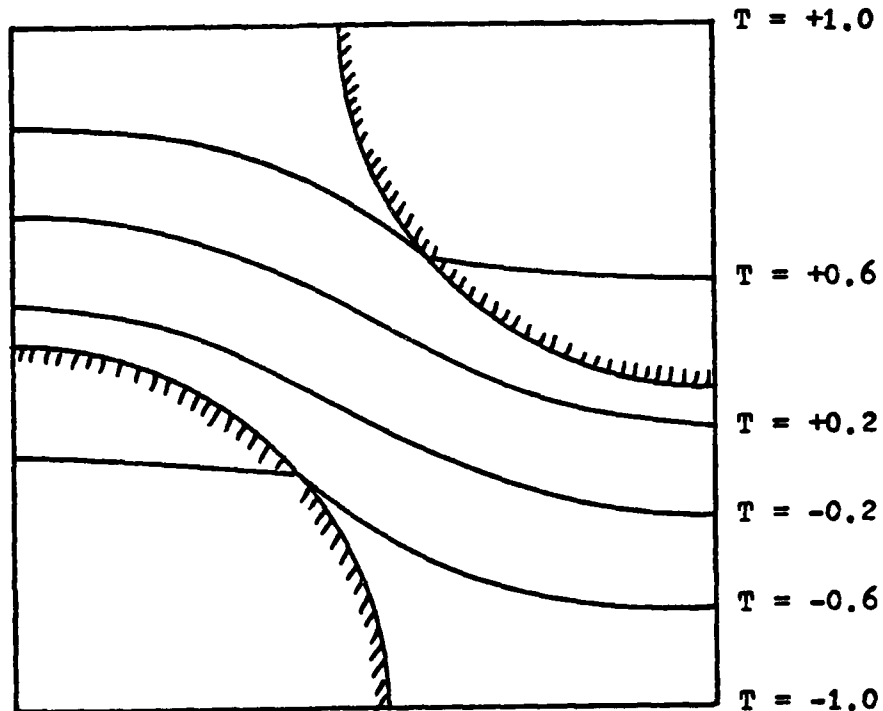
$$K_{fiber}/K_{matrix} = 4 \qquad \text{Volume Ratio} = .442$$

Figure 9. Staggered array constant temperature lines.

2.2 RECTANGULAR ARRAY

The general thermal energy balance equation for a solid material is the Fourier equation:

$$\rho c \frac{\partial T}{\partial t} = \nabla (k \nabla T) \qquad (15)$$

Here, the first term is the energy storage term, and the second is the heat transfer term.

When the problem is assumed to be steady state with no heat generation and with conductivity independent of temperature as it is here, the equation reduces to that below:

16

$$\nabla^2 T = 0 \tag{16}$$

This is commonly referred to as the Laplace equation and is valid for both the fiber and matrix regions. When this is written out in polar coordinates, the following expression is obtained:

$$\frac{\partial^2 T}{\partial r^2} + \frac{1}{r^2}\frac{\partial^2 T}{\partial \theta^2} + \frac{1}{r}\frac{\partial T}{\partial r} = 0 \tag{17}$$

The general solution to this two-dimensional equation is that shown below where A, B, C, and D are constants.

$$T = \sum_{n=1}^{\infty} r^n (A_n \cos n\theta + B_n \sin n\theta) + r^{-n}(C_n \cos n\theta + D_n \sin n\theta) \tag{18}$$

Now, consider the rectangular array which is the simpler of the two parallel-fiber arrangements. The problem to be solved is that shown in Figure 10. The temperatures across the top and bottom edges are arbitrarily taken as +1 and 0 respectively and the value of dT/dx must equal zero along the left and right sides. The horizontal side is of length a and the vertical of length b. The fiber radius is arbitrarily taken as 1.

Figure 10. Rectangular array problem.

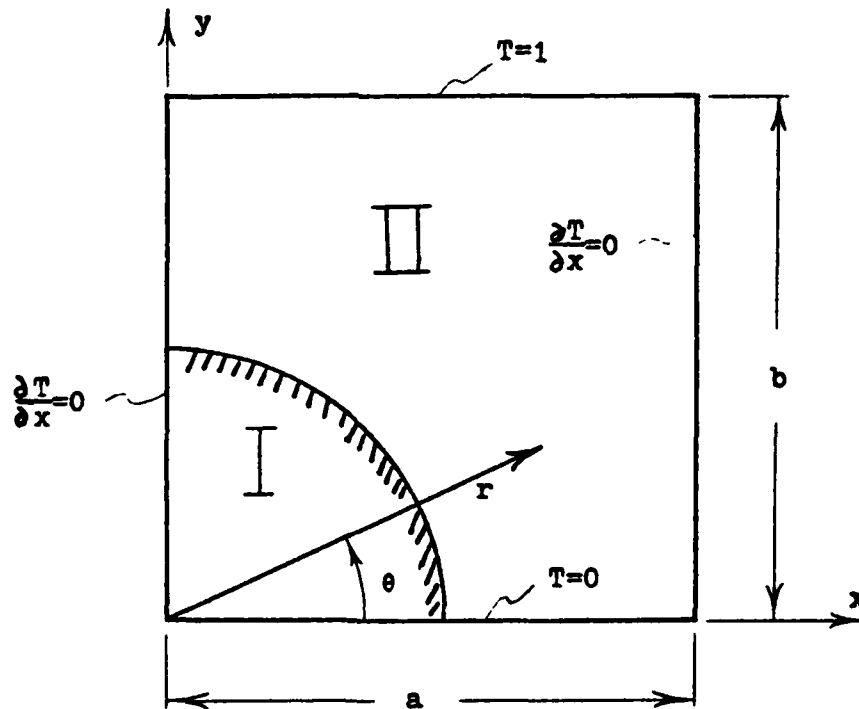The conductivities of the fiber and matrix are K_f and K_m respectively and the conductivity ratio, K_f/K_m is called β. Consider first the region I which is that region inside the fiber. On the lower edge where $\theta = 0$, then $T = 0$ and so the constants A_n and C_n of Equation 18 must both be zero. Furthur, at the origin the temperature is finite and so D_n must be zero so as not to have a singularity at that point. For the matrix (region II), A_n and C_n must be zero but there is no such restriction on D_n.

On the left side $\partial T/dx$ must be zero in both regions. This is equivalent to saying that $\partial T/d\theta$ must be zero at $\theta = \pi/2$. Since T consists strictly on sine terms, the derivative will consist strictly of cosine terms, and all coefficients where n is even must consequently be zero to satisfy the boundary condition. Therefore, the temperature in each region can be described as shown below where the constants have been redefined to avoid confusion between the two equations.

$$T_I = \sum_{n=1}^{\infty} A_n r^n \sin(n\theta) \tag{19}$$

$$T_{II} = \sum_{n=1}^{\infty} [B_n r^n + C_n r^{-n}] \sin(n\theta) \tag{20}$$

Consider now the interface between the fiber and the matrix. At this line where the radius, r, was chosen to be 1, the temperature in each region must be the same.

$$\text{at } r = 1, \quad T_I = T_{II}$$

$$\sum_{\substack{n=1 \\ \text{odd}}}^{\infty} A_n \sin(n\theta) = \sum_{\substack{n=1 \\ \text{odd}}}^{\infty} (B_n + C_n) \sin(n\theta) \tag{21}$$

From this expression, it can be seen that

$$A_n = B_n + C_n$$

for all n. Therefore, A_n can be eliminated from the expression for T_I to give the following equations for temperature:

$$T_I = \sum_{\substack{n=1 \\ \text{odd}}}^{\infty} (B_n + C_n) r^n \sin(n\theta) \tag{22}$$

$$T_{II} = \sum_{\substack{n=1 \\ \text{odd}}}^{\infty} (B_n r^n + C_n r^{-n}) \sin(n\theta) \tag{23}$$

18

The second condition that must be met at the interface is that the heat flux normal to the interface in region I must equal the heat flux normal to the interface in region II. This condition is described by the following equation:

$$K_I \frac{\partial T_I}{\partial r}\bigg|_{r=1} = K_{II} \frac{\partial T_{II}}{\partial r}\bigg|_{r=1} \tag{24}$$

When Equations 22 and 23 are differentiated with respect to r and the values for $r = 1$ substituted into Equation 24, then Equation 26 is obtained.

$$K_f\left[\sum_{\substack{n=1 \\ odd}}^{\infty} n(B_n + C_n)r^{n-1}\sin(n\theta)\right] =$$
$$K_m\left[\sum_{\substack{n=1 \\ odd}}^{\infty} n(B_n r^{n-1} - C_n r^{-n-1})\sin(n\theta)\right] \tag{25}$$

$$K_f\left[\sum_{\substack{n=1 \\ odd}}^{\infty} n(B_n + C_n)\sin(n\theta)\right] = K_m\left[\sum_{\substack{n=1 \\ odd}}^{\infty} n(B_n - C_n)\sin(n\theta)\right] \tag{26}$$

This can now be simplified to the expression of Equation 29. Here, the ratio K_f/K_m is referred to as β.

$$\beta \sum_{\substack{n=1 \\ odd}}^{\infty} [n(B_n + C_n)\sin(n\theta)] = \sum_{\substack{n=1 \\ odd}}^{\infty} [n(B_n - C_n)\sin(n\theta)] \tag{27}$$

$$\beta(B_n + C_n) = B_n - C_n \tag{28}$$

$$C_n = -B_n\left(\frac{\beta - 1}{\beta + 1}\right) \tag{29}$$

Using this equation for C_n, the equations for the temperatures can now be written in terms of one constant for each value of n as shown in Equations 30 and 31.

$$T_I = \sum_{\substack{n=1 \\ odd}}^{\infty} B_n\left(\frac{2}{1+\beta}\right)r^n\sin(n\theta) \tag{30}$$

$$T_{II} = \sum_{\substack{n=1 \\ odd}}^{\infty} B_n\left[r^n - \left(\frac{\beta - 1}{\beta + 1}\right)r^{-n}\right]\sin(n\theta) \tag{31}$$

19

A new constant E_n is now defined so as to give the equations for temperature in their final form.

$$E_n = \frac{2B_n}{\beta + 1} \tag{32}$$

$$T_I = \sum_{\substack{n=1 \\ \text{odd}}}^{\infty} E_n r^n \sin(n\theta) \tag{33}$$

$$T_{II} = \sum_{\substack{n=1 \\ \text{odd}}}^{\infty} E_n \left[\left(\frac{\beta + 1}{2} \right) r^n - \left(\frac{\beta - 1}{2} \right) r^{-n} \right] \sin(n\theta) \tag{34}$$

These are the general equations for temperature where the origin is placed at the center of the fiber. They incorporate the boundary conditions that $T = 0$ on the bottom and that $dT/dx = 0$ on the left side.

Now, the values of E_n have to be found. To do this, more boundary conditions are needed. All possible boundary conditions have been utilized in region I, but there are still two available in region II. These are namely that the temperature is constant at a value of 1 on the top edge and dT/dx is zero on the right edge. These conditions cannot be satisfied exactly at all points since polar coordinates are used in Equations 33 and 34. They can however be satisfied exactly at a finite number of points with the view point that they will be very closely satisfied at all other points along those edges. Let the boundary conditions be satisfied at five, or $M + 1$, equally spaced discrete points for the constant temperature condition and at four, or M, equally spaced discrete points for the constant dT/dx condition as shown below. At the top right corner point, both conditions are to be satisfied. In addition dT/dx is already made to equal zero in Equation 34 at the lower right corner and so this need not be one of the discrete points.

The expression for dT/dx in region II is found according to the following procedure using Equation 34.

$$\frac{\partial T}{\partial x} = \frac{\partial T}{\partial r} \frac{\partial r}{\partial x} + \frac{\partial T}{\partial \theta} \frac{\partial \theta}{\partial x} \tag{35}$$
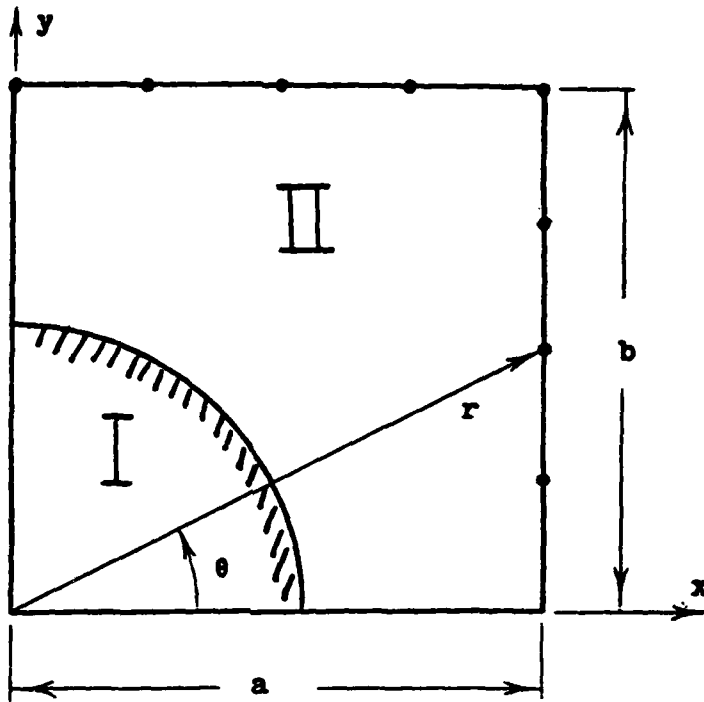
Figure 11. Rectangular array matching points.

$$\frac{\partial T}{\partial r} = \sum_{\substack{n=1 \\ \text{odd}}}^{\infty} n\Xi_n \left[(\frac{\beta + 1}{2})r^{n-1} + (\frac{\beta - 1}{2})r^{-n-1} \right] \sin(n\theta) \quad (36)$$

$$\frac{\partial T}{\partial \theta} = \sum_{\substack{n=1 \\ \text{odd}}}^{\infty} nE_n \left[(\frac{\beta + 1}{2})r^n - (\frac{\beta - 1}{2})r^{-n} \right] \cos(n\theta) \quad (37)$$

$$\frac{\partial r}{\partial x} = \cos(\theta) \quad (38)$$

$$\frac{\partial \theta}{\partial x} = \frac{-\sin(\theta)}{r} \quad (39)$$

21

$$\frac{\partial T}{\partial x} = \sum_{\substack{n=1 \\ odd}}^{\infty} nE_n \left\{ \left[\left(\frac{\beta+1}{2}\right)r^{n-1} + \left(\frac{\beta-1}{2}\right)r^{-n-1}\right][\sin(n\theta)\cos(\theta)] + \right.$$
$$\left. \left[\left(\frac{\beta+1}{2}\right)r^{n} - \left(\frac{\beta-1}{2}\right)r^{-n}\right]\left[\cos(n\theta)\frac{-\sin(\theta)}{r}\right] \right\} \quad (40)$$

$$\frac{\partial T}{\partial x} = \sum_{\substack{n=1 \\ odd}}^{\infty} nE_n \left\{ \left(\frac{\beta+1}{2}\right)r^{n-1}\sin[(n-1)\theta] + \right.$$
$$\left. \left(\frac{\beta-1}{2}\right)r^{-n-1}\sin[(n+1)\theta] \right\} \quad (41)$$

Therefore, Equation 41 can be set equal to zero for the coordinates of the M points shown in Figure 11 to give M equations. Similarly, Equation 34 for T_{II} can be set equal to 1 for the coordinates of the $(M + 1)$ points where it applies to give another $(M + 1)$ equation. This gives a total of $(2M + 1)$ equations. Now, if each equation is carried out to include $(2M + 1)$ terms, there will be $(2M + 1)$ unknowns in the $(2M + 1)$ equations. These unknowns are E_1, E_3, E_5, ---, E_{4M-1}, E_{4M+1}. Thus, the equations can be solved for these unknowns by various methods. They can then be substituted back into the temperature equations (33 and 34) to give the temperature at any point. The only approximation that has been made is to treat the power series as that of only $(2M + 1)$ terms instead of an infinite number. The assumption here is that the terms not included contribute to a negligible value compared with the sum of the first $(2M + 1)$ terms. As was shown earlier, this temperature field can then be used to calculate the effective conductivity which will be done in Section 2.4.

2.3 STAGGERED ARRAY

The problem to be solved for the staggered array is that shown in Figure 12. For reasons that will be discussed below, the temperature across the top will be taken as +1 and that across the bottom as -1.

Consider now the analysis in Section 2.2 for the rectangular array. The analysis leading to the general equations for temperature (Equations 33 and 34) is valid for the staggered array shown except that one minor change must be made. That change is that now the temperature across the bottom edge is taken as -1 instead of 0. To compensate for this, the constant 1 must be subtracted from the rectangular array equations to give the following equations for the staggered array:
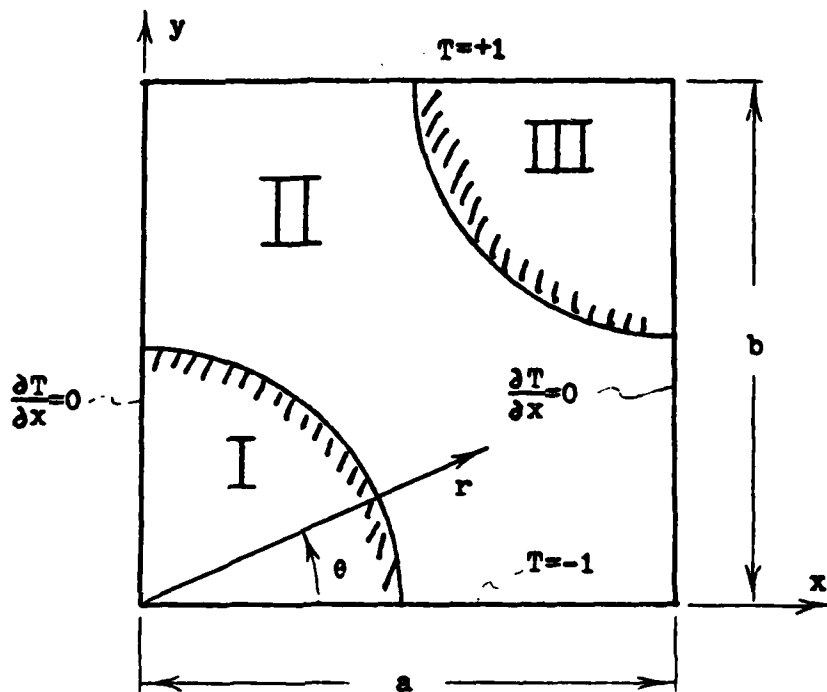
Figure 12. Staggered array problem.

$$T_I = -1 + \sum_{\substack{n=1 \\ odd}}^{\infty} E_n r^n \sin(n\theta) \tag{42}$$

$$T_{II} = -1 + \sum_{\substack{n=1 \\ odd}}^{\infty} E_n \left[\left(\frac{1 + \beta}{2} \right) r^n + \left(\frac{1 - \beta}{2} \right) r^{-n} \right] \sin(n\theta) \tag{43}$$

Because of the added complexity of region III, a similar equation cannot be written for the temperature in that region. However, an analytical solution similar to that used for the rectangular array is still possible and will now be discussed.

A typical plot of the constant temperature lines for a staggered array with a value of $\beta = 4$ and a volume ratio (fiber volume/total volume) of .442 was shown in Figure 9 previously. It is noted that a temperature field symmetry exists in this area. The symmetry is such that the temperature field in the top half is a mirror image of that in the bottom half. Figure 13 illustrates this symmetry.
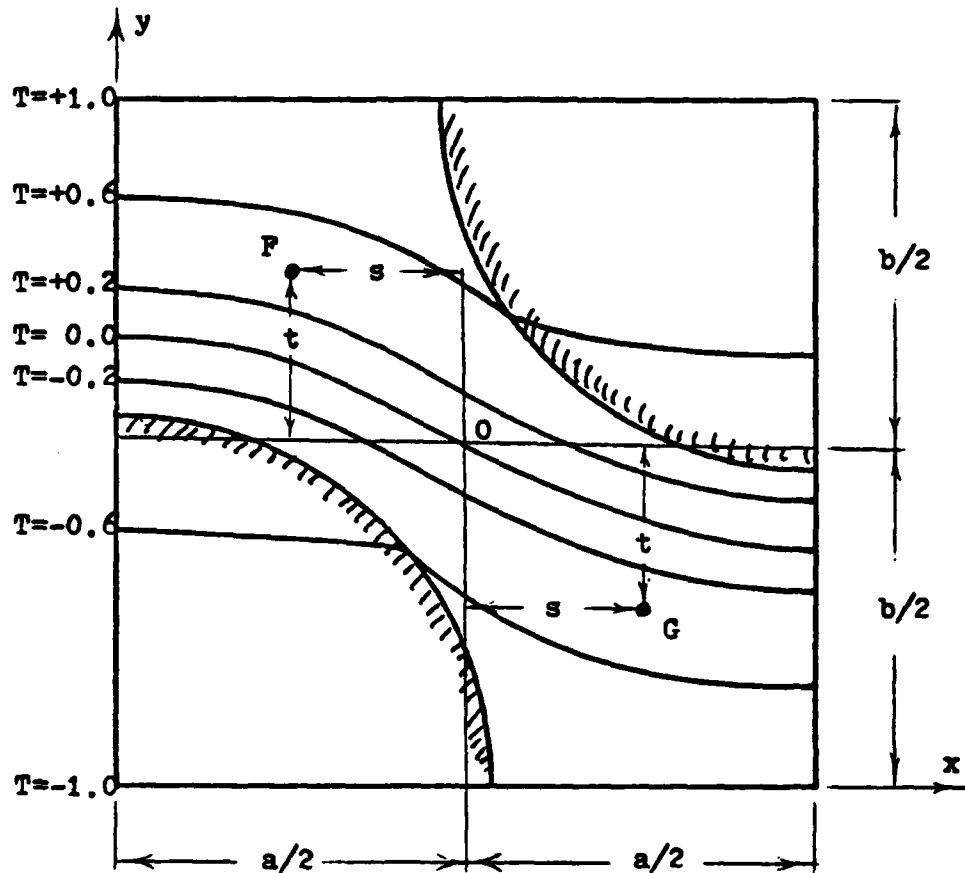
23

Figure 13. Staggered array temperature symmetry.

Consider points F and G which are located the same distance above and below the midplane respectively. They are also displaced by equal amounts horizontally from the center as shown. Thus, they are symmetric to point O at the center.

Because of symmetry, point O can be seen to have a temperature of zero because there are equal changes in conductivity above and below and to the left and right. By similar reasoning, points F and G can be seen to have opposite temperatures.

$$T_f = -T_g \tag{44}$$

This demonstrates the advantage of choosing the top and bottom temperatures as they were.

It can also be seen that symmetric points such as F and G have equal values of $\partial T/\partial y$.

$$\frac{\partial T}{\partial y}\Big|_F = \frac{\partial T}{\partial y}\Big|_G \qquad\qquad (45)$$

This can be reasoned in a way similar to that used in looking at the temperatures. Because the lines of constant temperature are symmetric, the gradient $(\partial T/\partial y)$ values must be the same. If $\partial T/\partial y$ varied, then the spacing between the constant temperature lines would have to vary accordingly which would cause at least some of the temperatures to be unsymmetric.

Because of this symmetry, if the temperature field is known in one-half of the area, then it is also known in the other half. Further, it does not matter which half of the area is studied so long as one of every pair of symmetric points is included in that half. It can be seen that any straight line drawn through the center point will separate the area into halves which will each include exactly one of every symmetric pair of points. Because points F and G are symmetric with respect to the center, it is impossible to draw a line through the center and have both points in the same half of the area.

The solution to the staggered array is similar to that for the rectangular array except that the discrete points will now be located on a line through the center. At these points, the symmetry discussed above will be enforced on pairs of symmetric points along this line. This will provide adequate boundary conditions for an area which includes the lower left fiber to be solved to get its temperature field. In this way the expressions for the temperature in areas I and II are all that is needed to solve for the entire temperature field, and the complexities of region III are now dispensed with.

There are a large number of choices as to which line through the center should be used for the discrete points. The only restriction on this choice is that the line should not cut across the fibers because no point may be used which exists in region III.

Consider the three possible geometries in which the volume ratio is made as large as is physically possible (see Figure 14) for a given ratio of the sides of the area. The cases shown are where the fibers are in contact along vertical, diagonal, and horizontal lines respectively. The best lines for the matching points are sketched on the figures as dashed lines.

In geometries where the fibers touch on the diagonal the only matching line that can be used is the one perpendicular to the diagonal that runs from the lower left to the upper right corners. Thus, this matching line is used for all geometries because it can never intersect the fiber. Then in cases where fibers touch along horizontal lines, additional points are used on the right side. When fibers touch along vertical lines, additional points are added along the top. These points
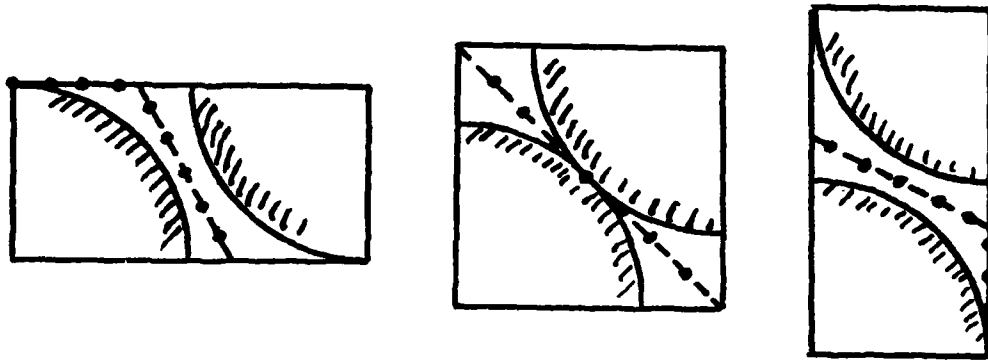
25

Figure 14. Staggered array matching lines.

that are on the top or right side introduce boundary condition equations identical to those that were derived for the square array. For completeness, these equations are repeated below.

For points on the top edge:

$$T_{II} = +1 = \sum_{\substack{n=1 \\ odd}}^{\infty} E_n \left[(\frac{\beta + 1}{2})r^n - (\frac{\beta - 1}{2})r^{-n} \right] \sin(n\theta) \qquad (46)$$

Along the right side:

$$\frac{\partial T}{\partial x}_{II} = 0 = \sum_{\substack{n=1 \\ odd}}^{\infty} nE_n \left\{ (\frac{\beta + 1}{2})r^{n-1}\sin[(n-1)\theta] + \right.$$
$$\left. (\frac{\beta - 1}{2})r^{-n-1}\sin[(n+1)\theta] \right\} \qquad (47)$$

$$T_f = -1 + \sum_{\substack{n=1 \\ odd}}^{\infty} E_n \left[(\frac{1 + \beta}{2})r_f^n + (\frac{1 - \beta}{2})r_f^{-n} \right] \sin(n\theta_f) \qquad (48)$$

$$T_g = -1 + \sum_{\substack{n=1 \\ odd}}^{\infty} E_n \left[(\frac{1 + \beta}{2})r_g^n + (\frac{1 - \beta}{2})r_g^{-n} \right] \sin(n\theta_g) \qquad (49)$$
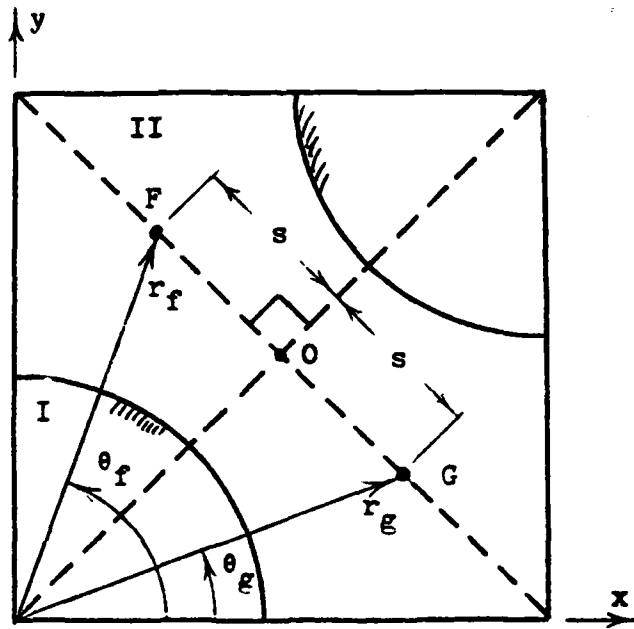
Figure 15. Staggered array matching points.

$$T_f = -T_g \tag{50}$$

$$\sum_{\substack{n=1 \\ odd}}^{\infty} E_n \left\{ \left[\left(\frac{1+\beta}{2} \right) r_g^n + \left(\frac{1-\beta}{2} \right) r_g^{-n} \right] \sin(n\theta_g) + \right.$$

$$\left. \left[\left(\frac{1+\beta}{2} \right) r_f^n + \left(\frac{1-\beta}{2} \right) r_f^{-n} \right] \sin(n\theta_f) \right\} = +2 \tag{51}$$

Everything in Equation 51 is known except for E_n. Therefore, this can be used to produce one equation with the required number of terms for every pair of points used. Further, another equation is produced by using Equation 43 to specify the temperature of point 0 at the center.

$$T_{II} = 0 = -1 + \sum_{\substack{n=1 \\ odd}}^{\infty} E_n \left[\left(\frac{1+\beta}{2} \right) r_o^n + \left(\frac{1-\beta}{2} \right) r_o^{-n} \right] \sin(n\theta_o) \tag{52}$$

27

Now, the value of $\partial T/\partial y$ must be made equal for the pair of points on the matching line. This calls for an expression for $\partial T/\partial y$ in region II, and it is therefore formulated below.

$$\frac{\partial T}{\partial y} = \frac{\partial T}{\partial \theta}\frac{\partial \theta}{\partial y} + \frac{\partial T}{\partial r}\frac{\partial r}{\partial y} \tag{53}$$

$$\frac{\partial T}{\partial r} = \sum_{\substack{n=1 \\ odd}}^{\infty} nE_n\left[\left(\frac{\beta+1}{2}\right)r^{n-1} + \left(\frac{\beta-1}{2}\right)r^{-n-1}\right]\sin(n\theta) \tag{54}$$

$$\frac{\partial T}{\partial \theta} = \sum_{\substack{n=1 \\ odd}}^{\infty} nE_n\left[\left(\frac{\beta+1}{2}\right)r^{n} - \left(\frac{\beta-1}{2}\right)r^{-n}\right]\cos(n\theta) \tag{55}$$

$$\frac{\partial r}{\partial y} = \sin(\theta) \tag{56}$$

$$\frac{\partial \theta}{\partial y} = \frac{1}{r}\cos(\theta) \tag{57}$$

$$\frac{\partial T}{\partial y} = \sum_{\substack{n=1 \\ odd}}^{\infty} nE_n\left\{\left[\left(\frac{1+\beta}{2}\right)r^{n} + \left(\frac{1-\beta}{2}\right)r^{-n}\right]\cos(n\theta)\frac{\cos(\theta)}{r} + \right.$$
$$\left. \left[\left(\frac{1+\beta}{2}\right)r^{n-1} - \left(\frac{1-\beta}{2}\right)r^{-n-1}\right]\sin(n\theta)\sin(\theta)\right\} \tag{58}$$

$$\frac{\partial T}{\partial y} = \sum_{\substack{n=1 \\ odd}}^{\infty} nE_n\left\{\left(\frac{1+\beta}{2}\right)r^{n-1}\cos[(n-1)\theta] + \right.$$
$$\left. \left(\frac{1-\beta}{2}\right)r^{-n-1}\cos[(n+1)\theta]\right\} \tag{59}$$

28

Equation 59 is the simplest form for $\partial T/\partial y$ in region II. Now the condition of symmetry will be imposed on points F and G in the same manner that the temperature symmetry was imposed to give Equation 61 below.

$$\left.\frac{\partial T}{\partial y}\right|_F = \left.\frac{\partial T}{\partial y}\right|_G \tag{60}$$

$$\sum_{\substack{n=1 \\ odd}}^{\infty} nE_n \left\{ \left(\frac{1+\beta}{2}\right)r_f^{n-1}\cos[(n-1)\theta_f] + \left(\frac{1-\beta}{2}\right)r_f^{-n-1}\cos[(n+1)\theta_f] - \left(\frac{1+\beta}{2}\right)r_g^{n-1}\cos[(n-1)\theta_g] - \left(\frac{1-\beta}{2}\right)r_g^{-n-1}\cos[(n+1)\theta_g] \right\} = 0 \tag{61}$$

Thus, Equation 61 can be used to produce one equation with the required number of terms for every pair of points used.

Therefore, for a given geometric arrangement the matching line is drawn as was discussed earlier. Then discrete points are placed along this line and either the top or right side--whichever is appropriate. For each pair of symmetric points, two equations are written (51 and 61). For the center point, Equation 52 is written. Then for each point on the top or right side, either Equation 46 or Equation 47 is written. Each equation is carried out to the same number of terms as there are equations so that the number of unknowns will equal the number of equations. The equations can then be solved for the unknowns which are E_1, E_3, E_5, ---, E_{2M-3}, E_{2M-1} for M equations. They can then be put back in the original temperature equations (42 and 43) to obtain the temperature field at any point. As with the rectangular array, the only approximation that has been made is that the power series has been reduced to a finite number of terms. This temperature field can then be used to calculate the effective conductivity in Section 2.4.

2.4 EFFECTIVE CONDUCTIVITY

Using the procedures described in the two previous Sections, the temperature field can be determined for both the rectangular and the staggered arrays. This temperature field can then be used to obtain the effective conductivity.

2.4.1 Rectangular Array

The temperature field for the rectangular array is given by the following equations:

29

$$T_I = \sum_{\substack{n=1 \\ \text{odd}}}^{2M-1} E_n r^n \sin(n\theta) \tag{62}$$

$$T_{II} = \sum_{\substack{n=1 \\ \text{odd}}}^{2M-1} E_n \left[\left(\frac{1+\beta}{2} \right) r^n + \left(\frac{1-\beta}{2} \right) r^{-n} \right] \sin(n\theta) \tag{63}$$

Here, M is the number of matching points that are used to satisfy the boundary conditions. The value of T_{II} is good for the entire region II for the rectangular array.

The heat flux must now be found through the unit area. As discussed previously, it can be found by Equation 64 by integrating across any line that cuts across the unit area.

$$Q = -\int \left(K \frac{\partial T}{\partial n} \right) dr \tag{64}$$

Here, n is the direction normal to the line of integration.

Since the heat flux will be the same across any line, the bottom edge will be used since it produces the simplest expressions. Thus, the normal direction is the y direction and the analysis proceeds as follows:

$$Q = -\int_0^1 \left(K_I \frac{\partial T_I}{\partial y} \Big|_{\theta=0} \right) dr - \int_0^a \left(K_{II} \frac{\partial T_{II}}{\partial y} \Big|_{\theta=0} \right) dr \tag{65}$$

Here the integration has been split up into the two regions since their conductivities differ. As was the case before, "a" is the length of the horizontal side. An expression for $\partial T / \partial y$ can be found as shown below.

$$\frac{\partial T}{\partial y} = \frac{\partial T}{\partial r} \frac{\partial r}{\partial y} + \frac{\partial T}{\partial \theta} \frac{\partial \theta}{\partial y} \tag{66}$$

$$\frac{\partial r}{\partial y} = \sin(\theta) \tag{67}$$

$$\frac{\partial \theta}{\partial y} = \frac{\cos(\theta)}{r} \tag{68}$$

30

However, the integration is being performed along the line $\theta = 0$ so the following expressions are obtained:

$$\frac{\partial T}{\partial y} = \frac{1}{r} \frac{\partial T}{\partial \theta}\bigg|_{\theta=0} \tag{69}$$

$$Q = -K_I \int_0^1 \left(\frac{1}{r} \frac{\partial R_I}{\partial \theta}\bigg|_{\theta=0}\right) dr - K_{II} \int_1^a \left(\frac{1}{r} \frac{\partial T_{II}}{\partial \theta}\bigg|_{\theta=0}\right) dr \tag{70}$$

Differentiating the expressions for temperature in each region with respect to θ gives Equations 71 and 72.

$$\frac{\partial T_I}{\partial \theta} = \sum_{\substack{n=1 \\ \text{odd}}}^{2M-1} n E_n r^n \cos(n\theta) \tag{71}$$

$$\frac{\partial T_{II}}{\partial \theta} = \sum_{\substack{n=1 \\ \text{odd}}}^{2M-1} n E_n \left[\left(\frac{1+\beta}{2}\right) r^n + \left(\frac{1-\beta}{2}\right) r^{-n}\right] \cos(n\theta) \tag{72}$$

For $\theta = 0$ the integration can now be carried out to give Equation 73 for the heat flux.

$$Q = -K_I \sum_{\substack{n=1 \\ \text{odd}}}^{2M-1} E_n - K_{II} \sum_{\substack{n=1 \\ \text{odd}}}^{2M-1} E_n \left[\left(\frac{1+\beta}{2}\right)(a^n-1) - \left(\frac{1-\beta}{2}\right)(a^{-n}-1)\right] \tag{73}$$

The effective conductivity is defined by Equation 74 where $\Delta T / \Delta n$ is the overall temperature gradient across the entire unit area under study.

$$K_{eff} = \frac{Q}{\text{Area} \frac{\Delta T}{\Delta n}} \tag{74}$$

$$K_{eff} = \frac{Q}{a\left(\frac{-1}{b}\right)} \tag{75}$$

$$K_{eff} = \frac{b}{a}\left\{K_I \sum_{\substack{n=1 \\ \text{odd}}}^{2M-1} E_n + K_{II} \sum_{\substack{n=1 \\ \text{odd}}}^{2M-1} E_n\left[\left(\frac{1+\beta}{2}\right)(a^n-1) - \left(\frac{1-\beta}{2}\right)(a^{-n}-1)\right]\right\} \tag{76}$$

31

By nondimensionalizing this expression by dividing through by the matrix conductivity, K_{II}, the following simplified expression can be obtained:

$$\frac{K_{eff}}{K_{II}} = \frac{b}{a} \sum_{\substack{n=1 \\ odd}}^{2M-1} E_n \left[(\frac{1+\beta}{2})a^n - (\frac{1-\beta}{2})a^{-n} \right] \qquad (77)$$

Therefore, once the constants, E_n, have been determined as was discussed in Section 2.2, they can immediately be inserted into Equation 77 to give the effective conductivity.

2.4.2 Staggered Array

Consider now the staggered array discussed in Section 2.3. In that analysis the temperature field was determined in only half of the rectangular unit area while symmetry was used to give the field in the other half. The two basic types of divisions of the rectangular area are repeated in Figure 16.
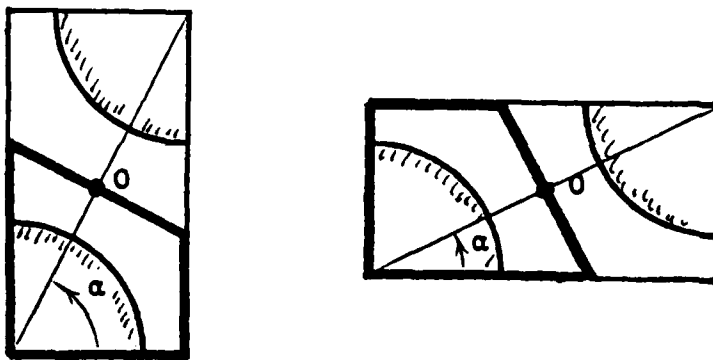
Figure 16. Staggered array solution regions.

The temperature within the regions outlined by heavy lines was found directly by the equations of 2.3 which are given below. The expression for T_{II} is not valid outside of the heavily outlined regions.

$$T_I = -1 + \sum_{\substack{n=1 \\ odd}}^{2M-1} E_n r^n \sin(n\theta) \qquad (78)$$

$$T_{II} = -1 + \sum_{\substack{n=1 \\ odd}}^{2M-1} E_n \left[(\frac{1+\beta}{2})r^n + (\frac{1-\beta}{2})r^{-n} \right] \sin(n\theta) \qquad (79)$$

32

It can be seen that as long as α is greater than or equal to 45 degrees, the entire bottom line is included in the region for which the equations are applicable. It can be seen that the effective conductivity for these cases can be analyzed in exactly the same manner as was done for the rectangular array. The expressions for temperature are the same except for a constant, and this constant does not affect the value of $\partial T/\partial \theta$ which is used to calculate the heat flux across the region. The only other change that must be made in that analysis is that the overall temperature gradient across the rectangular unit area, $\Delta T/b$, is now $-2/b$ instead of $-1/b$. This produces the following expression for the effective conductivity for staggered arrays where α is greater than or equal to 45 degrees:

$$\frac{K_{eff}}{K_{II}} = \frac{b}{2a} \sum_{\substack{n=1 \\ odd}}^{2M-1} E_n \left[\left(\frac{1+\beta}{2}\right) a^n - \left(\frac{1-\beta}{2}\right) a^{-n} \right] \qquad (80)$$

Consider now the other case for the staggered array where α is less than 45 degrees. Equations 78 and 79 are not valid along the entire bottom line and so they cannot be integrated along it to give a valid result. However it should be noted that the center point, O, and the line from it to the origin are always included in the region for which the equations are valid. Thus, an integration can be performed along this line to five the total heat flux across it. Further, because of the symmetry in the temperature field with respect to the center point, the heat flux across the line from the center to the top-right corner will be the same as that across the line segment just discussed. The major steps to this integration are shown below where z represents the distance from the origin to the center.

$$Q = \left[-\int_0^z \left(K \frac{\partial T}{\partial n} \right) dr \right](2) \qquad (81)$$

$$Q = [Q_y \cos(\alpha) - Q_x \sin(\alpha)](2) \qquad (82)$$

Here, the integration is being performed along a line of constant α while Q_x and Q_y refer to the s and y components of Q respectively. Equation 81 can then be rewritten as follows:

$$Q = \left[-\cos(\alpha) \int_0^z \left(K \frac{\partial T}{\partial y} \bigg|_\alpha \right) dr - \sin(\alpha) \int_0^z \left(K \frac{\partial T}{\partial x} \bigg|_\alpha \right) dr \right](2) \qquad (83)$$

These integrations are performed in the same manner as was done for the rectangular array. Then, the following expression for Q is obtained:

33

$$\frac{Q}{K_{II}} = -\sum_{\substack{n=1 \\ odd}}^{2M-1} 2E_n \left[\left(\frac{1+\beta}{2}\right) z^n - \left(\frac{1-\beta}{2}\right) z^{-n} \right] \cos(n\alpha) \qquad (84)$$

The effective conductivity can now be found in the same manner as was done before.

$$K_{eff} = \frac{Q}{Area\left(\frac{\Delta T}{\Delta n}\right)} \qquad (85)$$

$$K_{eff} = \frac{Q}{a\left(\frac{-2}{b}\right)} \qquad (86)$$

$$\frac{K_{eff}}{K_{II}} = \frac{b}{a} \sum_{\substack{n=1 \\ odd}}^{2M-1} E_n \left[\left(\frac{1+\beta}{2}\right) z^n - \left(\frac{1-\beta}{2}\right) z^{-n} \right] \cos(n\alpha) \qquad (87)$$

By inserting the previously obtained values of E_n into this equation, the effective conductivity can now be found. This is of a similar form as that obtained before, although now the angle α enters into the expression where as before it was made equal to zero.

2.5 GEOMETRIC RESTRICTIONS

The solution method evolved in this investigation for the staggered and the rectangular arrays was devised in such a way that the effective conductivity could be calculated for any physical arrangement. The equations that were derived will of course give numerical answers no matter what volume ratio (fiber volume/total volume is used. It is therefore desirable to know the maximum physical volume ratio for each of these arrays for various angles α.

For the rectangular array, the maximum volume ratio occurs when the radius of the fiber is made equal to either of the sides of the unit area. The two cases are shown below.

For the first case, where α is greater than 45 degrees, the critical volume ratio is given by Equation 88. For the case where α is less than 45 degrees, Equation 89 is the valid equation. It should be noted that at 45 degrees the two expressions are identical.
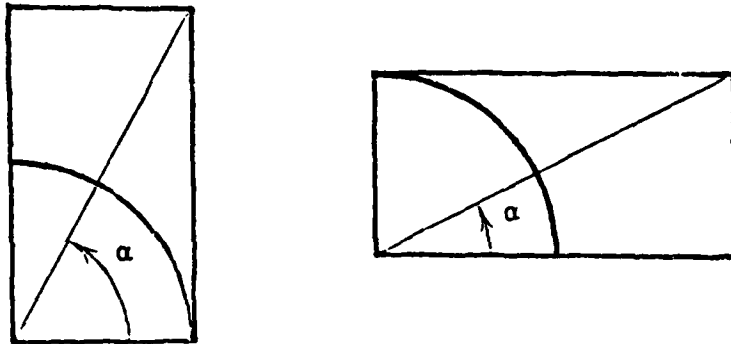
Figure 17. Rectangular array maximum volume ratios.

$$V_{critical} = \frac{\pi}{4\tan(\alpha)} \qquad \alpha \leq 45° \qquad (88)$$

$$V_{critical} = \frac{\pi\tan(\alpha)}{4} \qquad \alpha \leq 45° \qquad (89)$$

For the staggered array, three different situations occur which physically limit the value of the volume ratio. The limiting conditions are shown below.
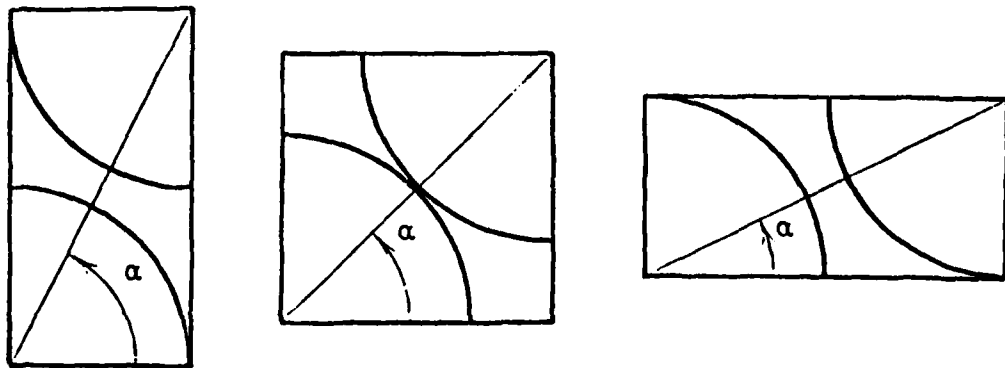

Figure 18. Staggered array maximum volume ratios.

The first case occurs for angles greater than 60 degrees when the fibers are in contact along a horizontal line. If the volume ratio were made any greater, the fibers would overlap, and this of course is impossible. The second case occurs for angles between 30 and 60 degrees

and is characterized by contact along diagonal lines. Finally, the third case shows contact along vertical lines and occurs for angles less than 30 degrees. The expressions for these critical volume ratios are given below.

$$V_{critical} = \frac{\pi}{2\tan(\alpha)} \qquad \alpha > 60° \qquad (90)$$

$$V_{critical} = \frac{\pi}{8\cos(\alpha)\sin(\alpha)} \qquad 60° \geq \alpha \geq 30° \qquad (91)$$

$$V_{critical} = \frac{\pi\tan(\alpha)}{2} \qquad \alpha < 30° \qquad (92)$$

Table 1 is a short table of the values of critical volume ratio. It should be noted that there is a large variation in these values demonstrating that some materials are much more efficient than others in terms of the quantity of fiber that can be included in the composite.

TABLE 1. CRITICAL VOLUME RATIOS

α	Critical Volume Ratio	
degrees	Staggered	Rectangular
25	.733	.366
30	.907	.453
35	.836	.550
40	.798	.659
45	.785	.785
50	.798	.659
55	.836	.550
60	.907	.453
65	.733	.366

2.6 RESULTS

The results for the rectangular arrays and the staggered arrays are presented in graphical form in Appendix A to this report. For both cases the value of K_{fiber}/K_{matrix} was varied from 0.1 to 100. The volume ratio was varied from 0.3 through the highest possible value. Finally, the fiber angle, α, was varied in 5 degree increments from 25 degrees through 65 degrees.

The accuracy of the data used to produce these graphs was good to three significant figures. This was deemed to be quite satisfactory from an engineering point of view.

Figures A-1 through A-7 for the rectangular array and A-21 through A-29 for the staggered array represent complete parametric studies. Equation 12 has been plotted on these graphs as this equation is by far the most common equation found in the literature for predicting effective conductivities. This equation does not take into account the varying packing geometry and so it is independent of α. Thus, only one curve for this equation is shown on each graph.

Equation 12 gives accurate effective conductivities for conductivity ratios below 5 or for volume ratios below 0.2. For values greater than these it is obvious it cannot be used because of the critical role that the angle α plays in the effective conductivity.

It is evident that at high conductivity ratios changes in the packing geometry (the angle α) can change the effective conductivity by an order of magnitude. This reflects the fact that the upper and lower bounds for the conditions [9, 11, 12] diverge greatly. More specifically, it can be seen that it is the spacings between fibers which are critically important.

For the high conductivity ratios, almost all the resistance to the heat flow is in the matrix material. Thus, the length of the path through which it must flow in the matrix is the most important factor. As an example, refer to Figure A-2 which is for the rectangular array with a volume ratio of 0.4. The 30 degree and the 35 degree geometries are shown below drawn to scale.
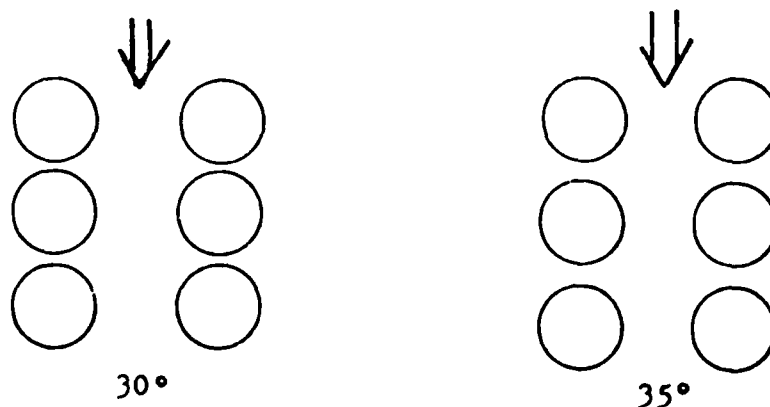
Figure 19. Rectangular arrays for volume ratio of 0.4.

37

For both cases, most of the heat is flowing vertically through the
fibers. But the vertical distance between fibers for the 35 degree
case is three times the distance for the 30 degree case and so there
is a large difference in the effective conductivities. It should be
realized that a volume ratio of 0.40 for the 30 degree case is very
near the maximum possible value of 0.45. This fact alone indicates
that the fibers are almost touching and that a high effective con-
ductivity should be expected.

For the rectangular array, the curves for the effective con-
ductivity line up in order of increasing angle, α, whereas this does
not occur for the staggered array. This can be explained by considering
which fiber spacings affect the effective conductivity for each case.
With the rectangular array, heat is flowing almost entirely across the
vertical spacings between fibers. Some heat will be flowing across
the diagonal spacings but they are a great deal larger and thus a
great deal more resistive so the heat flow across these spacings will
be a small fraction of the total. Thus, changes in these spacings
will affect the total heat flow very little. Then because the vertical
spacings are strictly increasing with increasing α, the thermal con-
ductivity will be strictly decreasing as is evident from the graphs.
A list of spacings normalized to the fiber radius for an arbitrary
volume ratio of 0.3 for both rectangular and staggered arrays is shown
below. These are the distances between fiber edges and not those
between fiber centers.

TABLE 2. FIBER SPACINGS NORMALIZED TO FIBER RADIUS

	Rectangular Array			Staggered Array		
α°	hor.	vert.	diag.	hor.	vert.	diag.
25	2.74	.21	3.23	4.70	1.12	1.70
30	2.26	.46	2.92	4.02	1.48	1.48
35	1.87	.70	2.72	3.47	1.83	1.34
40	1.53	.96	2.61	3.00	2.19	1.26
45	1.24	1.24	2.58	2.58	2.58	1.24
50	.96	1.53	2.61	3.00	2.19	1.26
55	.70	1.87	2.72	3.47	1.83	1.34
60	.46	2.26	2.92	4.02	1.48	1.48
65	.21	2.74	3.23	4.70	1.12	1.70

For both arrays the horizontal spacings are irrelevant since they
are perpendicular to the heat flow. For the rectangular array the
diagonal spacings are much larger than the vertical spacings and so
they are relatively insignificant. However, for the staggered array
the vertical diagonal spacings are of the same order of magnitude and
so both influence the effective conductivity. This is the reason why

the staggered array curves do not stack up according to increasing α. At different times different spacings carry most of the heat flow. Whenever either of the spacings becomes very small (fibers almost touching) the effective conductivity will become large no matter what the other spacing is like. Thus the 25-degree curve lies above the 30-degree curve because of the smaller vertical spacing, but the 45-degree curve lies above the 30 degree curve because of a smaller diagonal spacing.

It can be seen that in general the rectangular arrays produce higher effective conductivities than do the staggered arrays for the same volume ratios and conductivity ratios. This is the case because the fibers are stacked in rows parallel to the heat flow which naturally tends to give small fiber spacings in that direction. Thus, these materials provide low resistance paths for the heat flow. The staggered arrays however tend to have larger fiber spacings and thus lower effective conductivities. There is some overlap between the region covered by the staggered array and that covered by the equivalent rectangular array.

For a given type of array and a given volume ratio, consider the various pairs of angles which are complementary to each other such as 35 and 55, 25 and 65, and so forth. For a staggered array with a volume ratio of 0.2, the 25-degree and 65-degree cases are shown below in Figure 20.

25°   65°
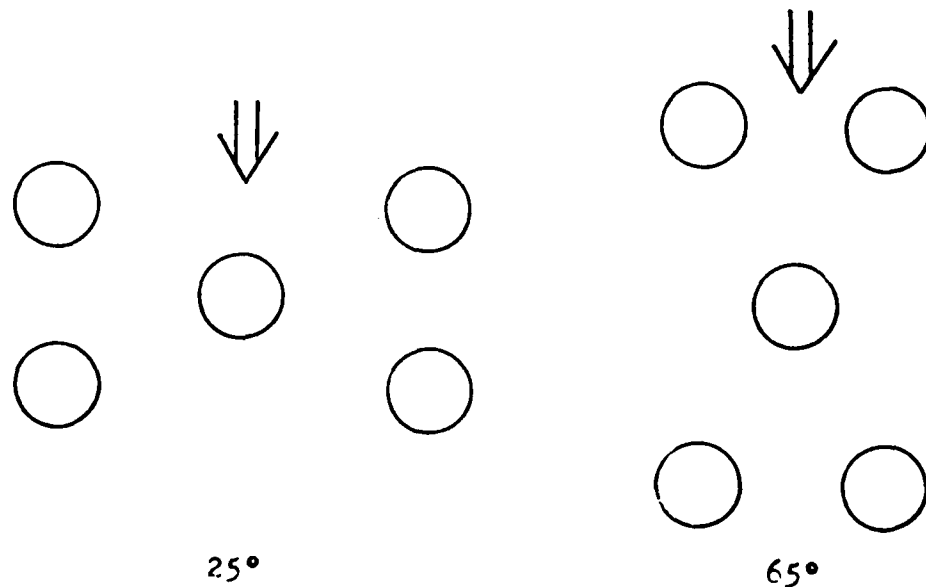
Figure 20. Complementary geometries for staggered array.

39

It is evident that these are really the same physical geometry which has merely been rotated by 90 degrees. Thus, the two effective conductivities which are given in the graphs for these values are in fact two of the three principal conductivities for the same material. The third principal conductivity is that for which heat is flowing into the paper parallel to the fibers. That effective conductivity is merely the weighted average of the individual conductivities based on the volume ratio and is given by the following equation:

$$\frac{K_{eff}}{K_{matrix}} = V \frac{K_{fiber}}{K_{matrix}} + 1 - V \qquad (93)$$

Figures A-8 through A-20 for the rectangular array and A-30 through A-56 for the staggered array present the three principal conductivities together for various materials. It should be noted that the effective conductivity parallel to the fibers for high conductivity ratios is always greater than both of the transverse conductivities because the high conductivity fibers provide an excellent heat conduction path. Further, the transverse conductivity curves level off at high conductivity ratios because most of the resistance is then in the matrix, and increasing the fiber conductivity does little to decrease the total resistance. However, for flow parallel to the fibers the curves become more and more linear at high conductivity ratios because more and more of the heat is flowing strictly through the fibers and the only resistance it sees is the fiber resistance.

It may be noted that the 45-degree curves for the staggered arrays are identical to the 45-degree curves for the rectangular arrays. The two cases are shown in Figure 21.

These are really the same configuration with the heat flow directions differing by an angle of 45 degrees. Further, it should be realized that the horizontal effective conductivities of these materials are the same due to geometric symmetry. By the equations of Section I, the reasoning can be extended to state that the effective conductivities of these materials will be the same for heat flow in any direction perpendicular to the fibers.
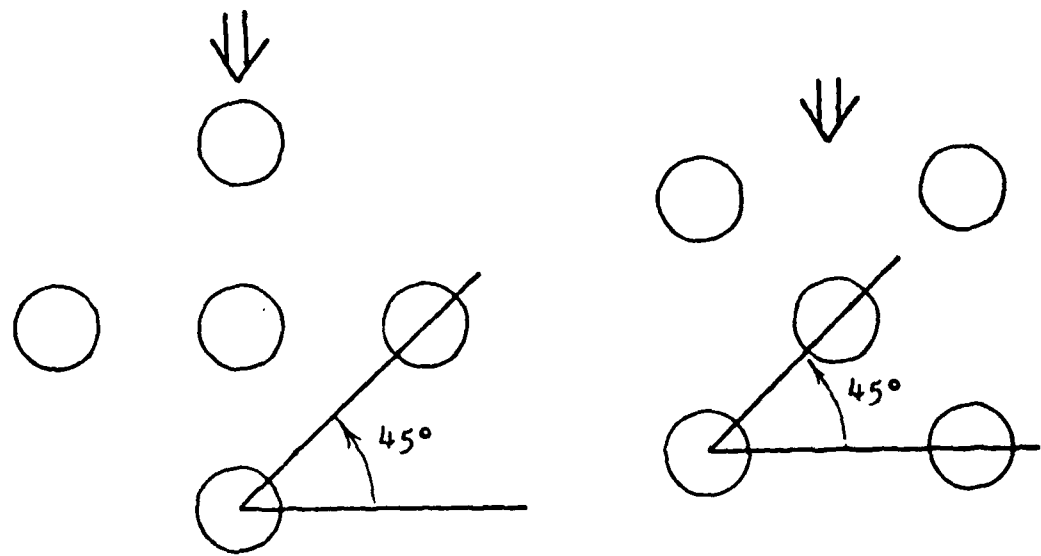
Rectangular Array   Staggered Array

Figure 21. 45-Degree configurations for parallel fibers.

CHAPTER III

0°-90° FIBER MATERIALS

3.1 PROBLEM DESCRIPTION

3.1.1 General Discussion

Composite materials in which the fibers are not all parallel will
now be considered. In particular, that group in which adjacent layers
of fibers are laid down at 90-degree angles to each other will be
studied. A sketch of a typical arrangement in this group is shown in
Figure 22.

From a geometric point of view, the independent variables are the
horizontal spacing between fibers, the vertical spacing between layers,
and the volume ratio. As was the case with the parallel fiber arrange-
ment, only those arrangements in which the horizontal spacing of all
layers is the same will be studied. Since the whole geometry can be
scaled up or down without changing the effective conductivity, only the
ratio of vertical spacing (between layers) to the horizontal spacing
(between fibers in a layer) is needed in addition to the volume ratio
to describe the geometry. This ratio will henceforth be referred to
as the aspect ratio.

The last variable which is needed is the ratio of fiber conductivity
to the matrix conductivity. Thus, when these three variables are
specified, there exists a unique value of the ratio of effective con-
ductivity to matrix conductivity which can be assigned to the material.
That effective conductivity ratio will then be valid for any geometrically
similar material which has the same ratio of fiber to matrix con-
ductivity.

As with the parallel fiber arrangements, it is first necessary to
find the temperature field in the material so that it can be integrated
across a plane to give the net heat flow through the material. The ef-
fective conductivity can then be seen to be given by Equation 94 where
$\Delta T / \Delta n$ refers to the uniform temperature gradient which exists over a
large section of the material.

$$K_{eff} = \frac{Q}{A \frac{\Delta T}{\Delta n}} \tag{94}$$

42
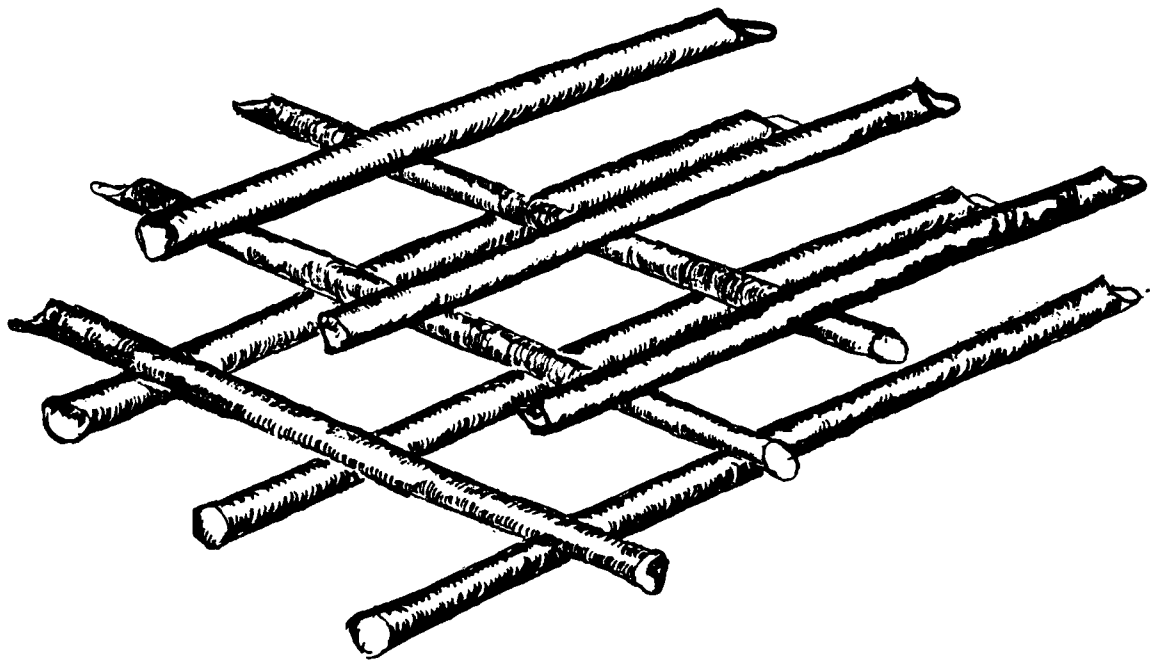
Figure 22.   0°-90° Fiber material.

3.1.2 Heat Flow Perpendicular to Both Fibers

First the case where heat flow is transverse to both directions of fibers will be considered. As with the parallel fiber arrays, a repeating unit cell can be isolated in which the temperature field is identical to, or a mirror image of that of every other unit cell. A typical unit cell is shown in Figure 23 where heat flow is along the y-axis.

Note that the two horizontal spacings are equal as this analysis is restricted to that case. Since the aspect ratio was defined as vertical spacing divided by horizontal spacing, and the horizontal spacing between fibers is $2(a)$, the aspect ratio is the quantity $b/(2a)$.

For a one-dimensional uniform temperature field, the top and bottom surfaces will be at a constant temperature. This is due to the fact that the geometric symmetry would not permit the temperature to vary on these planes since a conductivity change above the plane is exactly balanced by a conductivity change below the plane. By a similar

43
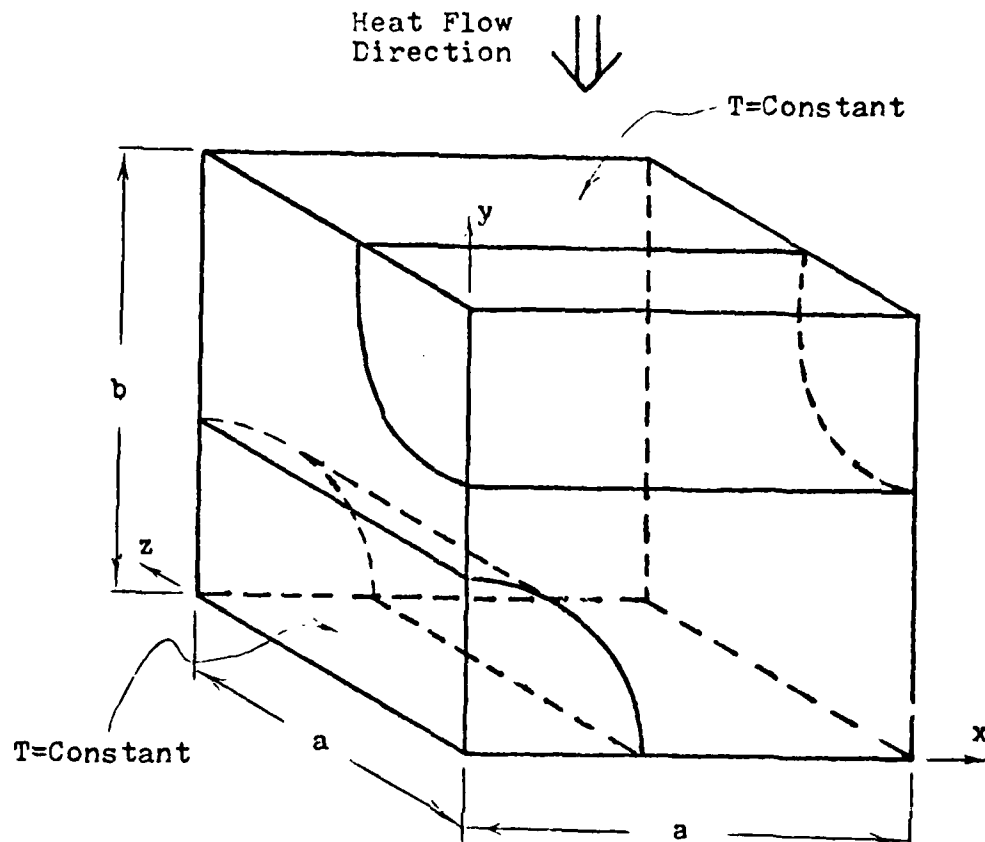
Figure 23. 0°-90° Array problem
(transverse-transverse).

reasoning, the four vertical planes of symmetry will be planes of zero
normal heat flux. Thus, the boundary conditions on these planes are
such that they can be considered perfectly insulated planes.

The obvious conditions which must be satisfied in the interior of
this unit cell are that at the fiber-matrix interfaces the temperature
in each region must be the same and the heat flux normal to the inter-
face must be the same. Therefore, a well defined boundary value problem
has been presented such that a unique temperature field exists. The
solution to this problem is presented in Section 3.2.

3.1.3 Heat Flow Perpendicular to One Fiber

Consider now the case where the one-dimensional uniform temperature
field is rotated 90 degrees so that heat flow is transverse to one
layer of fibers and axial to the adjacent layers. The same repeating
unit cell can be isolated although the boundary conditions are now
different. This cell is shown in Figure 24. It should be noted that

44
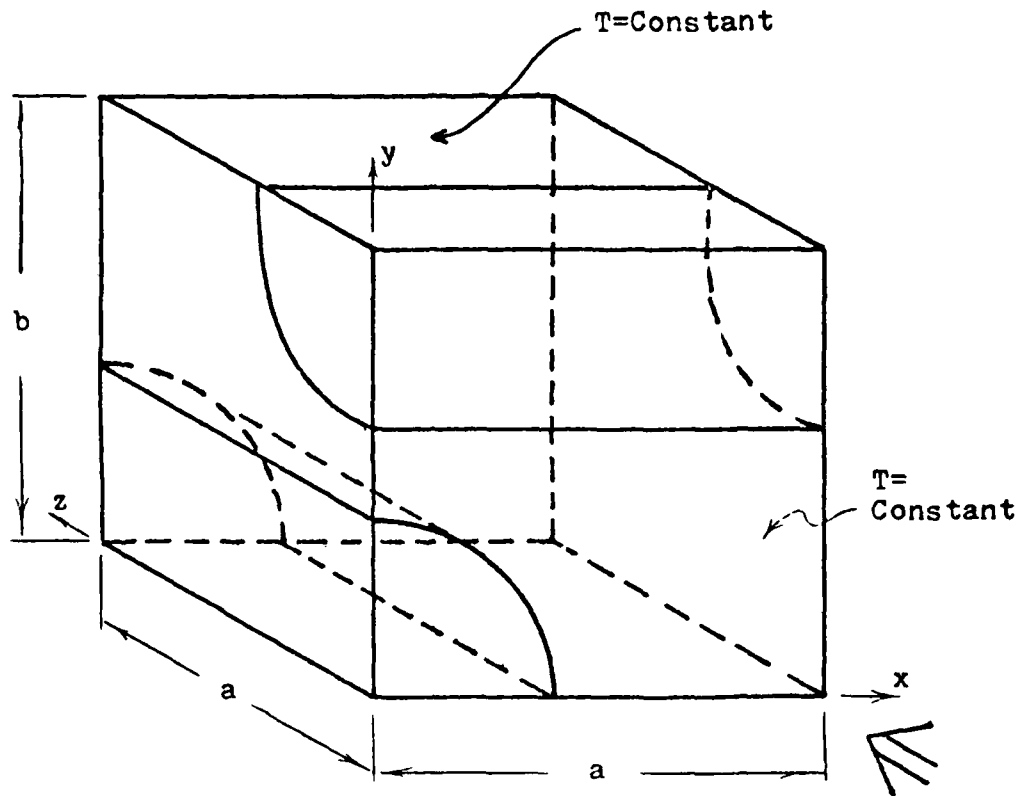
Figure 24.   0°-90° Array problem
(axial-transverse).

in this figure heat flow is along the z-axis. However, because the
horizontal spacings are the same, the case with heat flow in the x
direction is a similar problem and would therefore have the same ef-
fective conductivity.

The aspect ratio is defined as before and is equal to the quantity
b/(2a). By similar reasoning as was done for the previous case, the
boundary conditions on this unit cell can be described. On the front
and back planes which are normal to the heat flow, a constant
temperature condition exists. On the other four sides there is no
heat flow normal to the surface and they can be considered as planes
having perfect insulation on their surfaces. The interface conditions
in the interior are of course the same as for the other cases.

Thus, this constitutes another well defined boundary value problem
which can now be solved for the unique temperature field and from
which the heat flux can subsequently be determined. Then, once the
heat flux is known, the effective conductivity can be readily obtained.

3.2 GENERAL EQUATIONS

The general thermal energy balance equation for a solid material is the Fourier equation:

$$\rho c \frac{\partial T}{\partial t} = \nabla \cdot (K \nabla T) \tag{95}$$

For the problems being considered, Equation 95 simplifies to:

$$\nabla^2 T = 0 \tag{96}$$

This is commonly referred to as the Laplace equation and is valid for both the fiber and the matrix regions. This equation can be re-written in the following more conventional manner:

$$\frac{\partial^2 T}{\partial x^2} + \frac{\partial^2 T}{\partial y^2} + \frac{\partial^2 T}{\partial z^2} = 0 \tag{97}$$

In the previous cases where all the fibers were parallel to each other, a general solution was written in the form of a power series. The constants of the power series were then found by use of the boundary conditions and the temperature field was approximated by a finite number of terms.

In the problem being considered in this section, the boundary conditions are more complicated and there are two fiber-matrix interfaces that must be accounted for. This added complexity of the problem and made it impossible to satisfy all the conditions of the problem by a finite number of discrete points. Thus, an entirely different method of solution must be employed.

When it is not possible to satisfy all the boundary conditions at once by Equation 97, one must turn to a numerical method in which the original problem is broken up into a large number of smaller problems. Consider here that the large unit cell is broken up into thousands of smaller cells. Then these cells will have very simple boundary conditions which are imposed on them, and Equation 97 can be written for each one. If enough cells are used, then they can be considered to have constant temperatures throughout, and the temperatures can be solved for. The boundary conditions for the cell in question are the temperatures of the bordering cells. Because of this arrangement, the temperatures of all the cells must be solved for simultaneously and so an iterative solution is called for. This method is commonly referred to as the finite-difference method.

Consider a rectangular grid to be superimposed on the unit cell. It is layed down so that the intersection points lie at the center of the small cells, and thus the temperature at the center is the temperature of the entire cell. Thus, the Laplace equation must be satisfied for each of these points in finite-difference form. Figure 25 shows an arbitrary point as it is surrounded by its six nearest neighbors with subscripting included to identify the points.
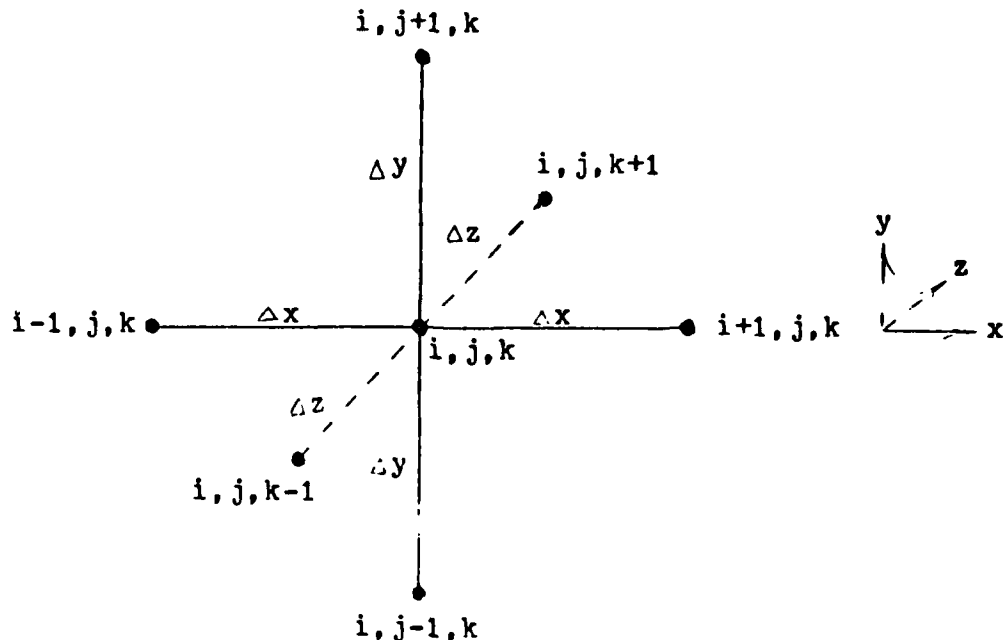
Figure 25. Interior grid point.

The first derivative of the temperature with respect to distance can now be written in terms of the finite difference in temperature between adjacent points as follows. Here, only the x direction will be considered although the other directions are of a similar form. At the position $i + \frac{1}{2}, j, k$ the first derivative can be approximated as:

$$\frac{\partial T}{\partial x}\bigg|_{i+\frac{1}{2},j,k} = \frac{T_{i+1,j,k} - T_{i,j,k}}{2\Delta x} \tag{98}$$

At the point $i - \frac{1}{2}, j, k$ the first derivative is:

$$\frac{\partial T}{\partial x}\bigg|_{i-\frac{1}{2},j,k} = \frac{T_{i,j,k} - T_{i-1,j,k}}{2\Delta x} \tag{99}$$

The second derivative at the point i,j,k can now be approximated using the above expressions as follows:

$$\left.\frac{\partial^2 T}{\partial x^2}\right|_{i,j,k} = \frac{\left.\frac{\partial T}{\partial x}\right|_{i+\frac{1}{2},j,k} - \left.\frac{\partial T}{\partial x}\right|_{i-\frac{1}{2},j,k}}{\Delta x} \tag{100}$$

$$\left.\frac{\partial^2 T}{\partial x^2}\right|_{i,j,k} = \frac{T_{i+1,j,k} + T_{i-1,j,k} - 2T_{i,j,k}}{2\Delta x} \tag{101}$$

Equation 101 is commonly referred to as a central-difference equation. By combining the similar equations for the y and z directions, the Laplace equation can now be written in finite difference form to give the following expression:

$$\frac{T_{i+1,j,k} + T_{i-1,j,k} - 2T_{i,j,k}}{2\Delta x} + \frac{T_{i,j+1,k} + T_{i,j-1,k} - 2T_{i,j,k}}{2\Delta y}$$

$$+ \frac{T_{i,j,k+1} + T_{i,j,k-1} - 2T_{i,j,k}}{2\Delta z} = 0 \tag{102}$$

If Δx, Δy, Δz are all taken to be equal, then Equation 103 below is obtained.

$$T_{i,j,k} = (T_{i+1,j,k} + T_{i-1,j,k} + T_{i,j+1,k} + T_{i,j-1,k} +$$

$$T_{i,j,k+1} + T_{i,j,k-1})/6 \tag{103}$$

Thus, the temperature of the point in question (point i,j,k) is given in terms of the temperatures of the neighboring points. Further, for the equal spacing here, it is merely the average of the temperature of these points. This is the finite-difference representation of the solution to the Laplace equation for these points.

Using Equation 103, the temperature of each point in the regular grid can be estimated using the estimated temperatures of neighboring points. By successively re-estimating the temperatures of all the points and by doing this repeatedly, the temperature values assigned to each point will converge to values such that Equation 103 is as closely satisfied as is desired at every point simultaneously. Depending on the number of points chosen, the resulting values will then approximate the actual temperature at those points in the real material. A numerical integration can then be performed using these values across

any plane through the material to determine the heat flux and thus the effective conductivity.

For the points just described which are in a uniform section of the material, the Laplace equation can be written for each one by using the boundary conditions which are the temperatures of the neighboring points. Thus, a boundary value problem has been defined with very simple boundary conditions, and a very simple solution has been obtained. There are however many points to be considered which are affected by the boundary conditions that are impressed on the large unit cell itself. These points exist at the sides of the unit cell and next to the fiber-matrix interfaces. They must reflect those boundary conditions, and by doing so the effect of those conditions will be impressed on the problem as a whole and it will be forced to converge to the unique solution for the temperature field which exists. The finite-difference representations of the solutions to the Laplace equation for these various types of boundary points are presented in Section 3.3.

3.3 BOUNDARY CONDITION EQUATIONS

There are basically three types of boundary conditions which must be impressed on the various points that are being considered in the finite-difference representation of this problem. They are the fixed temperature condition on two surfaces of the unit cell, the insulated condition of four surfaces, and the conditions at the fiber-matrix interfaces.

3.3.1 Fixed Temperature Boundary Points

The first condition of constant temperature is very easily handled by the finite-difference method. It is merely necessary to assign the desired temperature to these points and never include them in the set of points which will be used in the iteration scheme and made to satisfy the Laplace equation.

3.3.2 Insulated Boundary Points

Consider now an arrangement of these nodal points in the same regular grid such that $\Delta x = \Delta y = \Delta z$ but located at an insulated boundary (see figure 26). The position $i + 1,j,k$ is where a point would exist were it not for the fact that the insulated boundary is the edge of the unit cell and no nodal points exist outside of it. A finite difference solution to the Laplace equation is now desired for the point i,j,k taking into account the insulated condition.

Consider now the physical situation which exists in the composite material when many cells exist side by side. The insulated condition is a representation of the symmetry that exists in the temperature field across the plane. This symmetry means that the temperature at the point $i + 1,j,k$ which actually exists as a point in the adjacent

49
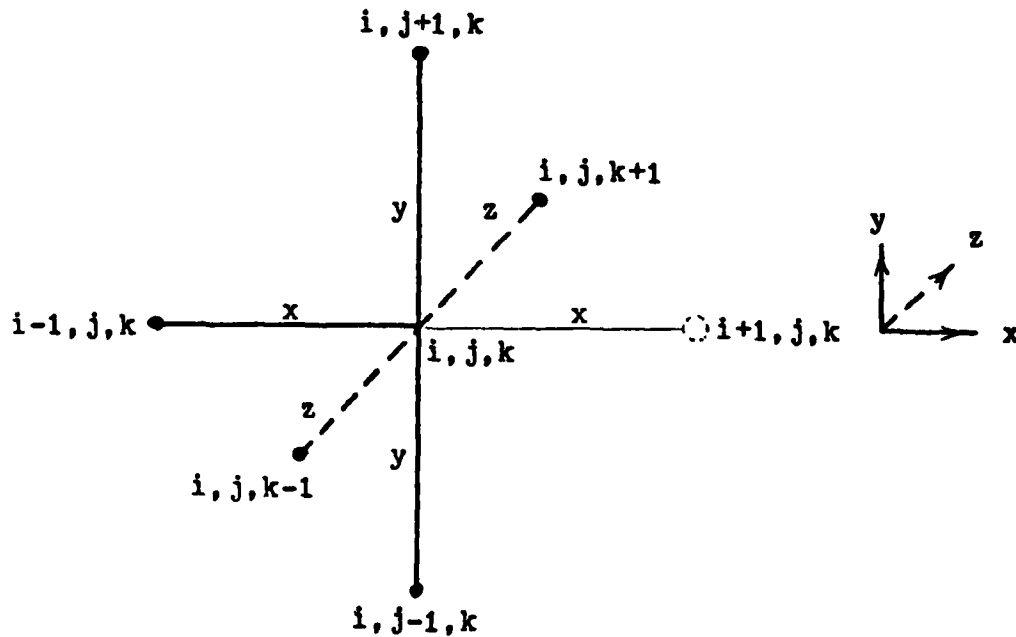
Figure 26. Insulated boundary point.

unit cell will be the same as the temperature at the point i - 1,j,k. Similarly, the temperatures of the points i + 2,j,k and i - 2,j,k will be the same so that complete symmetry between the cells is achieved.

If a node is considered to be at the point i + 1,j,k and to have the temperature of point i - 1,j,k, then the point i,j,k is seen to have six neighbors for the purpose of calculation. The general finite difference equation is then applicable here and can be written as below with the appropriate equality of temperatures introduced.

$$T_{i+1,j,k} = T_{i-1,j,k} \qquad (104)$$

$$T_{i,j,k} = (2T_{i-1,j,k} + T_{i,j+1,k} + T_{i,j-1,k} + T_{i,j,k+1} +$$

$$T_{i,j,k-1})/6 \qquad (105)$$

Similar expressions are of course obtained when the insulated condition occurs on a plane other than the x-plane.

3.3.3 Interface Points

The last condition which must be satisfied occurs at the fiber-matrix interfaces. The condition is that the temperatures in the two regions must be the same at the interface and that the heat flux normal to the interface must be the same in each region.

Consider the following section of an interface in which additional nodal points have been added where the regular grid lines cross the interface. The assumption will be made throughout this analysis the $\Delta x = \Delta y$.
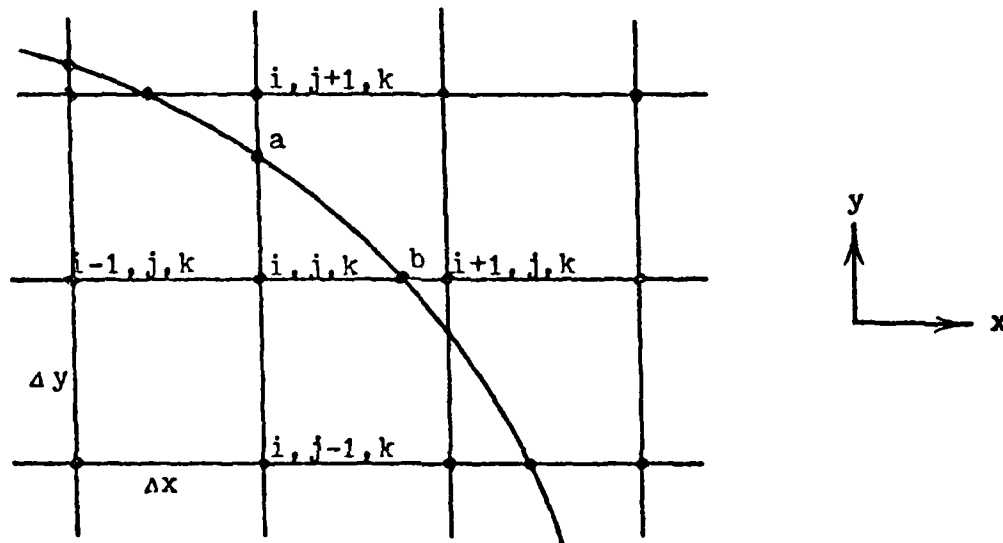
Figure 27. Interface point.

It must be kept in mind that the z direction goes into the paper, and thus similar arrangements of nodes lie in front of and behind the one shown in Figure 27.

It is desired to find the temperature at i,j,k given the temperatures of all other nodal points. The temperature must be based solely on the temperatures of those points located in the same region or on the interface. The points in the other region cannot be used because there is a change in conductivity at the interface. Thus, the temperature at i,j,k must be found from that at points i - 1,j,k; i,j-1,k; i,j,k+1; i,j,k-1; a; and b. This requires a solution to the Laplace equation when unequal spacings are involved. In this way, the temperature at the points next to the interface can be found although no effort has yet been made to satisfy the heat flux requirements at the interface. The temperatures of the points on the interface will be calculated so as to satisfy those requirements.

A finite-difference formulation of the Laplace equation using unequal spacings will now be found. The general result can then be used to find the temperatures of any points which adjoin points on the interface and thus have unequal spacings involved.

Consider the general arrangement of a nodal point with six neighbors positioned on an orthogonal set of axes in Figure 28. The notation is such that T refers to the temperature at the specified point and D refers to the distance between points. The subscripts L, R, U, D, F, and B refer to the directions left, right, up, down, forward, and backward.
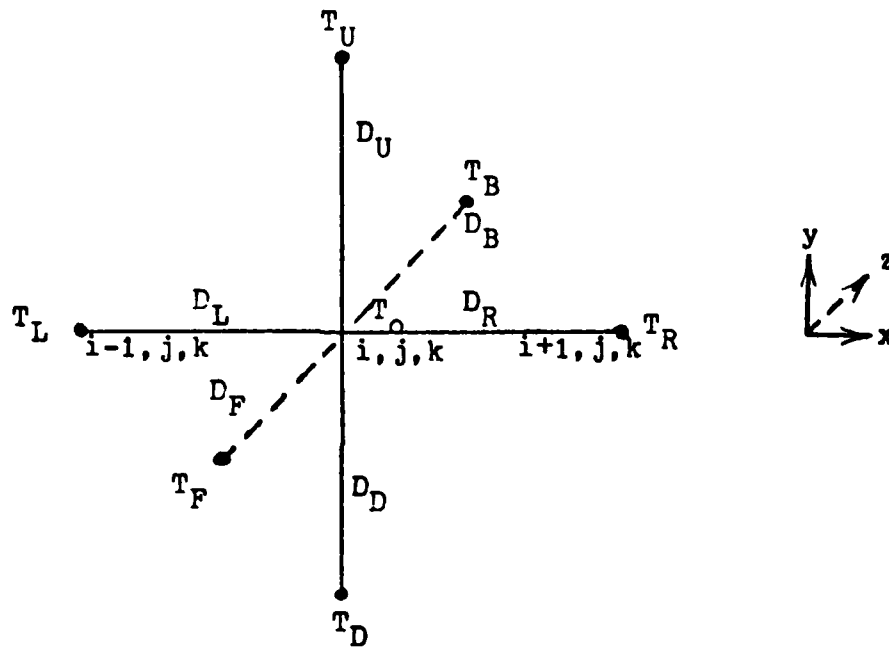
Figure 28. Point with unequal spacings.

The first derivatives at the positions $i + \frac{1}{2}, j, k$ and $i - \frac{1}{2}, j, k$ can be represented in finite-difference form by the following equations:

$$\frac{\partial T}{\partial x}\bigg|_{i+\frac{1}{2}, j, k} = \frac{T_R - T_0}{D_R} \tag{106}$$

$$\frac{\partial T}{\partial x}\bigg|_{i-\frac{1}{2}, j, k} = \frac{T_0 - T_L}{D_L} \tag{107}$$

52

From these, an expression for the second derivative with respect to x at the point i,j,k can be obtained.

$$\frac{\partial^2 T}{\partial x^2}\bigg|_{i,j,k} = \frac{\frac{\partial T}{\partial x}\big|_{i+\frac{1}{2},j,k} - \frac{\partial T}{\partial x}\big|_{i-\frac{1}{2},j,k}}{\frac{1}{2}(D_R + D_L)} \tag{108}$$

$$\frac{\partial^2 T}{\partial x^2}\bigg|_{i,j,k} = \frac{\frac{T_R - T_o}{D_R} - \frac{T_o - T_L}{D_L}}{\frac{1}{2}(D_R + D_L)} \tag{109}$$

Similar expressions can be written for the y and the z directions. These expressions can now be inserted into the Laplace equation to obtain a representation of that equation in finite-difference form.

$$\frac{\partial^2 T}{\partial x^2} + \frac{\partial^2 T}{\partial y^2} + \frac{\partial^2 T}{\partial z^2} = 0 \tag{110}$$

$$\frac{\frac{T_R - T_o}{D_R} - \frac{T_o - T_L}{D_L}}{\frac{1}{2}(D_R + D_L)} + \frac{\frac{T_U - T_o}{D_U} - \frac{T_o - T_D}{D_D}}{\frac{1}{2}(D_U + D_D)} + \frac{\frac{T_B - T_o}{D_B} - \frac{T_o - T_F}{D_F}}{\frac{1}{2}(D_B + D_F)} = 0 \tag{111}$$

This equation can then be solved to obtain an expression for T_o in terms of the six spacings and six temperatures. That solution is as follows:

$$T_o = \left\{ D_U D_D D_B D_F \frac{\left(T_R D_L + T_L D_R\right)}{\left(D_L + D_R\right)} + D_R D_L D_B D_F \frac{\left(T_U D_D + T_D D_U\right)}{\left(D_D + D_U\right)} + \right.$$
$$\left. + D_R D_L D_U D_D \frac{\left(T_B D_F + T_F D_B\right)}{\left(D_F + D_B\right)} \right\} \Bigg/ \left\{ D_U D_D D_B D_F + D_R D_L D_B D_F + D_R D_L D_U D_D \right\} \tag{112}$$

It can be noted that this equation reduces to the general equation, 103, when all of the spacings are equal. By use of this equation, all those points next to a fiber-matrix interface can now be calculated according to the governing Laplace equation.

53

The temperature at the nodal points which lie on the fiber-matrix interface can be assigned so as to satisfy the condition of equal heat glux normal to the interface in each region. This condition can be described as follows where n is the direction normal to the interface:

$$q_I = q_{II} \tag{113}$$

$$K_I \frac{\partial T_I}{\partial n} = K_{II} \frac{\partial T_{II}}{\partial n} \tag{114}$$

Refer now to the general section of an interface in Figure 29 where the temperature at point 0 is to be determined from those nearest points around it. Since the interface is in the shape of a quarter circle, the normal direction is the same as the r direction when polar coordinates are used. Using this fact and simple geometric identities, Equation 114 can be rewritten as in Equation 115.

$$K_I \left(\frac{\partial T_I}{\partial x} \frac{\partial x}{\partial r} + \frac{\partial T_I}{\partial y} \frac{\partial y}{\partial r} \right) = K_{II} \left(\frac{\partial T_{II}}{\partial x} \frac{\partial x}{\partial r} + \frac{\partial T_{II}}{\partial y} \frac{\partial y}{\partial r} \right) \tag{115}$$

It should be noted that the normal direction is perpendicular to the z direction and so derivatives with respect to the z direction do not enter into the problem. The expressions for the derivatives below (116 through 121) can now be inserted into Equation 115 to obtain a finite-difference representation of that equation. The derivatives are defined in finite-difference form by the use of the four points right, left, up, and down with respect to point 0. The point to the left is point 3, and the point to the right is point 8. The point above is point 5 and its temperature can be estimated by interpolation between points 1 and 7. The temperature of point 6 below point 0 can be estimated in a similar manner.

$$\frac{\partial T_I}{\partial x} = \frac{T_o - T_L}{D_L} \tag{116}$$

$$\frac{\partial T_I}{\partial y} = \frac{T_o - T_D}{D_D} \tag{117}$$

54
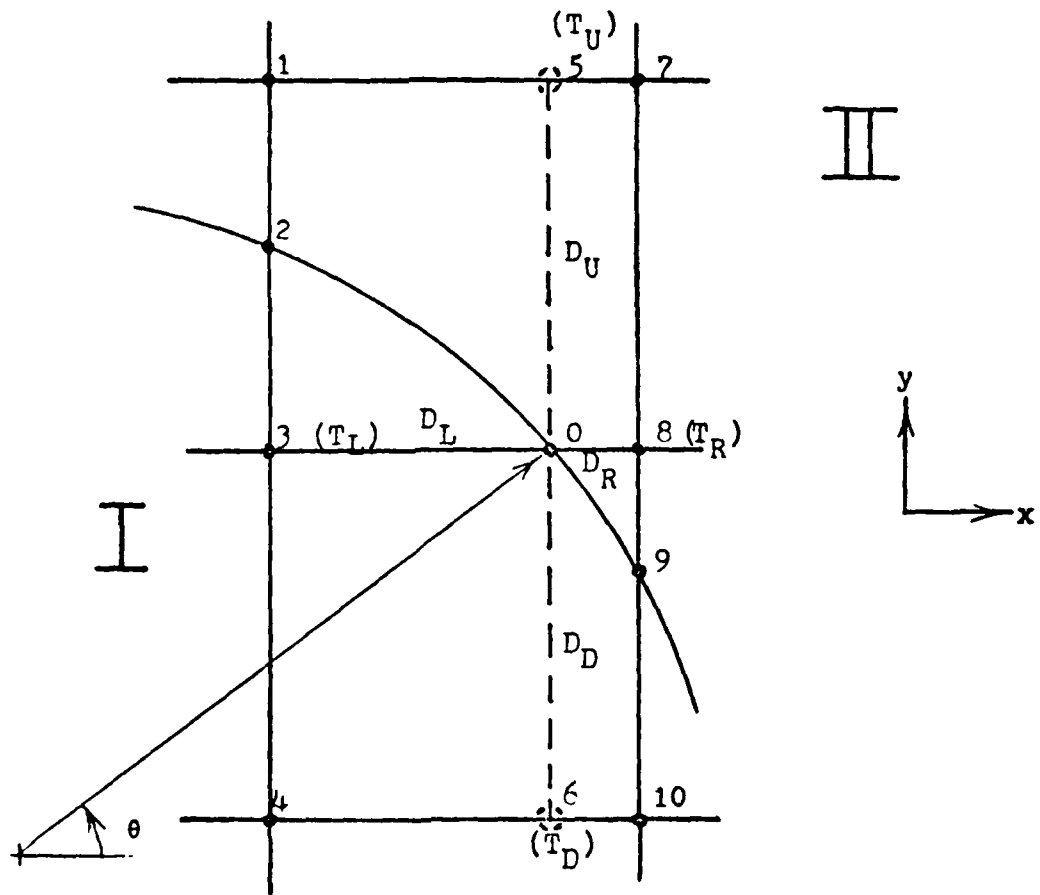
Figure 29. Interface point.

$$\frac{\partial T_{II}}{\partial x} = \frac{T_R - T_o}{D_R} \qquad (118)$$

$$\frac{\partial T_{II}}{\partial y} = \frac{T_U - T_o}{D_U} \qquad (119)$$

$$\frac{\partial x}{\partial r} = \cos(\theta) \qquad (120)$$

55

$$\frac{\partial y}{\partial r} = \sin(\theta) \tag{121}$$

$$K_I\left[\left(\frac{T_o - T_L}{D_L}\right)\cos(\theta) + \left(\frac{T_o - T_D}{D_D}\right)\sin(\theta)\right] =$$

$$K_{II}\left[\left(\frac{T_R - T_o}{D_R}\right)\cos(\theta) + \left(\frac{T_U - T_o}{D_U}\right)\sin(\theta)\right] \tag{122}$$

This finite-difference representation can now be solved for T_o to give the following expression:

$$T_o = \frac{K_I\left[\frac{T_R}{D_R}\cos(\theta) + \frac{T_U}{D_U}\sin(\theta)\right] + K_{II}\left[\frac{T_L}{D_L}\cos(\theta) + \frac{T_D}{D_D}\sin(\theta)\right]}{K_I\left[\frac{\cos(\theta)}{D_R} + \frac{\sin(\theta)}{D_U}\right] + K_{II}\left[\frac{\cos(\theta)}{D_L} + \frac{\sin(\theta)}{D_D}\right]} \tag{123}$$

By setting the point on the interface to this value, the difference in conductivities between the materials is taken into account. Thus, it can be seen that the purpose of putting these points on the interface was not to improve the accuracy of the solution, but rather it was simply to institute the boundary condition.

Thus, the basic equations governing every point in the unit cell have been developed. A computer can now be used to calculate the temperatures of all points in turn. Then by using the new temperature estimates, it can keep recalculating all the temperatures until they converge to stable values which are approximations to the temperatures at the respective points in the actual composite material.

3.4 SOLUTION METHOD

3.4.1 General Discussion

Two Fortran programs were written for the arrangement where alternate layers of fibers are crossed at 90-degree angles. They both appear in the appendix to this report.

The first case was where the heat transfer is axial to one layer of fibers and transverse to the adjacent layers of fibers. This boundary value problem was presented earlier in this section.

The program models this problem by placing a regular grid on it where $\Delta x = \Delta y = \Delta z$. The proper equation is used for each point, and

the computer succesively calculates the temperature of each point while at all times using the most recent values of temperatures at the neighboring points.

The computer keeps iterating through the entire set of points until no temperature of any point changes more than a specified value in a specified number of iterations. It is then determined that adequate convergence has been achieved. Then the computer performs a numerical integration across either the top face or the bottom face, depending on which is more accurate. These factors which affect accuracy are discussed in detail in the following section.

The heat flux is found according to the following equation which can be broken up into that part in the fiber and that part in the matrix:

$$Q = \int_{Area} (K\frac{dT}{dy})dA \qquad (124)$$

$$Q = K_I \sum_{fiber} (\frac{\Delta T}{\Delta y}) A + K_{II} \sum_{matrix} (\frac{\Delta T}{\Delta y}) A \qquad (125)$$

The value of ΔT is found by a two point derivative, or just the difference between the temperatures of the two adjacent points at one of the sides of the unit cell. These values of ΔT are summed according to Equation 125 and the appropriate values of Δy and ΔA, depending on the grid used, are inserted. The effective conductivity is then found by Equation 126 where ΔT is the macro temperature gradient across the unit cell and Δn is the unit cell dimension in the direction of the heat flow.

$$K_{eff} = Q/A(\frac{\Delta T}{\Delta n}) \qquad (126)$$

Two methods were used to reduce the calculation time of the computer. The first was to use a very coarse grid with large spacings and few points and an initial guess of constant temperature to give a quick estimate. A finer grid was then established using the values from the coarse grid as initial guesses. The computer then iterated through to the desired level of convergence. This downsizing of the grid was performed several times and resulted in a much faster program than if the final grid was used from the start with a constant temperature initial guess.

The second method of speeding up the program was by a method known as over-relaxation. Here the change in the estimate of the temperature at a point is calculated according to those equations derived previously. Then, instead of changing the temperature by that amount, it is changed by that amount plus an additional fraction of that amount.

57

The general equation (Equation 103) would be altered in the following manner, and the other equations from Section 3.3 would be altered similarly.

$$T^{new}_{i,j,k} = (T_{i+1,j,k} + T_{i-1,j,k} + T_{i,j+1,k} + T_{i,j-1,k} + T_{i,j,k+1} + T_{i,j,k-1})/6$$

(127)

$$T^{new}_{i,j,k} = \lambda(T_{i+1,j,k} + T_{i-1,j,k} + T_{i,j+1,k} + T_{i,j-1,k} + T_{i,j,k+1} + T_{i,j,k-1})/6 + (1-\lambda)T^{old}_{i,j,k}$$

(128)

Here, λ is known as the relaxation factor. If it is 1 then Equation 128 reduces to that of 127. However, if it is between 1 and 2 the temperature, $T_{i,j,k}$, will be changed by a factor of λ more than it would have otherwise. If a value of 2 or greater is used then numerical oscillations will occur, and the problem will not converge. A relaxation factor of 1.5 was found to be optimum in terms of the number of iterations needed to achieve convergence.

3.4.2 Temperature Field Symmetry

The program for the case where heat flow is transverse to both fibers works in a similar manner to the one described above. There is, however, one additional feature that can be used to reduce the amount of computer time that is needed to reach convergence. This feature is an additional plane of symmetry that exists within the unit cell.

Consider Figure 30 which is the unit cell with the midplane, which is the plane of symmetry, outlined in heavy lines. Also, shown are representative lines of constant temperature as they would appear on the front and left faces of the cell.

The temperature has been arbitrarily taken as +1 on the top surface and -1 on the bottom surface. First, consider point d on the corner of the cell. It can be seen that due to symmetry the conductivity changes above it exactly counteract the conductivity changes below it, and so it must be at a temperature of zero. The same reasoning holds for point b as well as all other points on the heavy line from d to b.
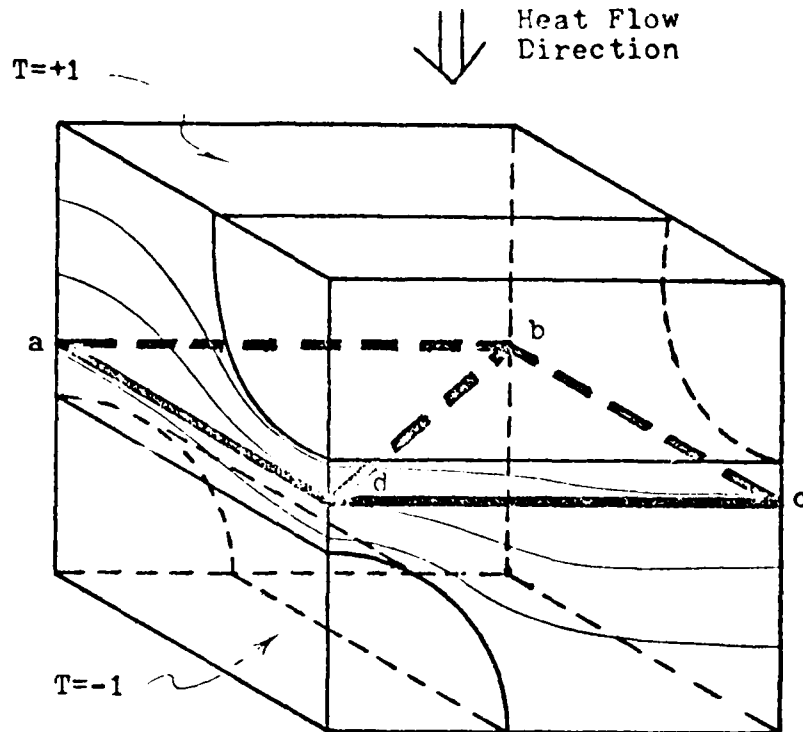
Figure 30. Symmetry for transverse-transverse heat flow.

Consider now two points which lie on the midplane and which are symmetric with respect to the line b-d. Points a and c are two such points. It can be seen that the conductivity effects above c are the same as those below a. Similarly, the conductivity effects below c are the same as those above a. Thus, a symmetry exists in the temperature field at these two points. It is such that the temperatures will be symmetric with respect to the temperature on the diagonal b-d, and this is caused by the constant temperature lines on the faces of the unit cell. Because the boundary condition temperatures were chosen in such a way so as to make the temperature on the diagonal b-d equal to zero, then temperatures of symmetric points in the midplane, such as a and c, will be negatives of each other. In addition, because of the symmetry in the temperature field at these points the heat flux will be the same, and so the value of $\partial T/\partial y$ will be the same.

Therefore, only one-half of the unit cell needs to be used to obtain a solution to this problem. The above described conditions are then required of the points on the midplane so that a completely defined boundary value problem exists. This is a very similar approach to that used to obtain a reduction of the unit area used for the staggered array with parallel fibers. The benefit of this approach is that only half as many points need to have their temperatures calculated for each interation. Thus, the computer time needed for convergence is reduced by approximately half.

59

3.5 ACCURACY

There are a number of factors which affect the accuracy of the results of these finite-difference calculations. They include the number of points used, the plane of integration for the heat flux calculation, and the criteria used to determine when adequate convergence has been achieved.

3.5.1 Number of Points

The number of points used is a critical factor affecting the accuracy of the result. In general, the result is more accurate for a larger number of points because with more points the spacings between points are smaller and so the finite-difference derivatives more closely represent the true values. Thus, one would like to use a very large number of points. However, as the number of points increases, the computer time needed increases sharply, and eventually the result could become worse due to roundoff errors. All of these differences must be added in the integration process with roundoff occurring after each operation, and with the number of points being increased, the number of calculations is increased.

A finite-difference program was written for the rectangular array of Section II to study the effects of the various parameters on the accuracy of the result. A very good result had been obtained by other methods to which the finite-difference results could be compared. As an example, all parameters were kept the same except the number of divisions along each side of the cell was varied.

TABLE 3. EFFECTS OF NUMBER OF DIVISIONS

Number of Divisions per Side	k_{eff}/k_{matrix}	Interations
10	1.6546	320
25	1.6516	1060
50	1.6459	3260
100	1.6355	7800

Accurate Value Using Other Method---$k_{eff}/k_{matrix} = 1.6520$

These data demonstrate the decrease in accuracy for a small number of divisions and for a large number of divisions. The value for a high number of divisions can, however, be greatly improved by requiring a better tolerance for each of the individual temperatures. By iterating through more times to obtain more significant figures in each of the temperature values, the effect of roundoff errors can be reduced substantially. This will of course increase the computing time even more than has already accumulated because of the large number of points. For these reasons and because some of the figures above are correct to four significant figures already, it does not seem necessary to use an

extremely large number of points. For the 3-dimensional problem considered here, 28 points per side were used along the base and the number of points used along the vertical dimension was determined by the dimensions of the specific problem.

3.5.2 Convergence Criterion

The criterion that is used to determine when the computer should stop iterating the temperatures of the points has a significant effect on the accuracy of the result. The program was designed to stop when every temperature changed no more than a specified amount in 20 iterations. A figure of 20 was chosen to guarantee that convergence really had been reached and that all the temperatures had stopped fluctuating more than the specified amount. That specified amount will now be referred to as the tolerance.

If the tolerance is too large, then when the program stops there will not be enough significant figures in the temperature values to survive the effects of roundoff in the numerical integration. If the tolerance is too small, then the time that the program runs may become excessive. The following table shows the effect of tolerance on the accuracy of the result and the number of iterations required to achieve it. This data is from the 2-dimensional finite-difference program which models the rectangular array of Section II.

TABLE 4. EFFECTS OF TOLERANCE

Tolerance	K_{eff}/K_{matrix}	Iterations
.001	1.6489	580
.0001	1.6516	1060
.00005	1.6523	1160
.00001	1.6529	1420

Accurate Value Using Other Method --- $K_{eff}/K_{matrix} = 1.6520$

For the results presented in the appendix to this report, a value of 0.0001 was used. In the table above, this provided a result accurate to four significant figures. Further, another order of magnitude improvement in the tolerance did not provide any more significant figures. Since three significant figures is adequate, a value of 0.0001 was more than satisfactory, and approximately three-figure accuracy was obtained for all the results presented in the appendix.

3.5.3 Integration Plane

The other factor that can affect the accuracy of the result is the choice of which plane to use for the numerical integration to find the heat flux. The surface planes of the unit cell are the best planes to use because either the fiber-matrix interface is not present there or

it intersects the plane at a right angle. Either way, these planes provide for the simplest numerical integration.

The accuracy of the result deteriorates as the volume ratio increases and as the ratio of fiber conductivity to matrix conductivity is increased. Consider the following 2-dimensional finite-difference representation which will show the same effects that occur with a 3-dimensional problem:
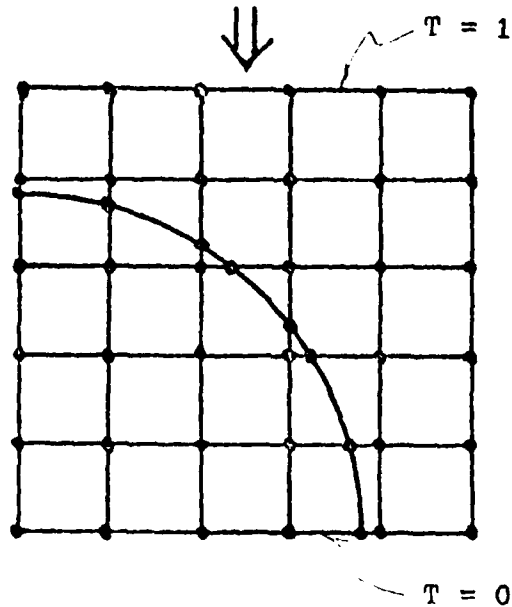
Figure 31. High volume ratio array.

In this case a high volume ratio is used, and only two nodal points exist on a line from the fiber to the edge of the unit cell. Assume also that a high conductivity ratio has been used. Because of these conditions, most of the heat flow along the top surface will occur in those nodal points on the left. On the bottom surface though, the heat flow will be spread throughout the fiber, and thus it will occur through a much higher number of points. For this case, integration across the bottom surface will give a more accurate answer than across the top surface. The result from an integration across the top will be less accurate because there are not as many points to give a description of the temperature field in that region that will contribute the most to the heat flux.

Consider now the case where there are more nodes between the fiber and the top edge in Figure 32. Again, assuming a high conductivity ratio, the heat flow will now be spread out through the top surface

much more uniformly than was the case before. Further, the integration
across the bottom will be worse. This is because most of the resistance
to the heat flow is occuring in the matrix, so most of the temperature
drop will occur at those points. Thus, the fiber will be very close to
a constant temperature. When the differences are found between the
temperatures on the bottom plane and those on the adjacent plane above
it, the differences will be very small and so roundoff errors will
reduce the accuracy. Therefore, for this case the integration is best
performed along the top edge.
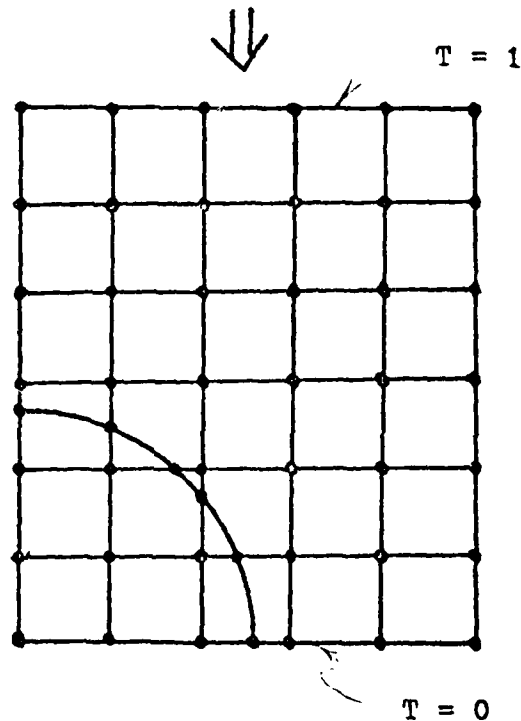
Figure 32. Low volume ratio array.

It should be noted that roundoff errors are less when the case of
only a few points between the fiber and edge is considered. This is
because a higher portion of the resistance to heat flow is then located
in the fiber region. Thus, there will be more of a temperature drop
in the fiber than when almost all of the resistance is located in the
matrix. Thus, the top surface should be used when there are a number
of nodes between the fiber and edge. Otherwise the bottom surface
should be used.

Consider now the case where heat flow is transverse to both fibers.
The unit cell that was modelled by the computer is shown below.
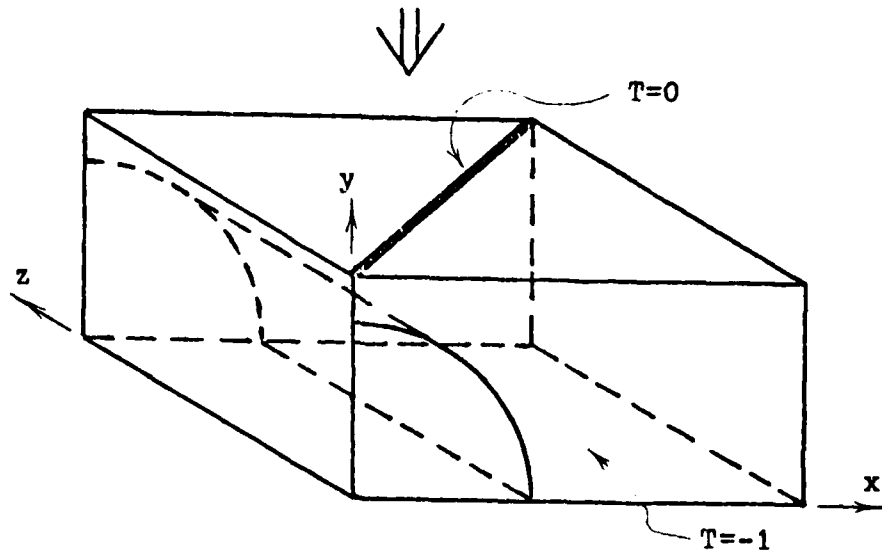
Figure 33. 0°-90° Unit cell for heat flow
transverse to both fibers.

   This problem is much like the 2-dimensional case described above.
Thus, integration should be performed according to the considerations
discussed for it.   It should be noted though that the two integration
schemes will give better agreement as the conductivity ratio is
reduced.

   Consider now the case of heat flow axial to one fiber and transverse
to the other.   The axial fiber will carry most of the heat flow for
high conductivity ratios.   Because of its orientation, the temperature
drop from front to back will be quite uniform along its length.   Also
because of this fiber's dominant effect on the heat transfer, the
temperature drop through the entire cell will tend to be more uniform
than was the case for the previous problem.   Thus, the roundoff errors
on the front face will not be as severe as they were across the bottom
face of the previous problem since the temperature differences between
adjacent points are much greater.   In addition, with this arrangement
most of the heat flux is occurring across the axial fiber which is a
much larger region than was the case for the previous problem.   This
would tend to indicate that integration across the back plane would
provide an accurate result.

   The actual results showed that both methods were accurate and that
they agreed to three significant figures for all the results presented
in the appendix to this report.   This showed that the effects of roundoff
errors on the front face were just as small as the effects of heat
transfer through a small number of points on the back face.

64

3.6 RESULTS

The results for the 0°-90° array are presented in graphical form in Appendix A. These graphs present the effective conductivities for aspect ratios of 1 and 2 (layer spacing to fiber spacing). Further, the conductivity ratio is varied from 0.1 to 100, and the volume ratio takes on the values 0.4, 0.5, 0.6, 0.65 and 0.70. The spacing between fibers in adjacent layers is taken to be the same throughout the material.

Of the three principal conductivities in these materials, two will always be the same. These are the two in which heat flow is transverse to one layer of fibers and parallel to the adjacent layers of fibers. Parametric curves for these conditions are presented in Figures A-59 and A-60. The third principal conductivity is such that the heat flow is transverse to all fibers, and these results are presented in Figures A-57 and A-58. The results from which all of these curves were drawn were accurate to at least three significant figures.

For the cases where heat flow is transverse to both layers of fibers, it can be seen that the curves level off at high conductivity ratios. This is because all of the heat must pass through a portion of the matrix, and at high conductivity ratios almost all of the resistance to heat flow is in the matrix. Thus, decreasing the resistance of the fiber still further affects the total resistance that the heat passes through very little, and the effective conductivity is increased very little.

Consider now the case where heat flow is axial to one layer of fibers and transverse to the other. There the axial fibers provide a very low resistance path for the heat flow when the conductivity ratio is high. Most of the heat flow will be within the axial fiber, and as the conductivity of that fiber is increased, the overall effective conductivity will increase by the same order of magnitude. Thus, the curves for the axial-transverse case are steeply sloped at high conductivity ratios and will approach linear lines as the additional contribution of the transverse fiber becomes negligible.

Consider the graph of transverse-transverse heat flow for an aspect ratio of 1.0. If alternate layers of fibers were turned 90 degrees the 45 degree case for the parallel fibers in a rectangular array would be obtained. In this way the 0°-90° array is similar to the rectangular array of 45 degrees.

By comparing the curves of these two cases it can be seen that they are identical for volume ratios less than or equal to 0.40. This shows that at low volume ratios the orientation of the fibers does not affect the effective conductivity significantly. As the volume ratio is increased, the curves for the 0°-90° case fall further and further below the corresponding curves for the rectangular array. This is because the

heat conduction paths in the 0°-90° array are not as straight, and the heat is forced to pass through a greater amount of resistive matrix material. When the fibers are parallel, it can pass much more directly from one fiber to the next and pass through a minimum amount of matrix material.

For the 0°-90° array with an aspect ratio of 2, alternate layers can be turned to produce a rectangular array with $\alpha = 63.4°$. Thus, these two materials are much alike. As is expected, the curves for these materials are identical for volume ratios less than 0.39 which is the highest value that is physically possible. Thus, for low volume ratios, the data for parallel fibers can be used for other orientations as the effective conductivity is almost entirely independent of the orientation.

APPENDIX A

EFFECTIVE CONDUCTIVITY GRAPHS
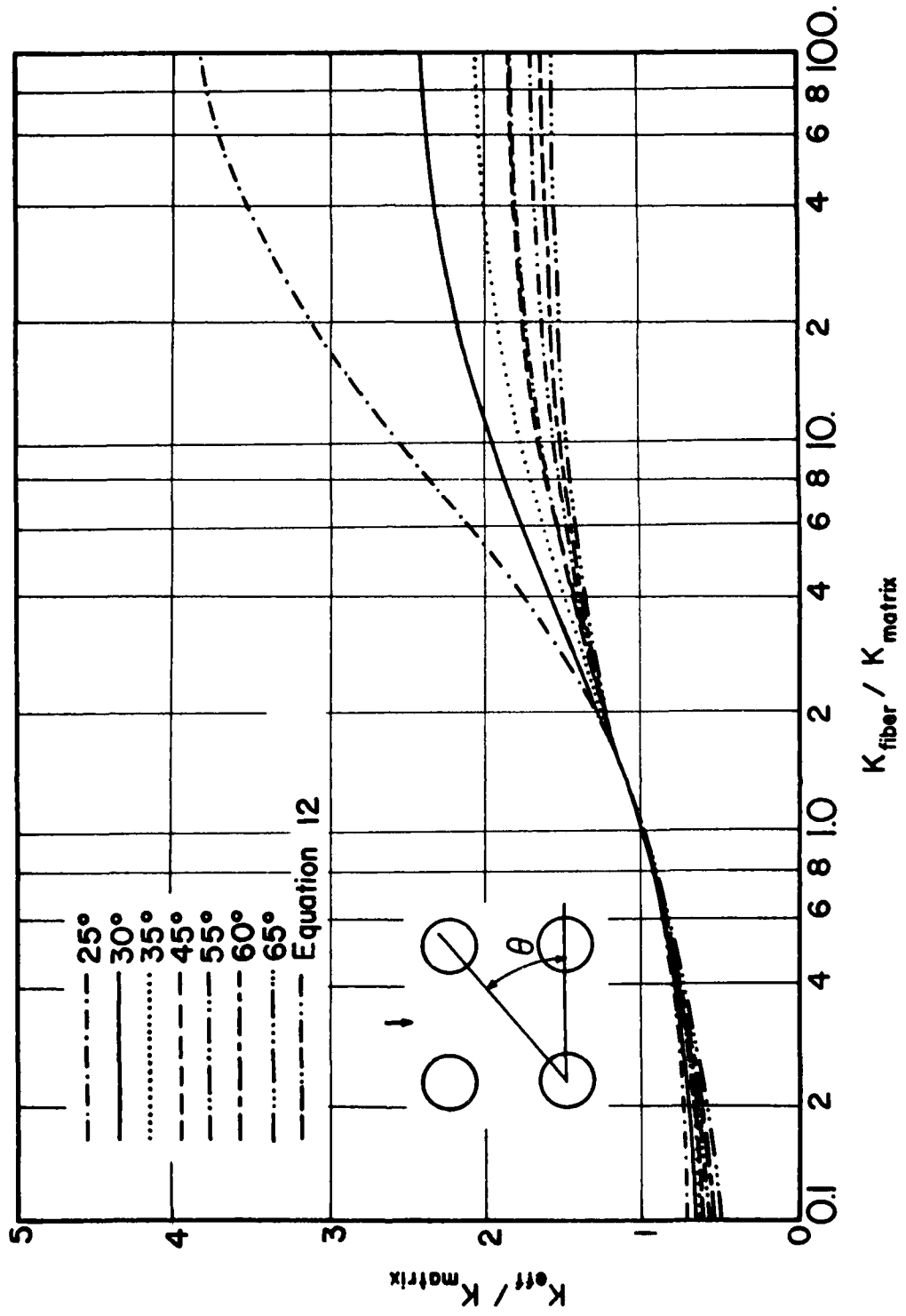
Figure A-1 Parallel Fiber (Rectangular Array) Volume Ratio = .30
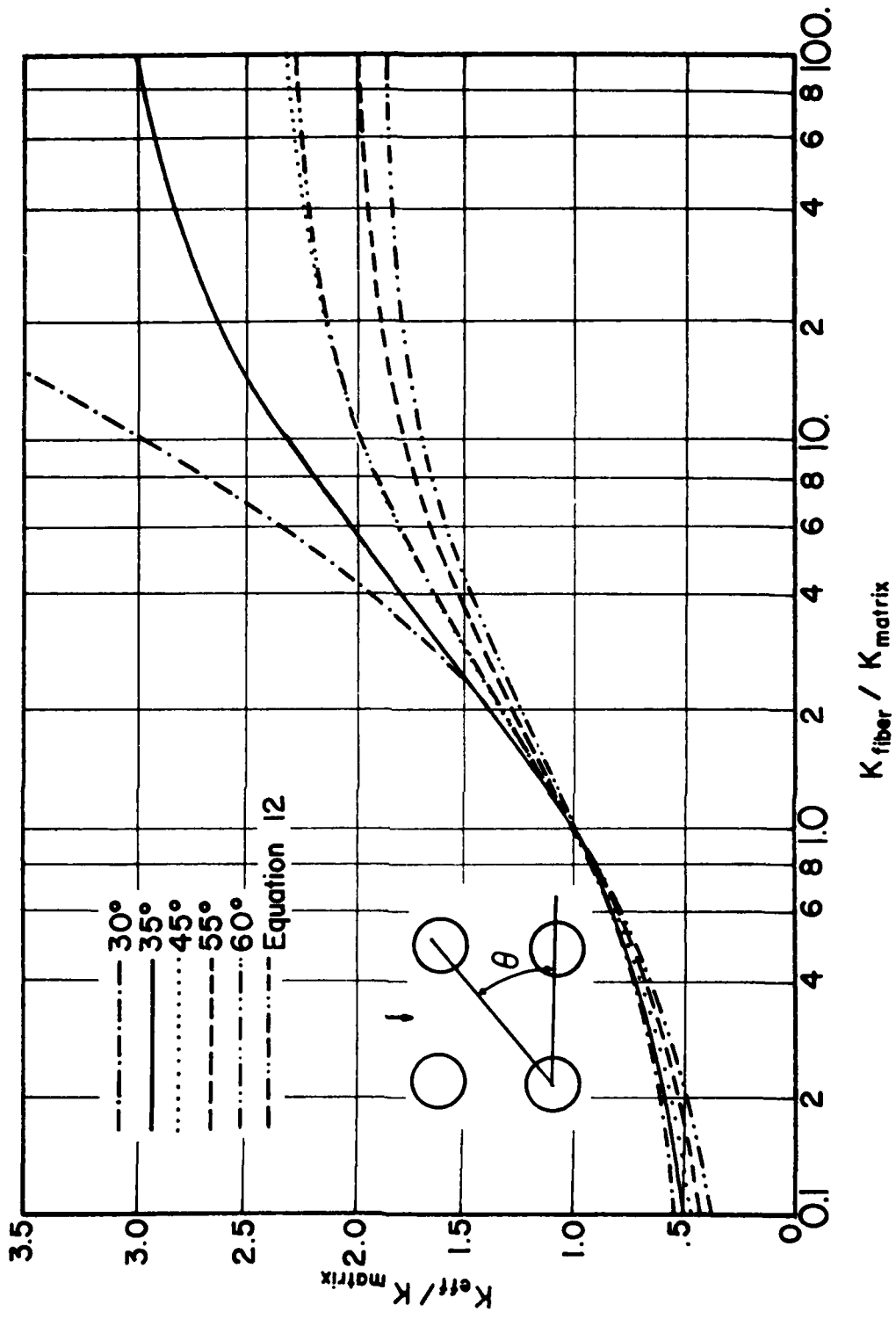
Figure A-2 Parallel Fiber (Rectangular Array) Volume Ratio = .40

69
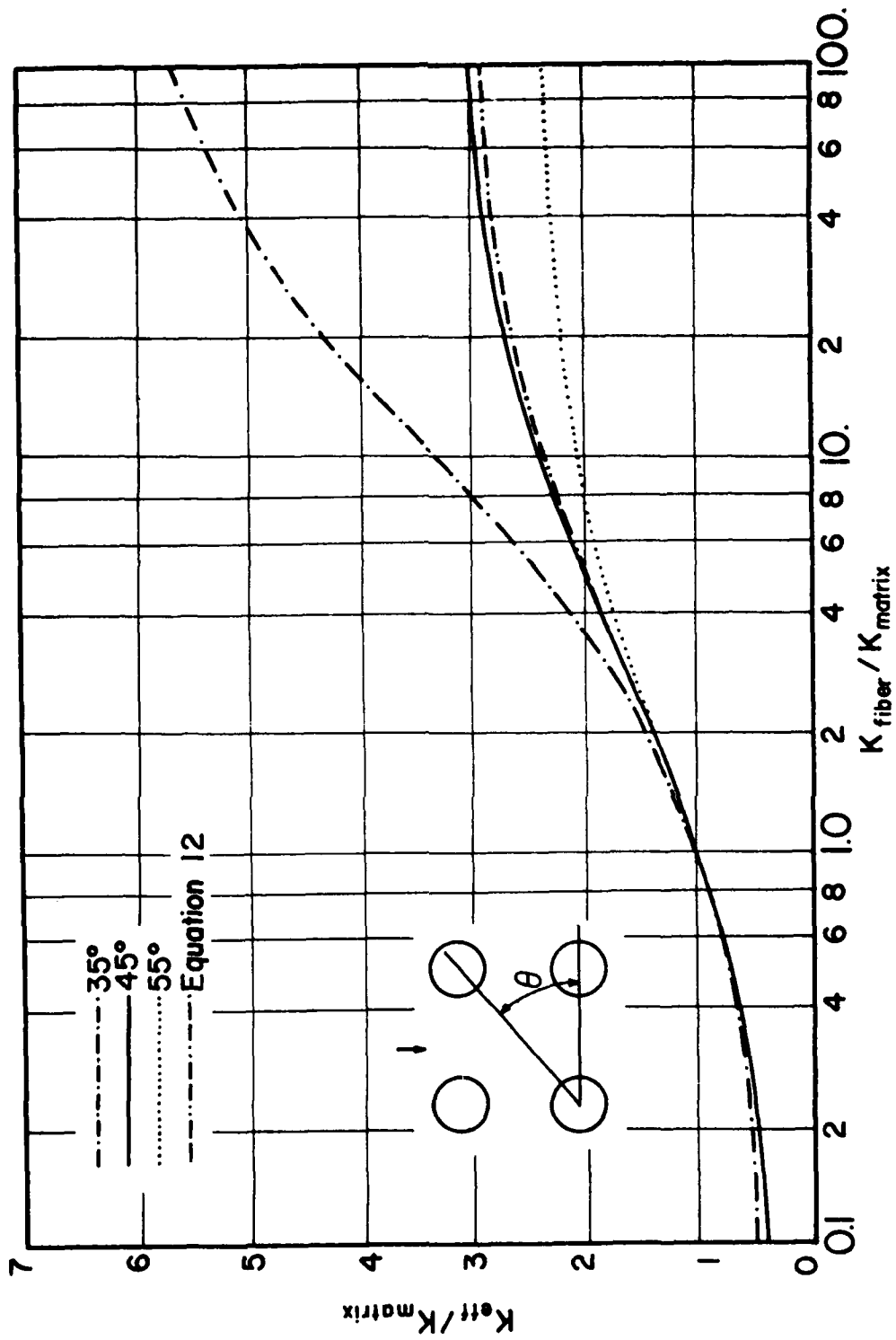
Figure A-3 Parallel Fiber (Rectangular Array) Volume Ratio = .50
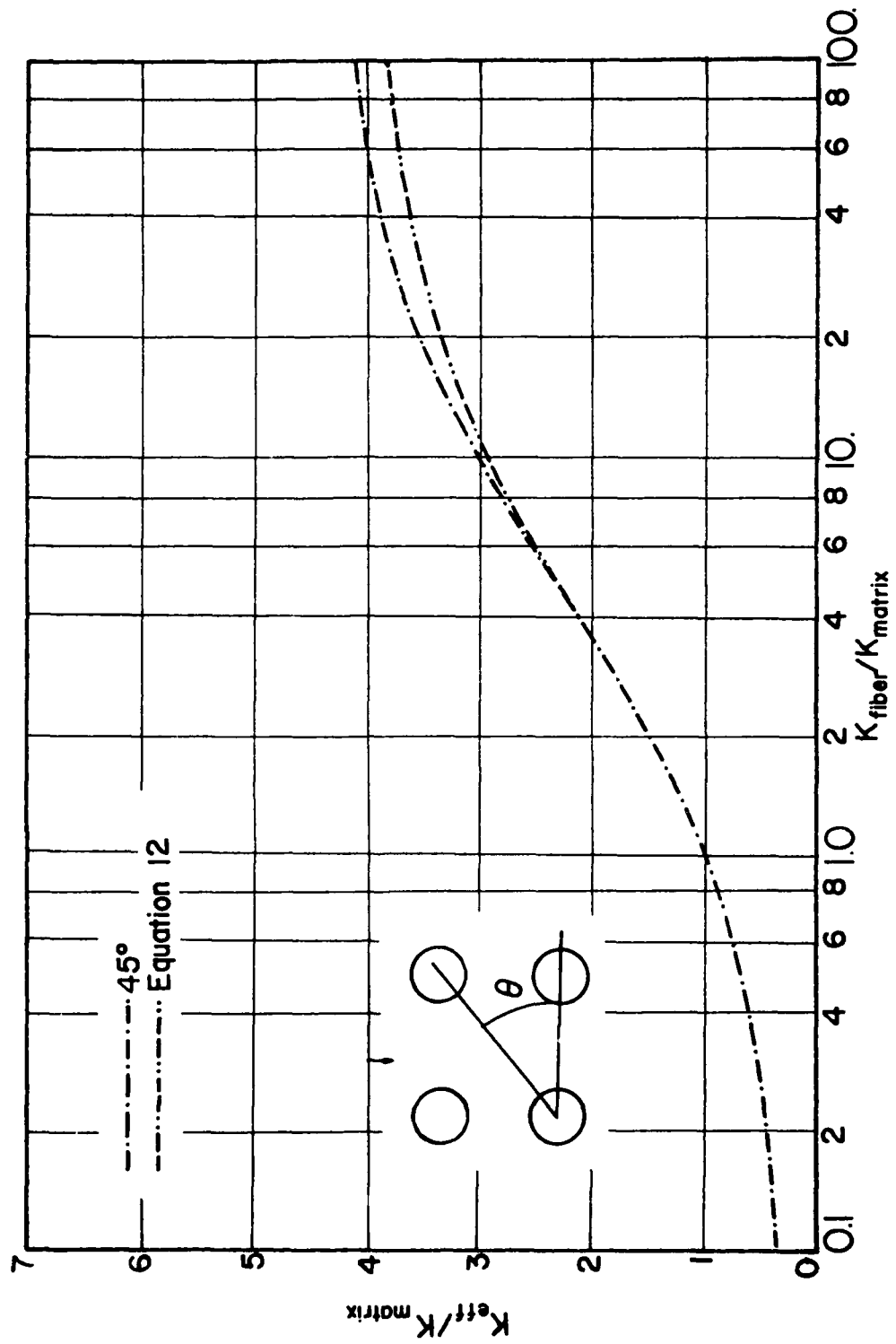
Figure A-4   Parallel Fiber (Rectangular Array) Volume Ratio = .60

71
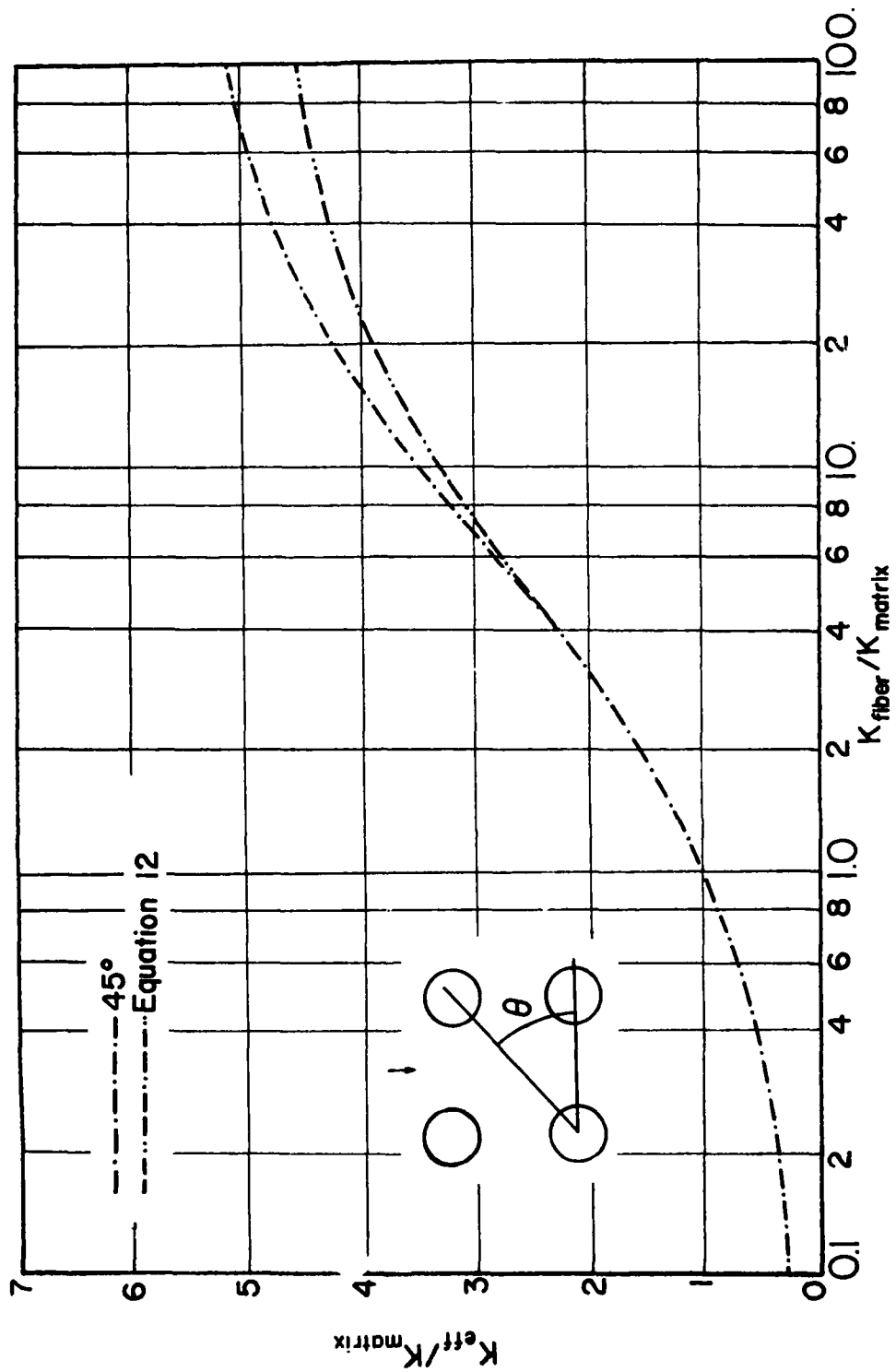
Figure A-5 Parallel Fiber (Rectangular Array) Volume Ratio = .65
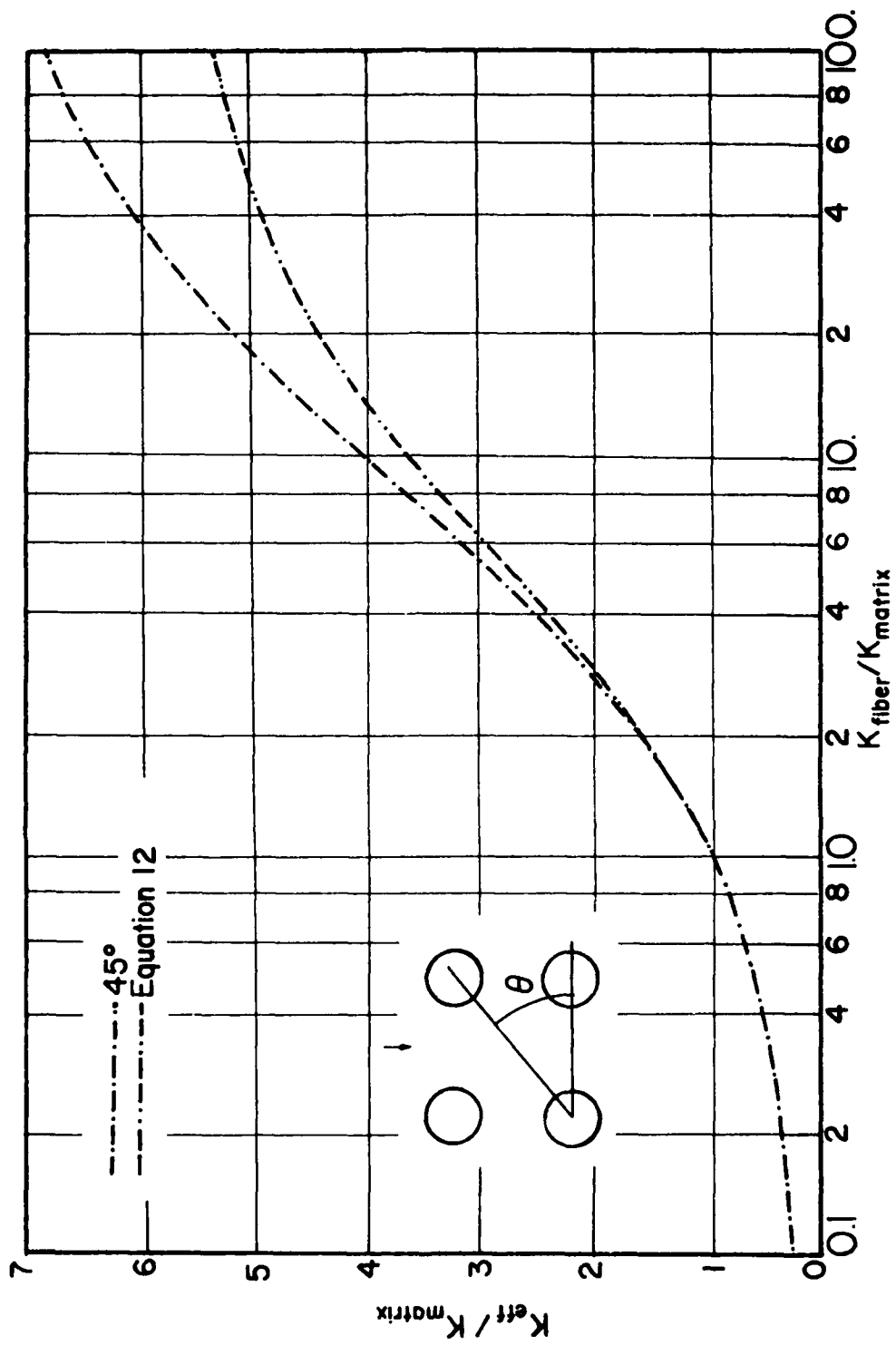
Figure A-6 Parallel Fiber (Rectangular Array) Volume Ratio = .70

K_{eff} / K_{matrix}

K_{fiber}/K_{matrix}

......45°
Equation 12

θ

73
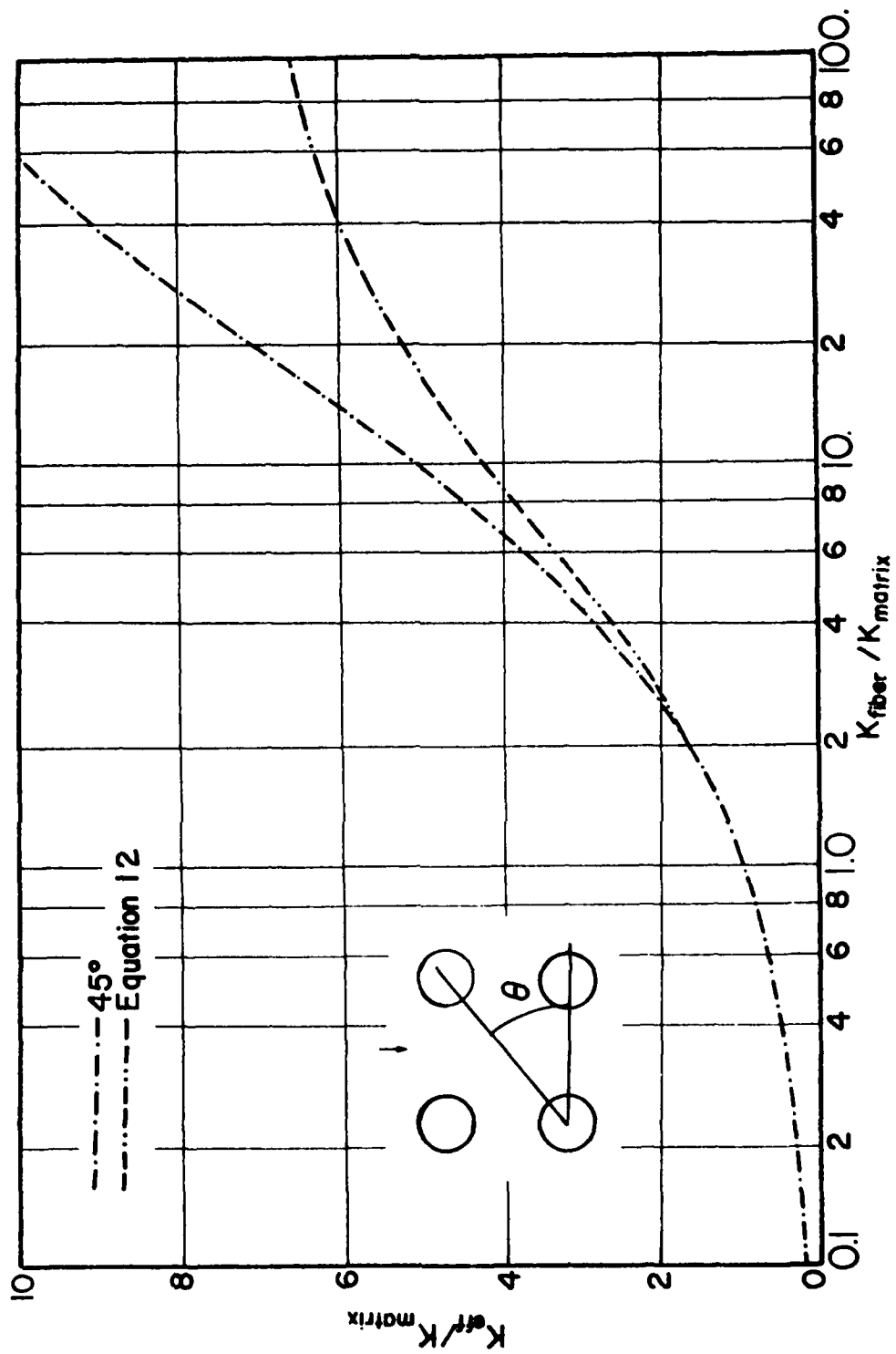
Figure A-7 Parallel Fiber (Rectangular Array) Volume Ratio = .75

74
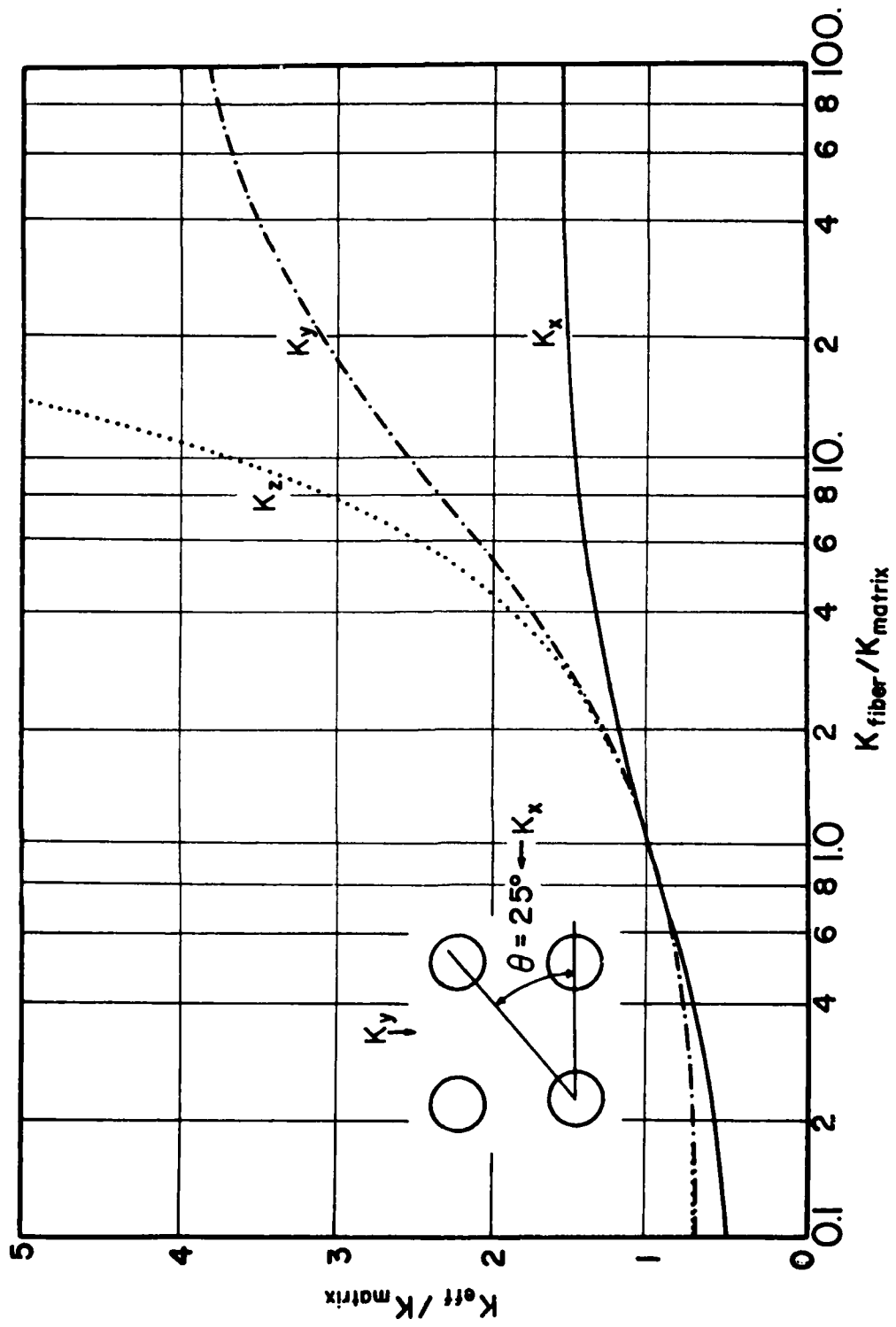
Figure A-8 Parallel Fiber (Rectangular Array) Volume Ratio = .30
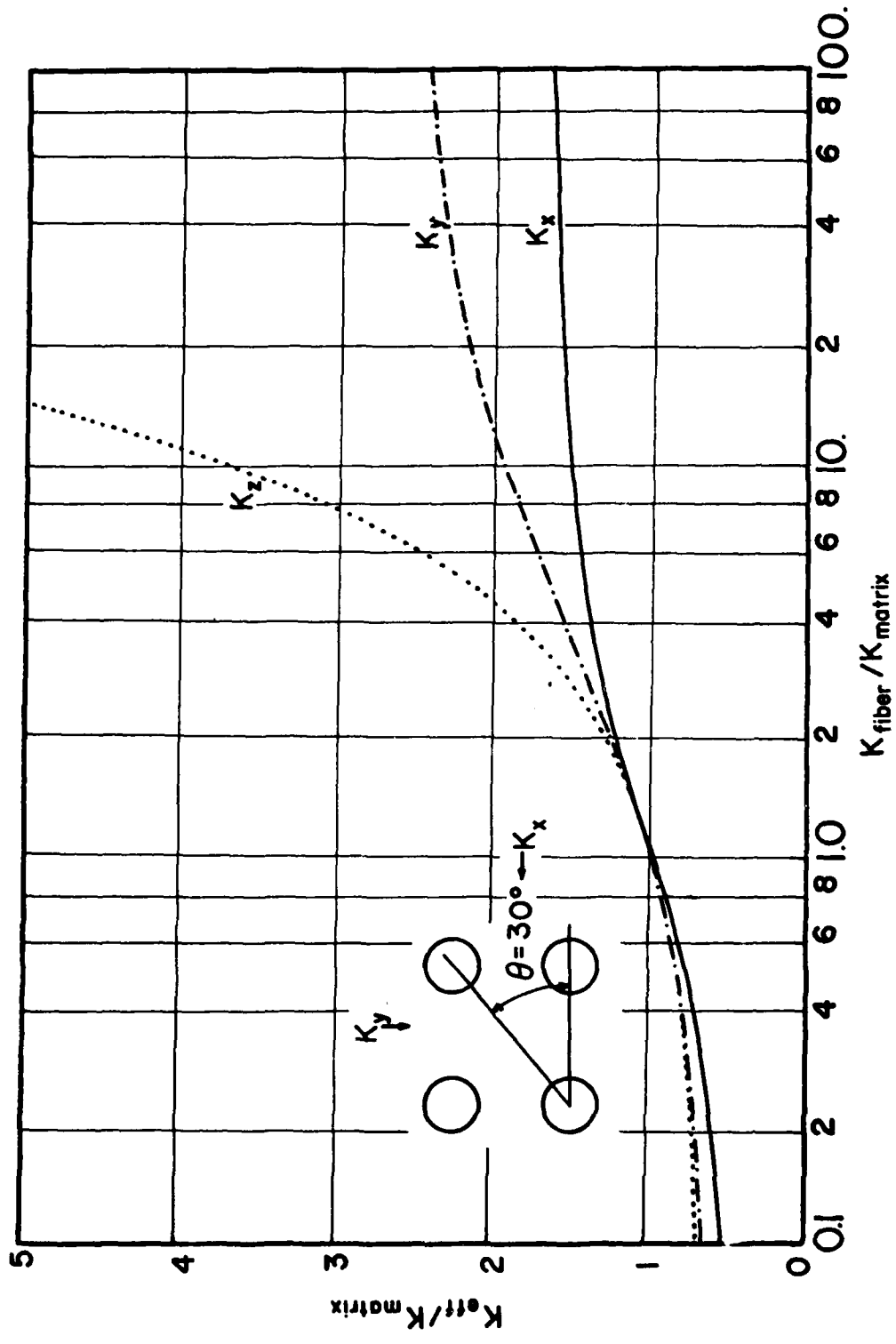
Figure A-9 Parallel Fiber (Rectangular Array) Volume Ratio = .30

76
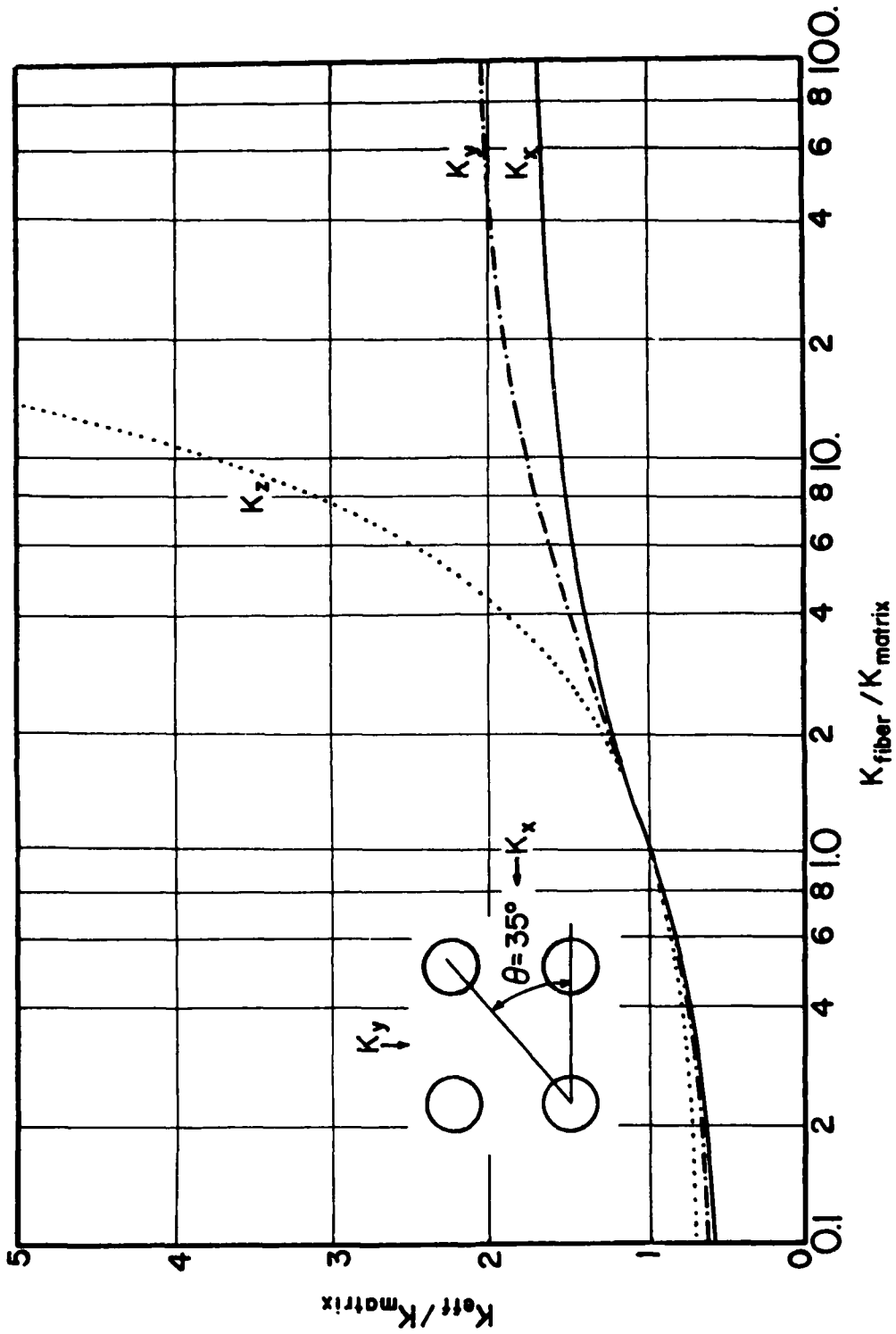
Figure A-10 Parallel Fiber (Rectangular Array) Volume Ratio = .30
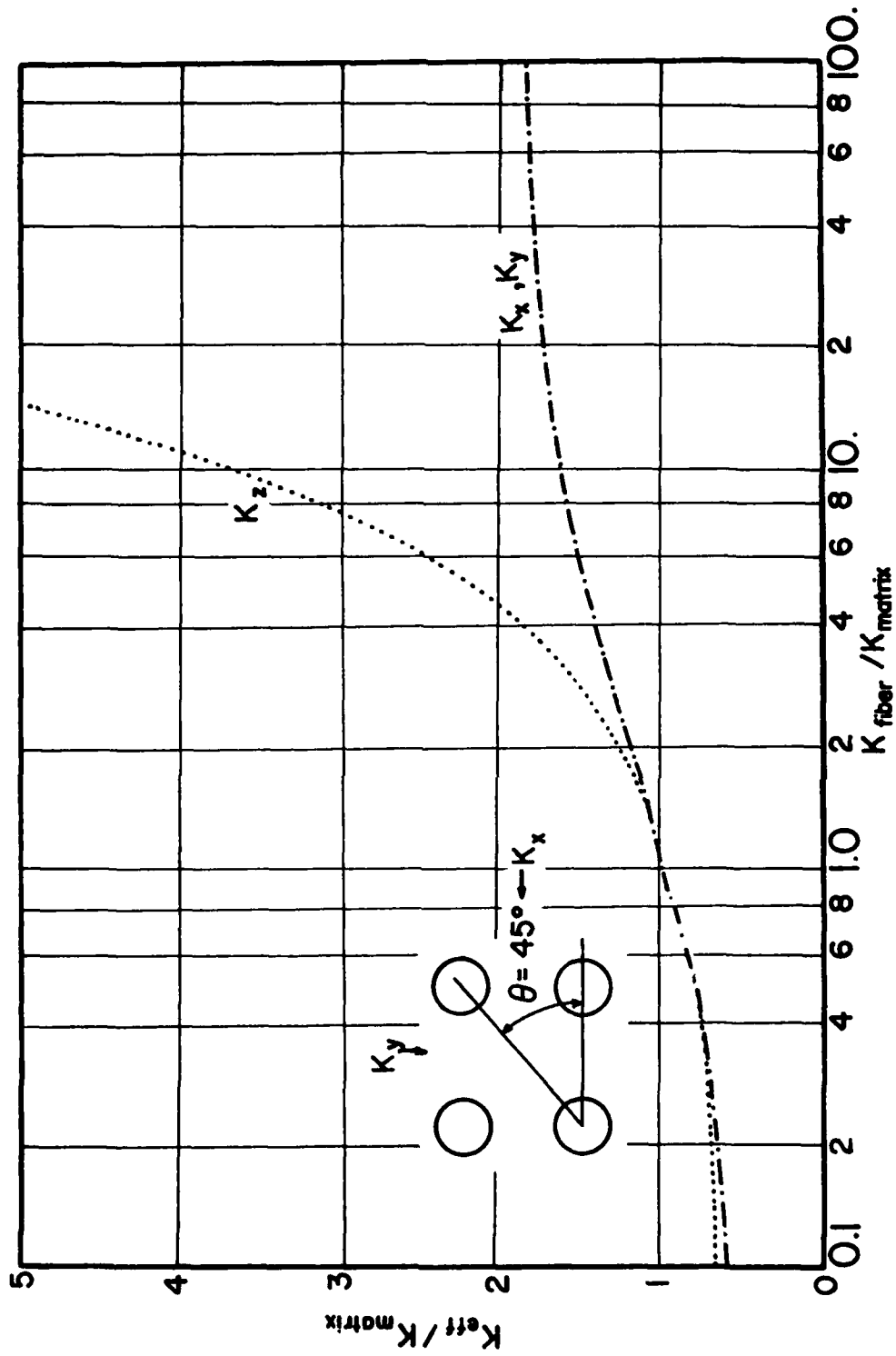
Figure A-11 Parallel Fiber (Rectangular Array) Volume Ratio = .30

78
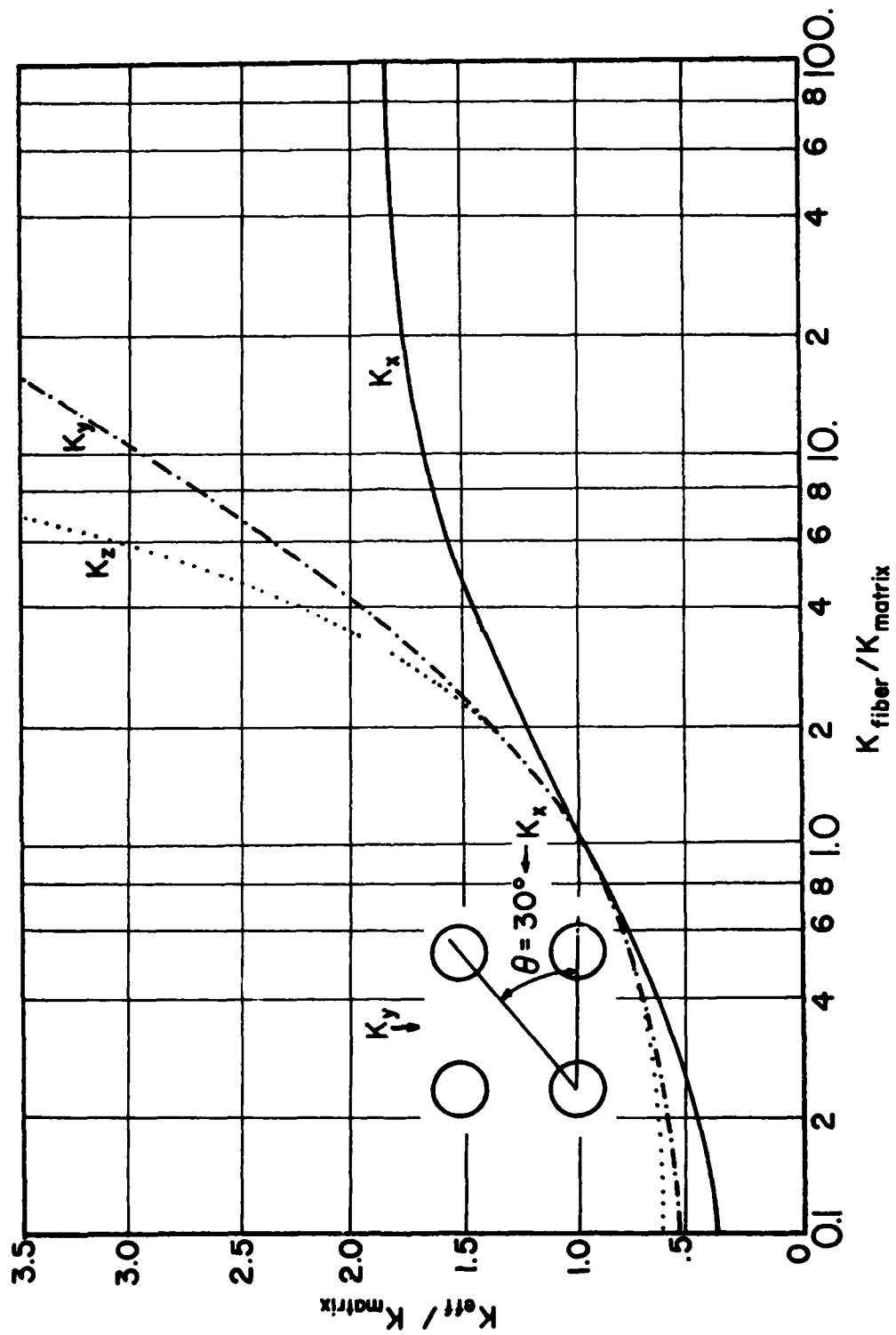
Figure A-12 Parallel Fiber (Rectangular Array) Volume Ratio = .40
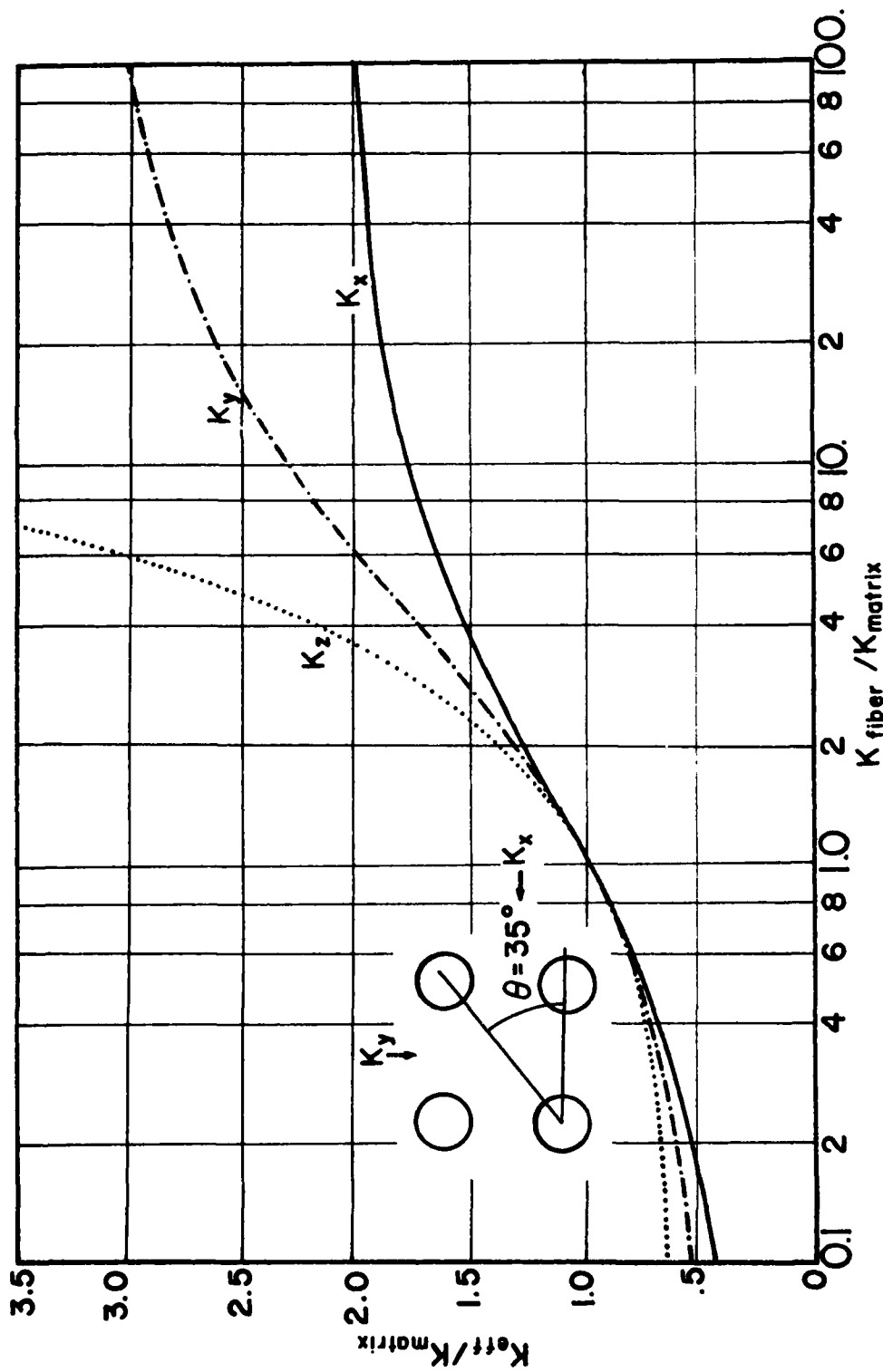
Figure A-13 Parallel Fiber (Rectangular Array) Volume Ratio = .40
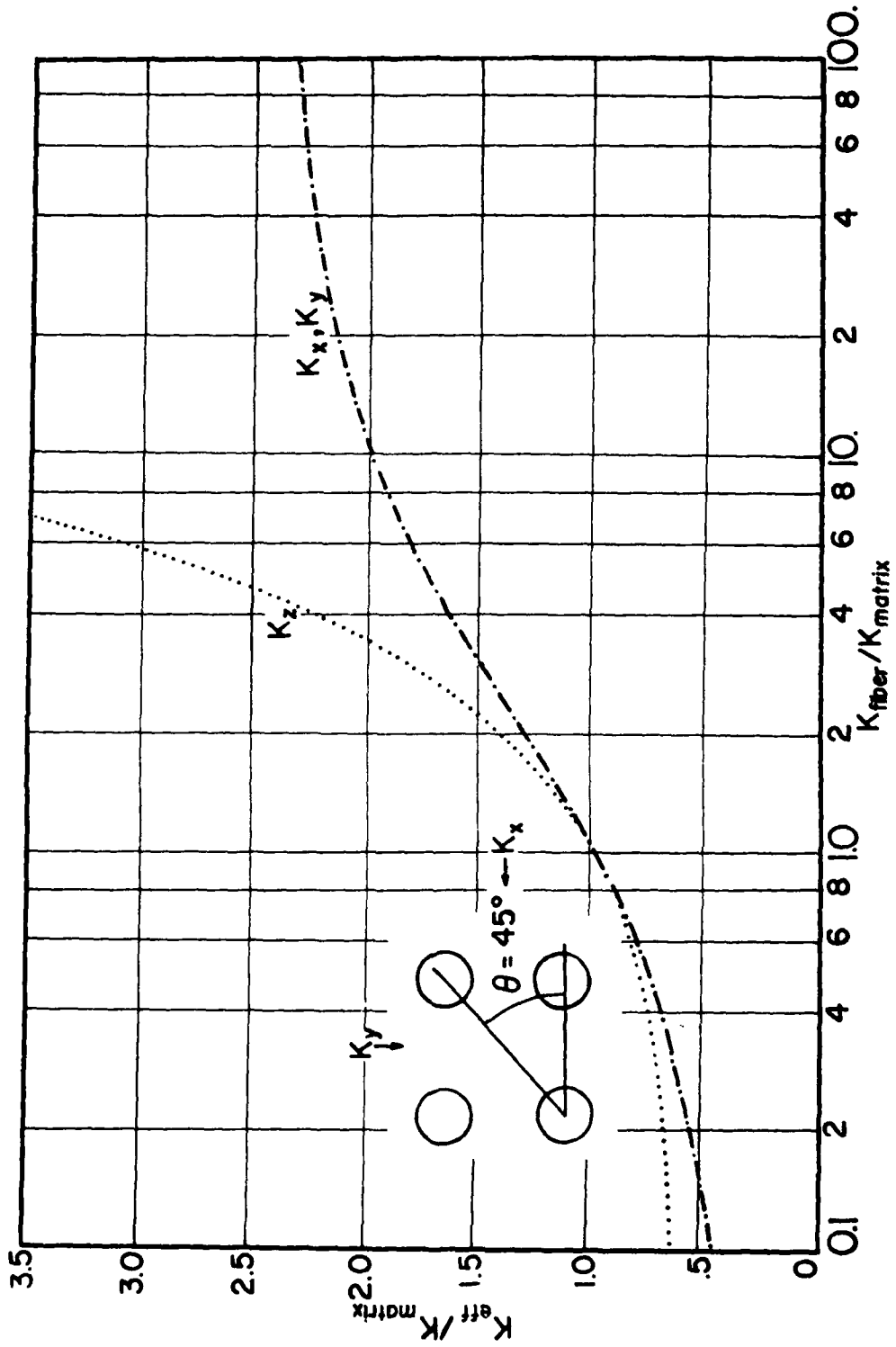
Figure A-14 Parallel Fiber (Rectangular Array) Volume Ratio = .40
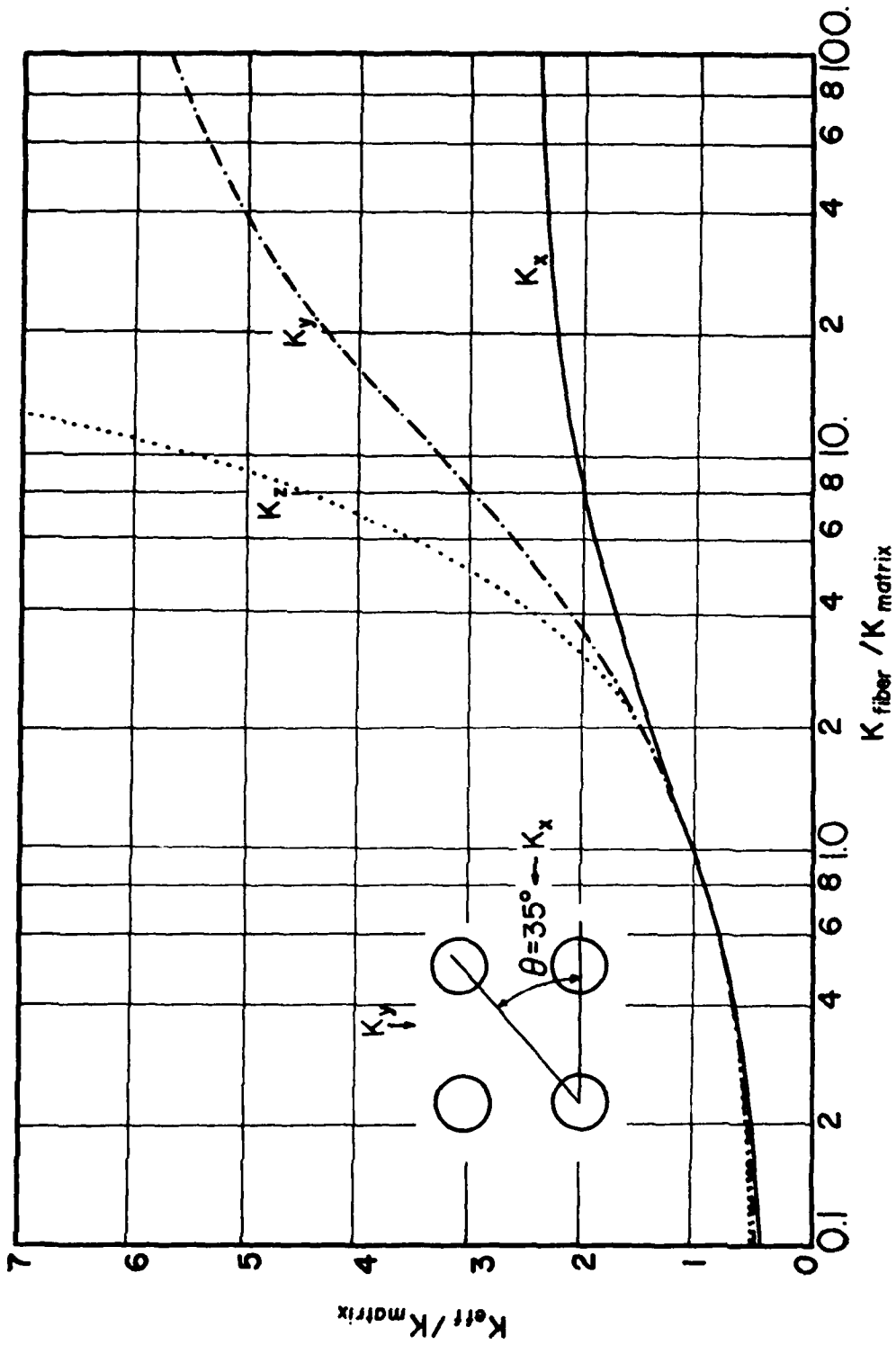
Figure A-15 Parallel Fiber (Rectangular Array) Volume Ratio = .50

82
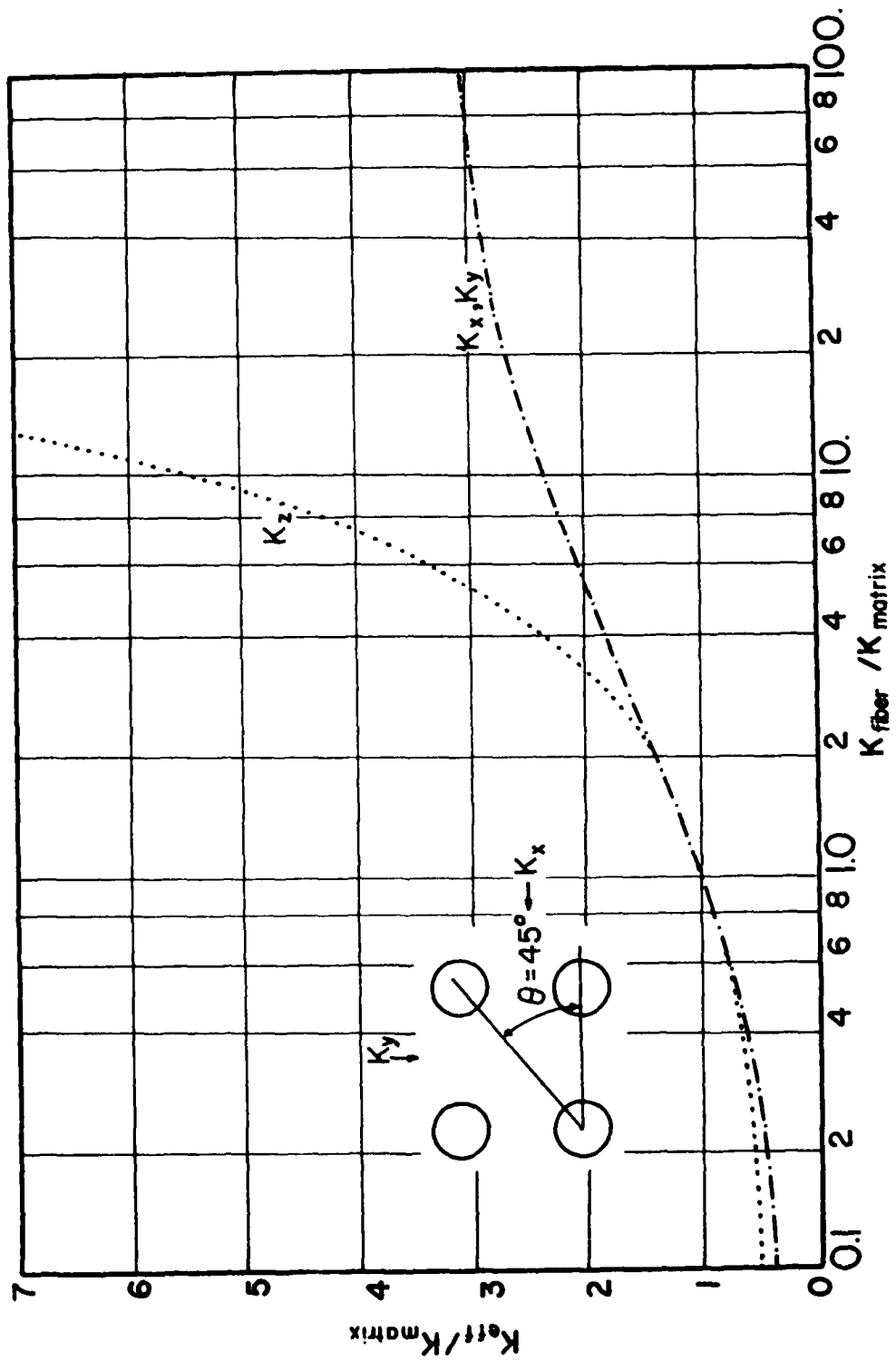
Figure A-16 Parallel Fiber (Rectangular Array) Volume Ratio = .50
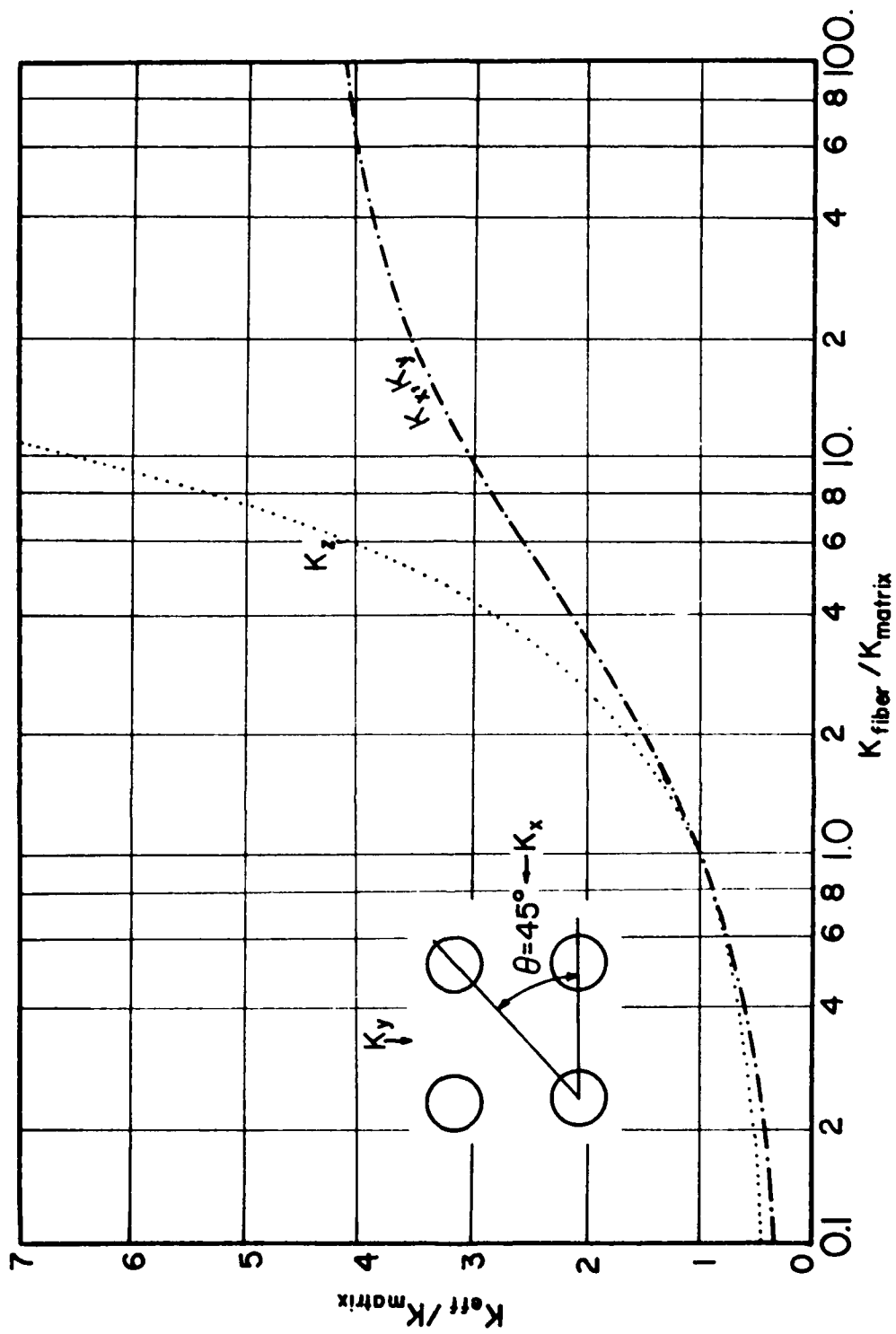
Figure A-17 Parallel Fiber (Rectangular Array) Volume Ratio = .60
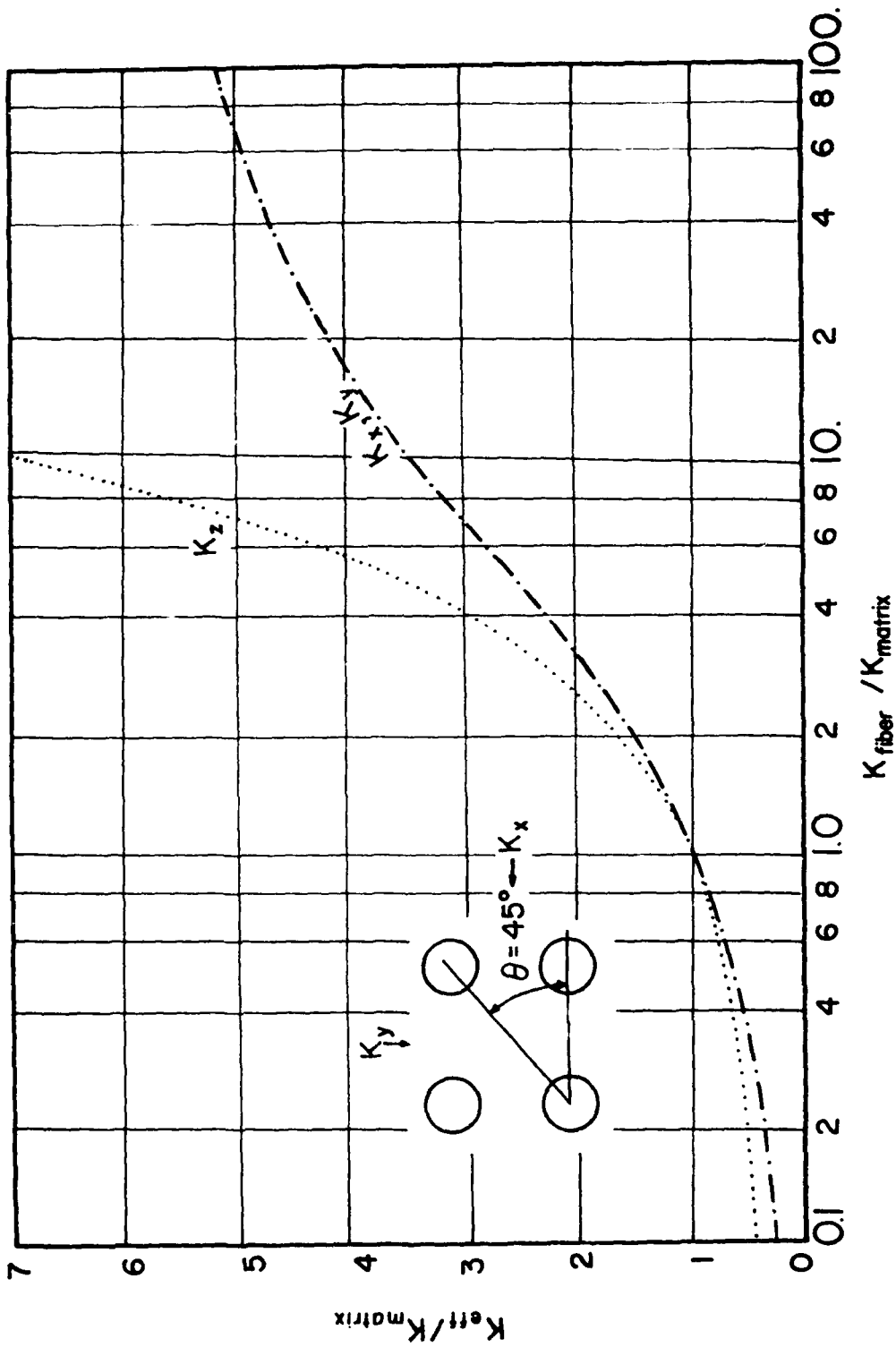
Figure A-18 Parallel Fiber (Rectangular Array) Volume Ratio = .65
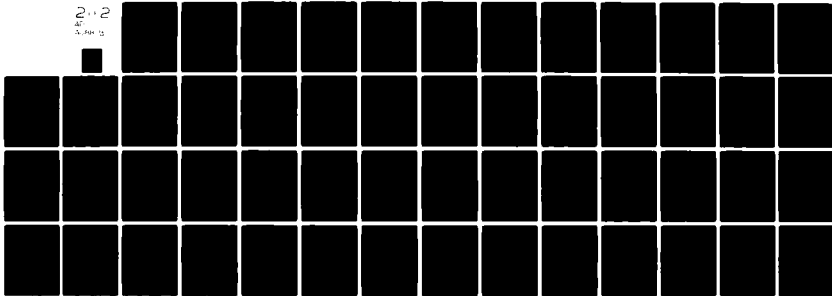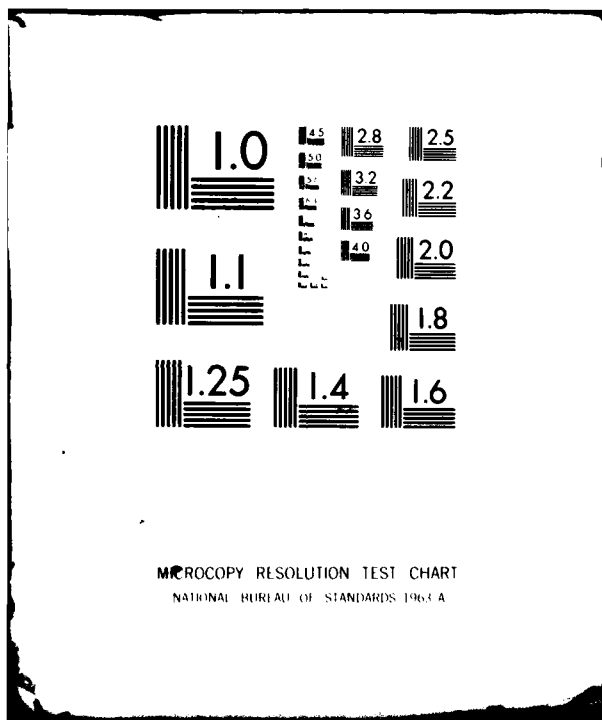
MICROCOPY RESOLUTION TEST CHART
NATIONAL BUREAU OF STANDARDS 1963 A
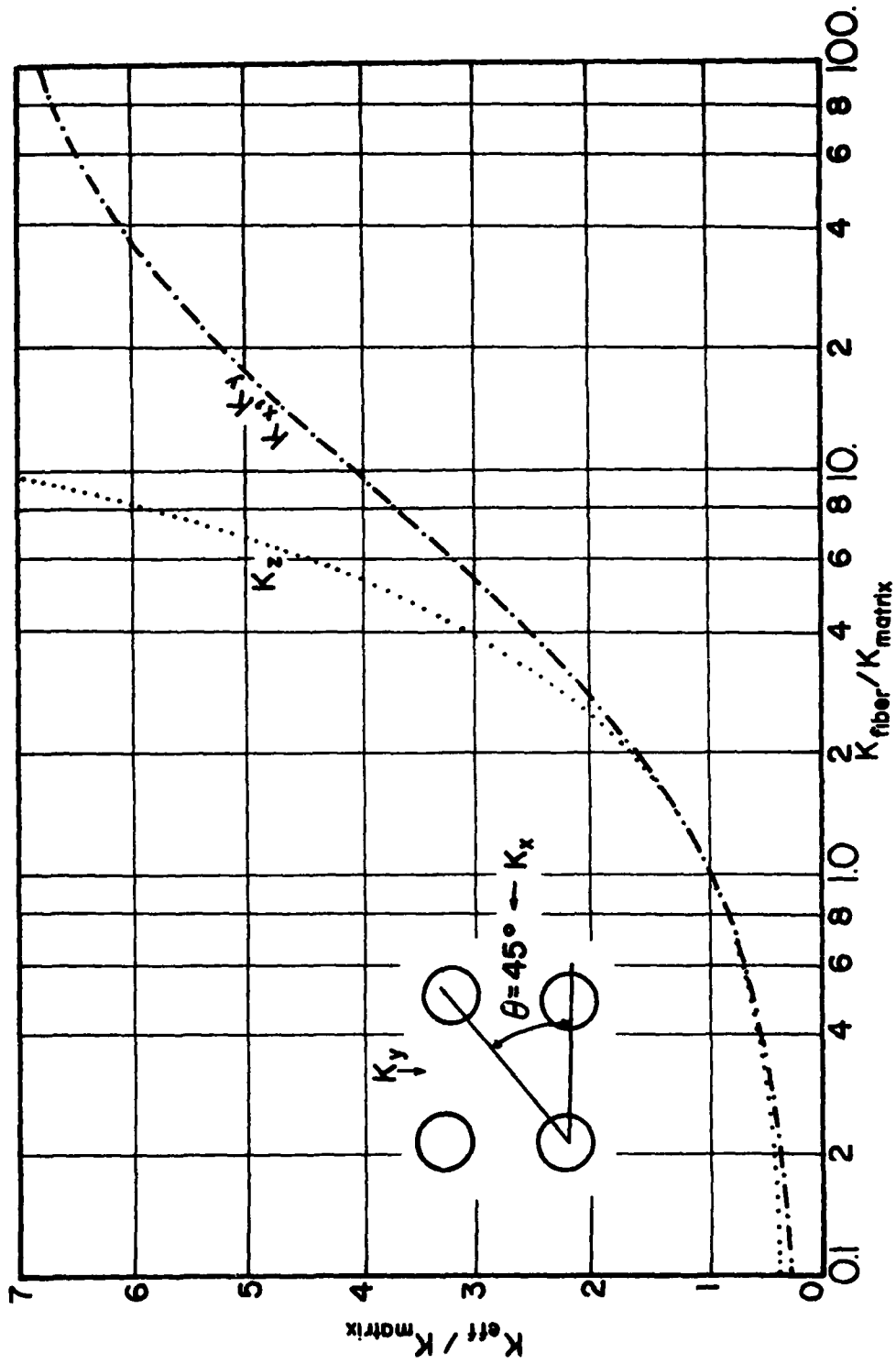
Figure A-19 Parallel Fiber (Rectangular Array) Volume Ratio .70

86
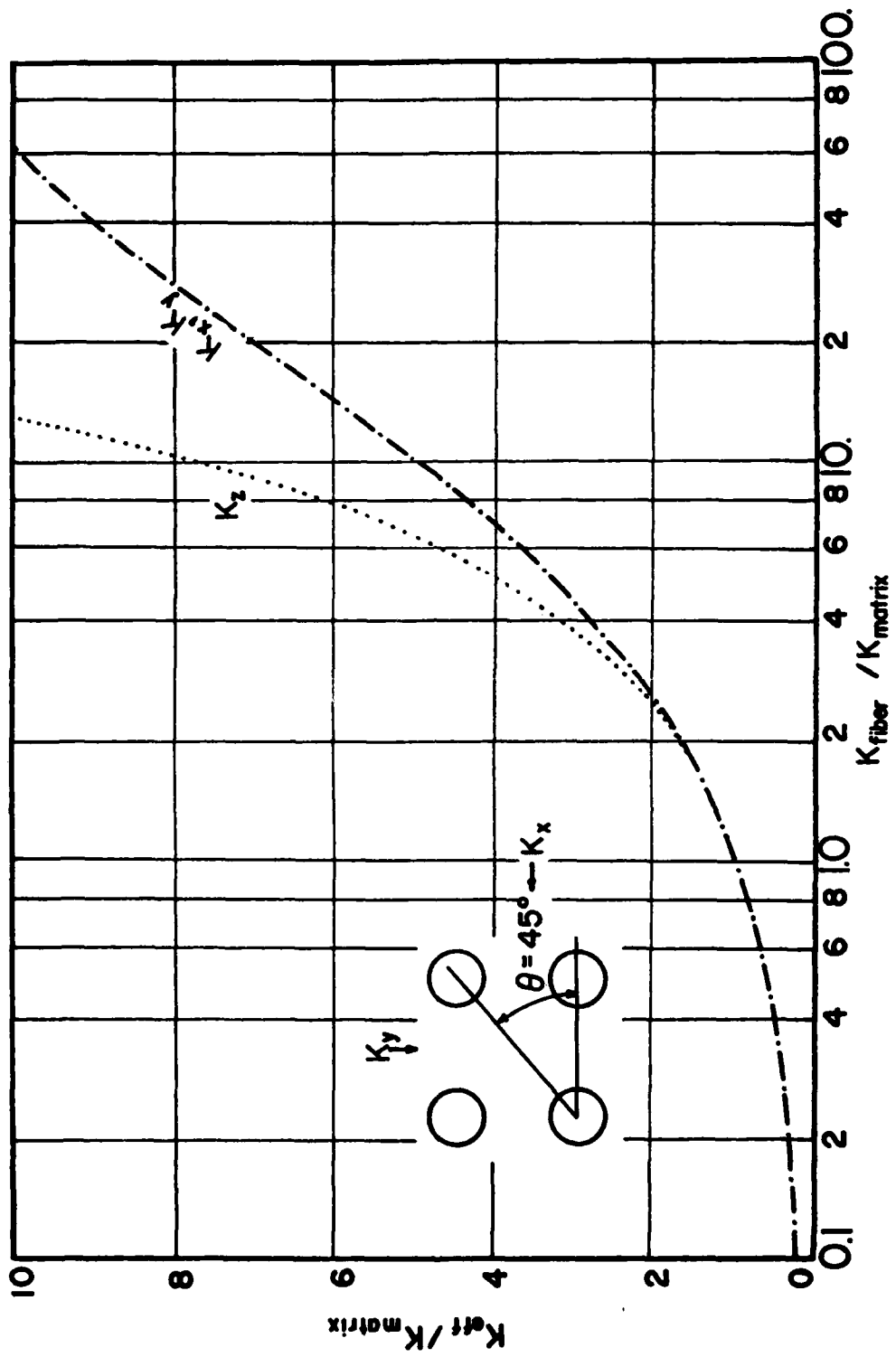
Figure A-20 Parallel Fiber (Rectangular Array) Volume Ratio = .75
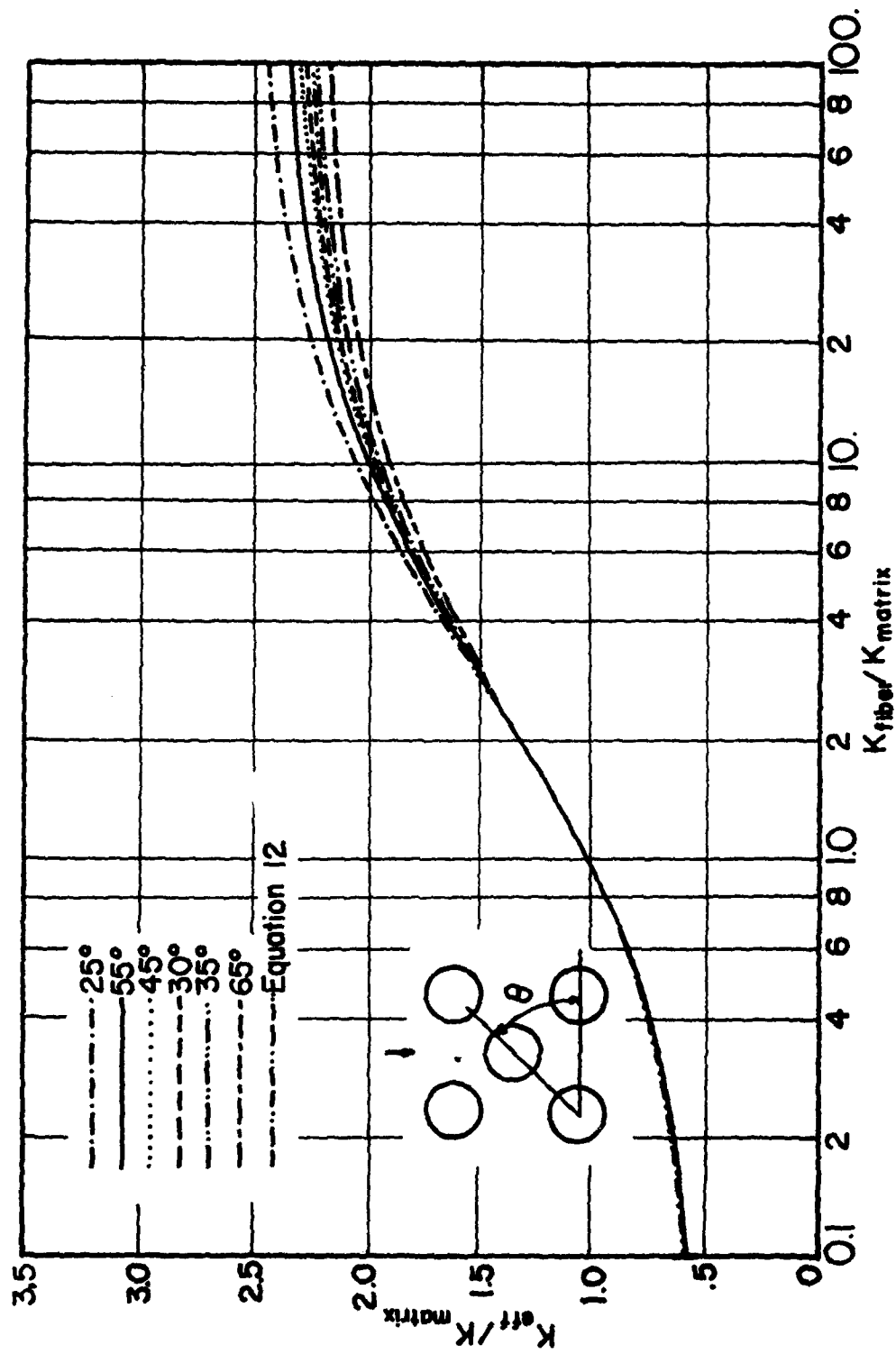
Figure A-21 Parallel riber (Staggered Array) Volume Ratio = .50
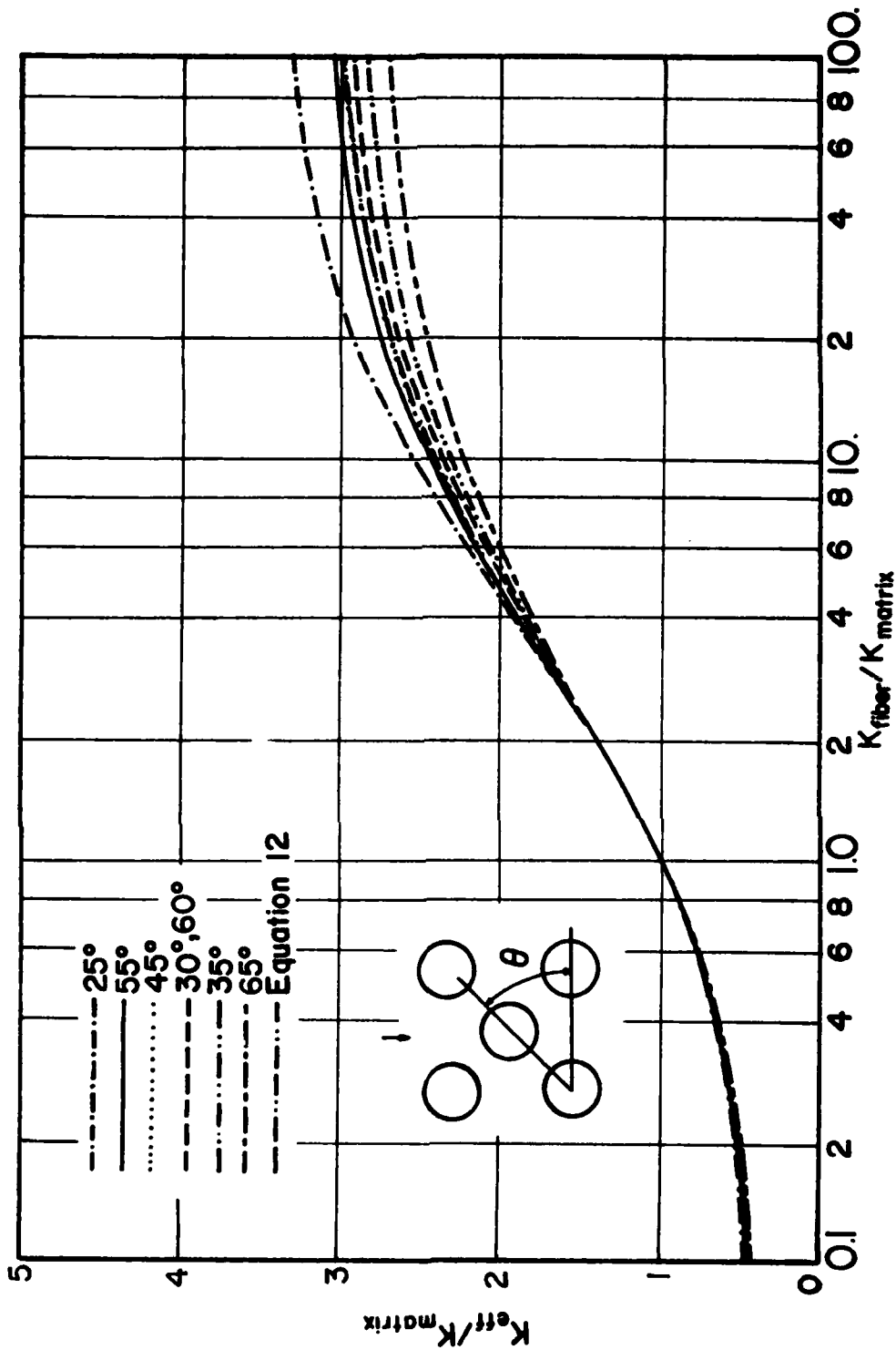
Figure A-22 Parallel Fiber (Staggered Array) Volume Ratio = .50
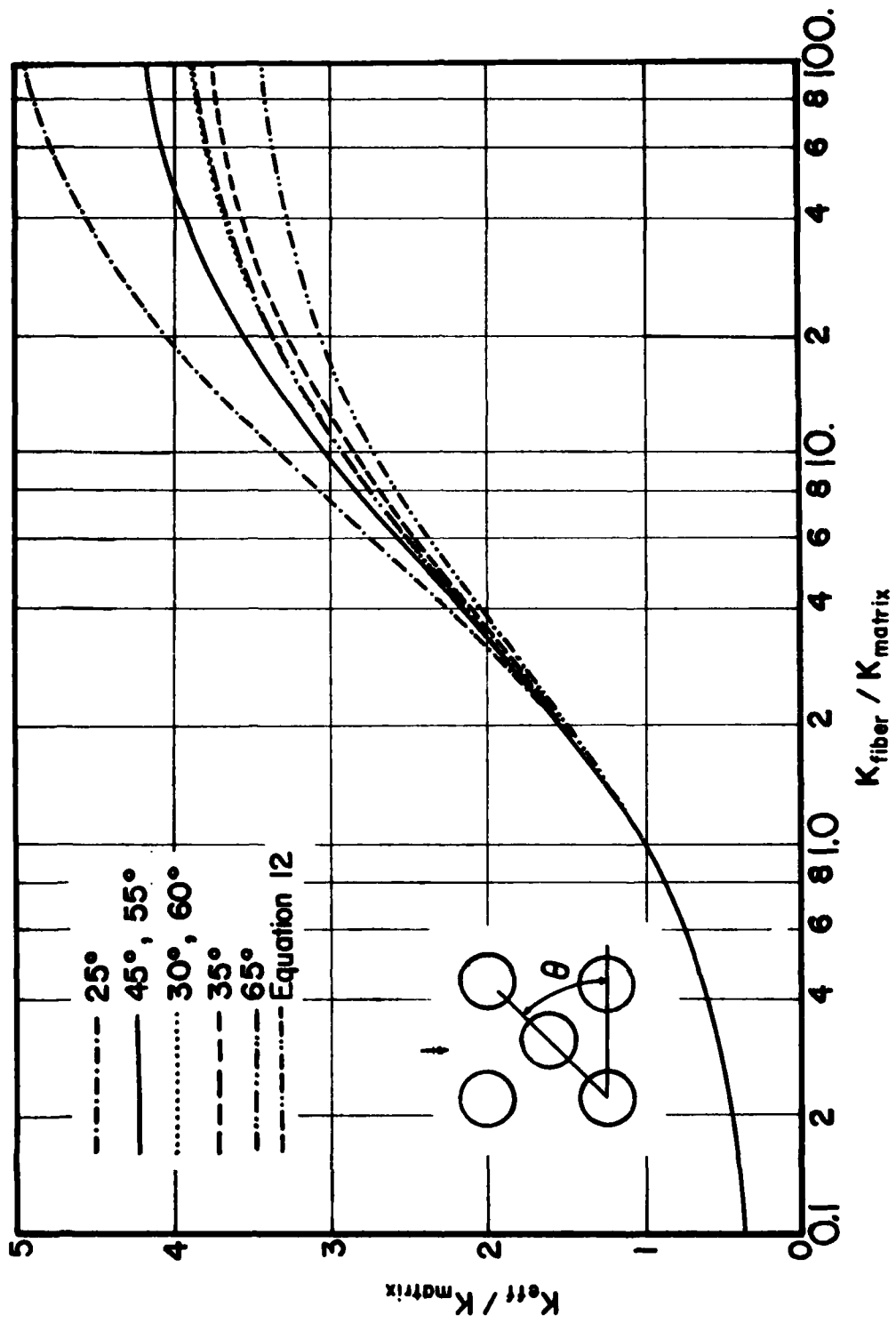
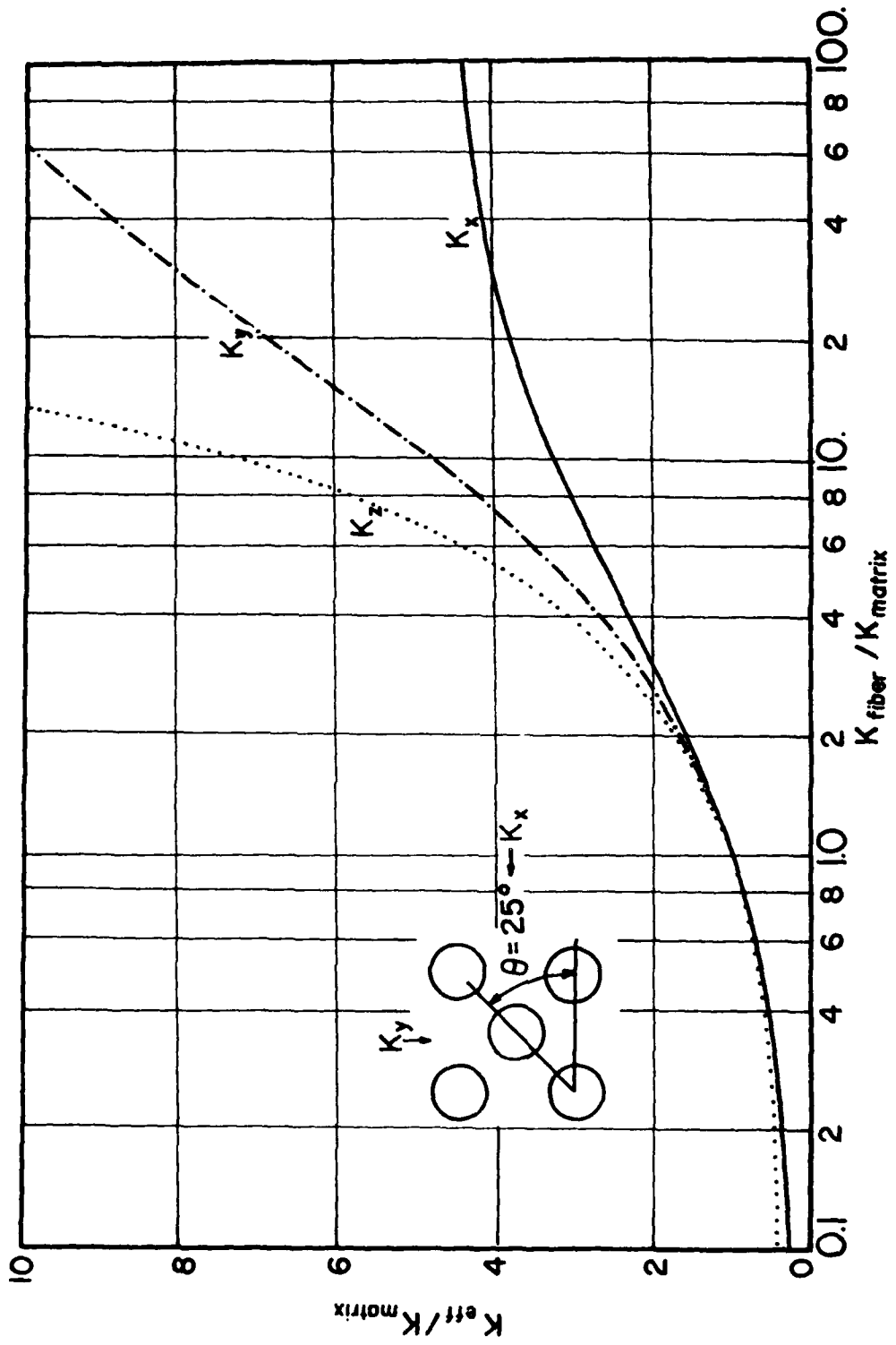Figure A-23 Parallel Fiber (Staggered Array) Volume Ratio = .60
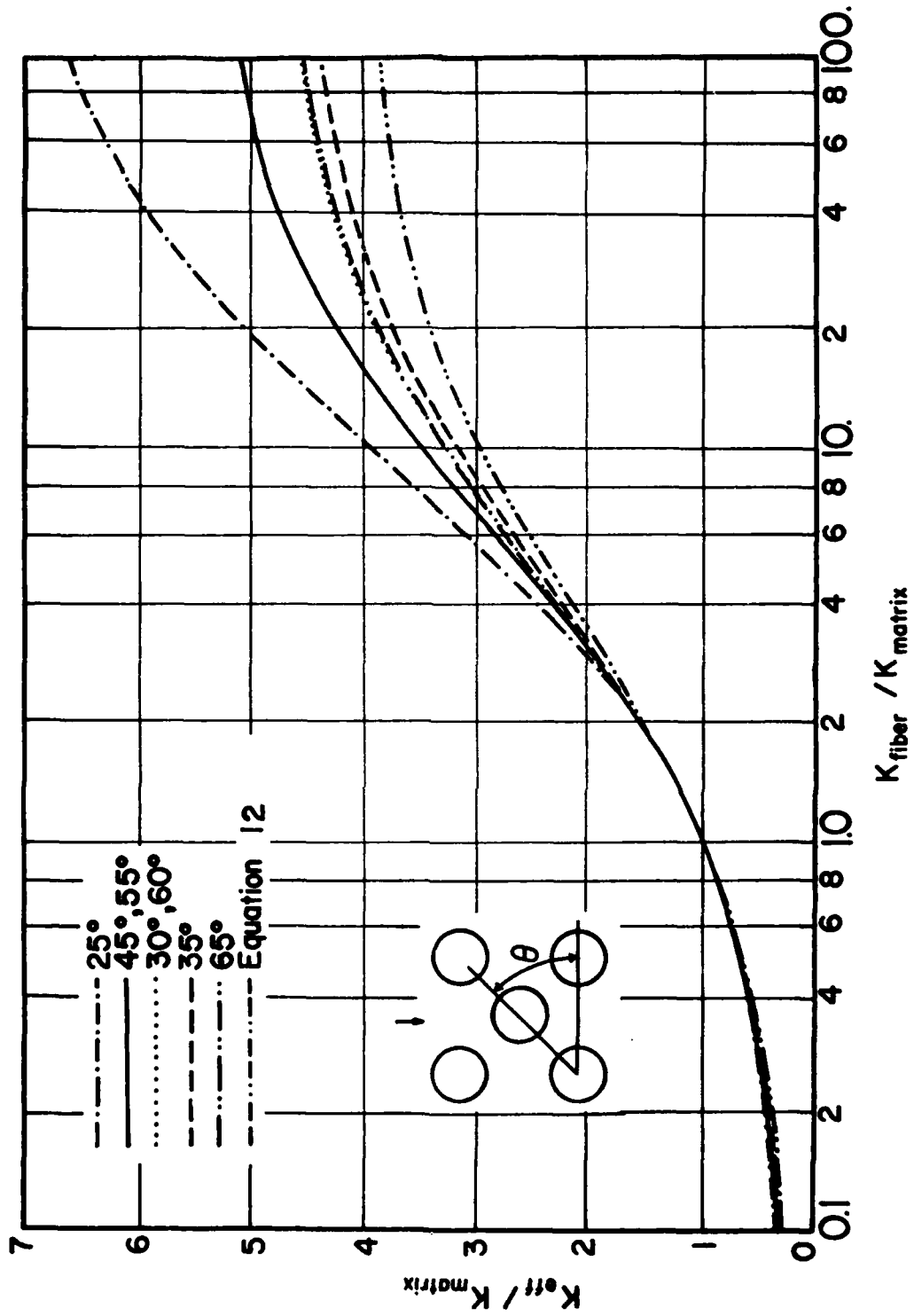
Figure A-24 Parallel Fiber (Staggered Array) Volume Ratio = .65
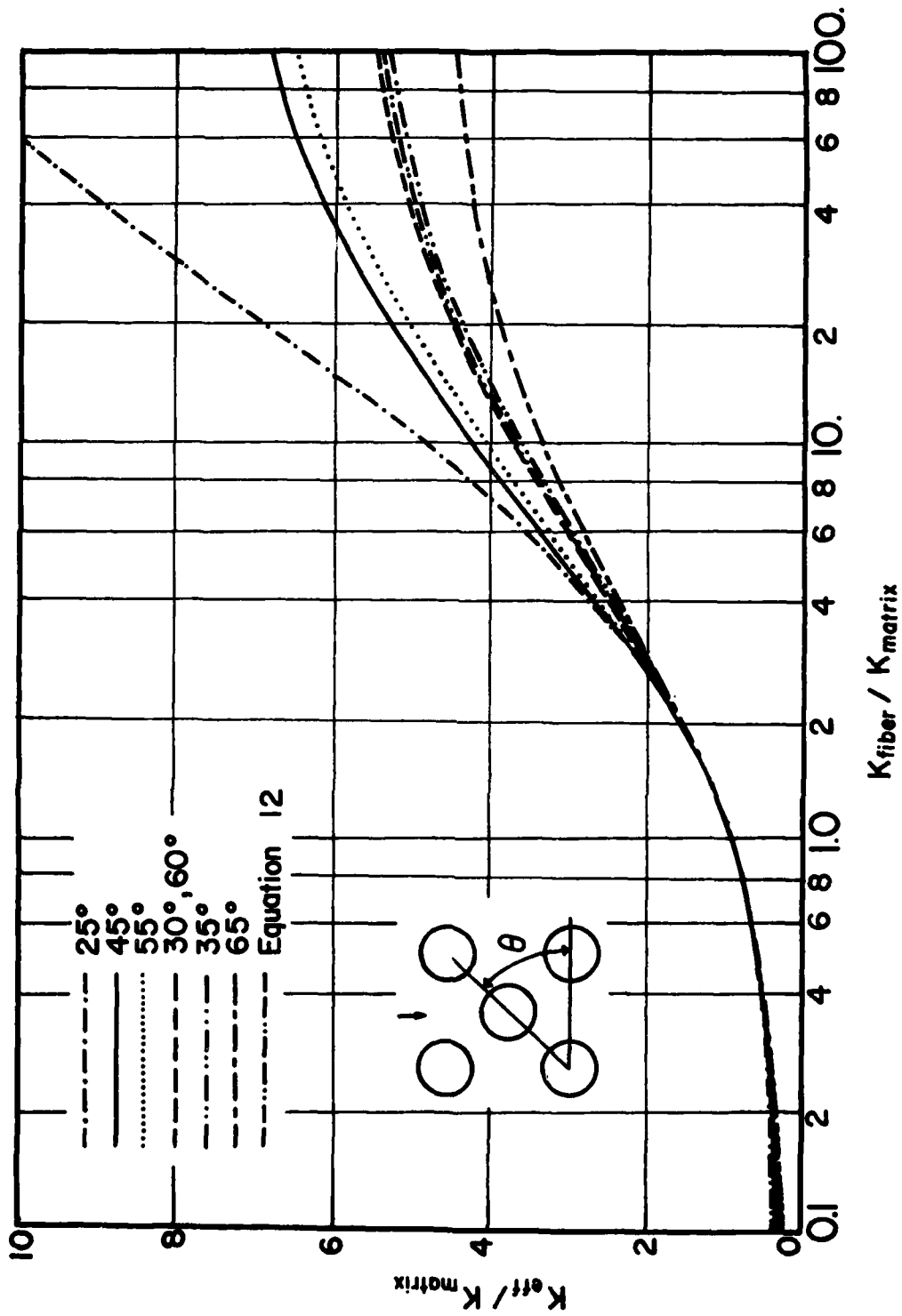
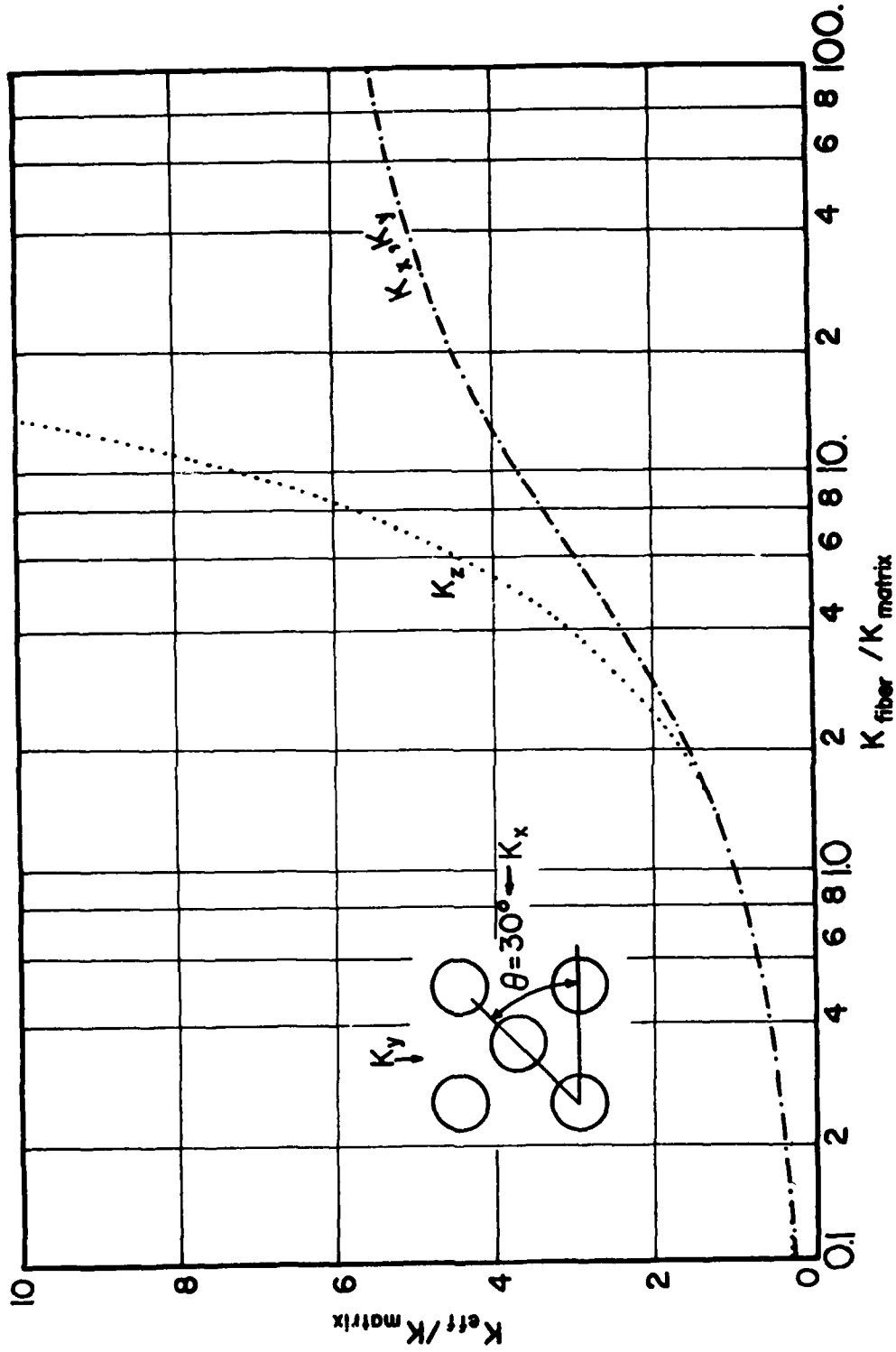Figure A-25 Parallel Fiber (Staggered Array) Volume Ratio = .70
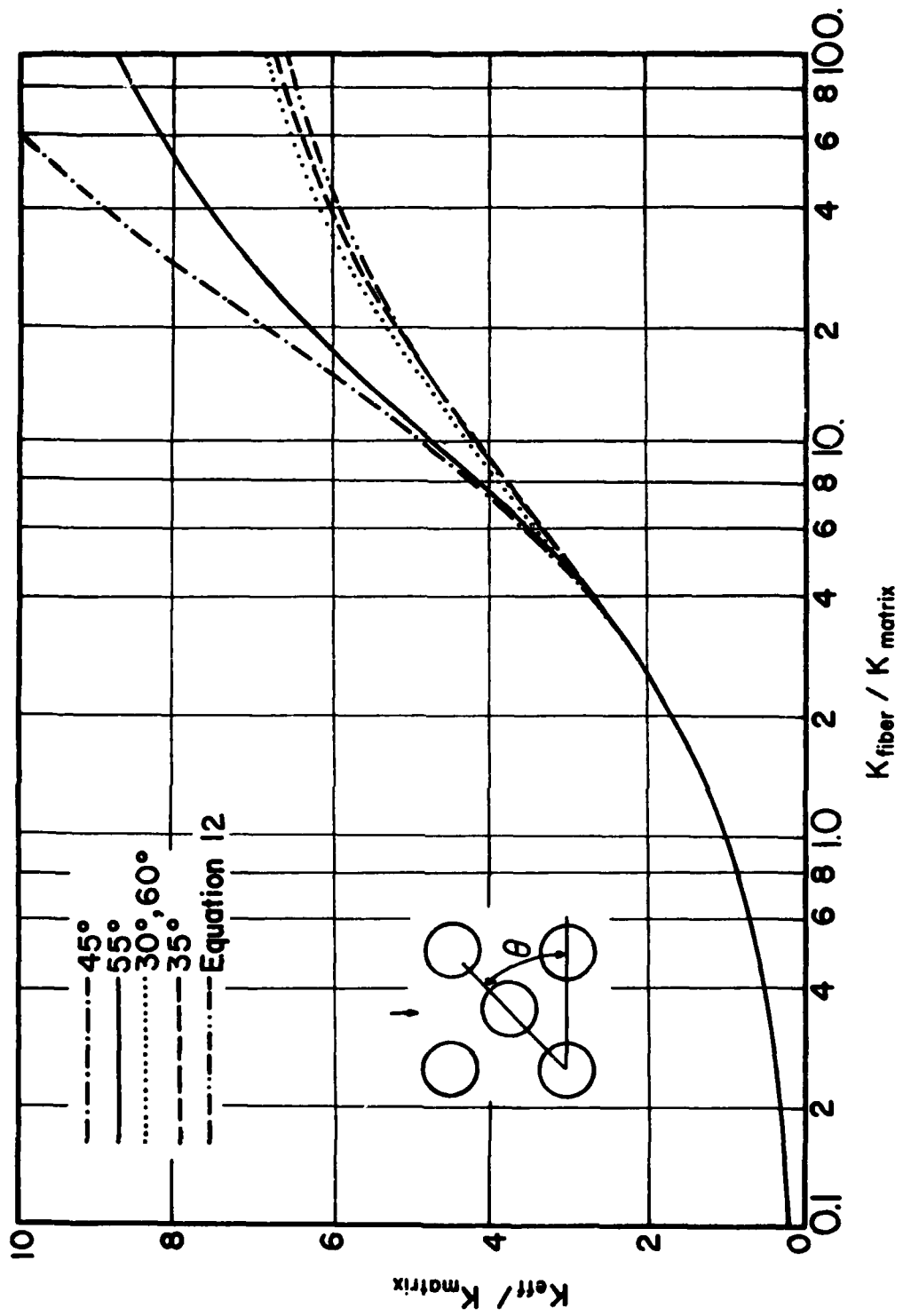
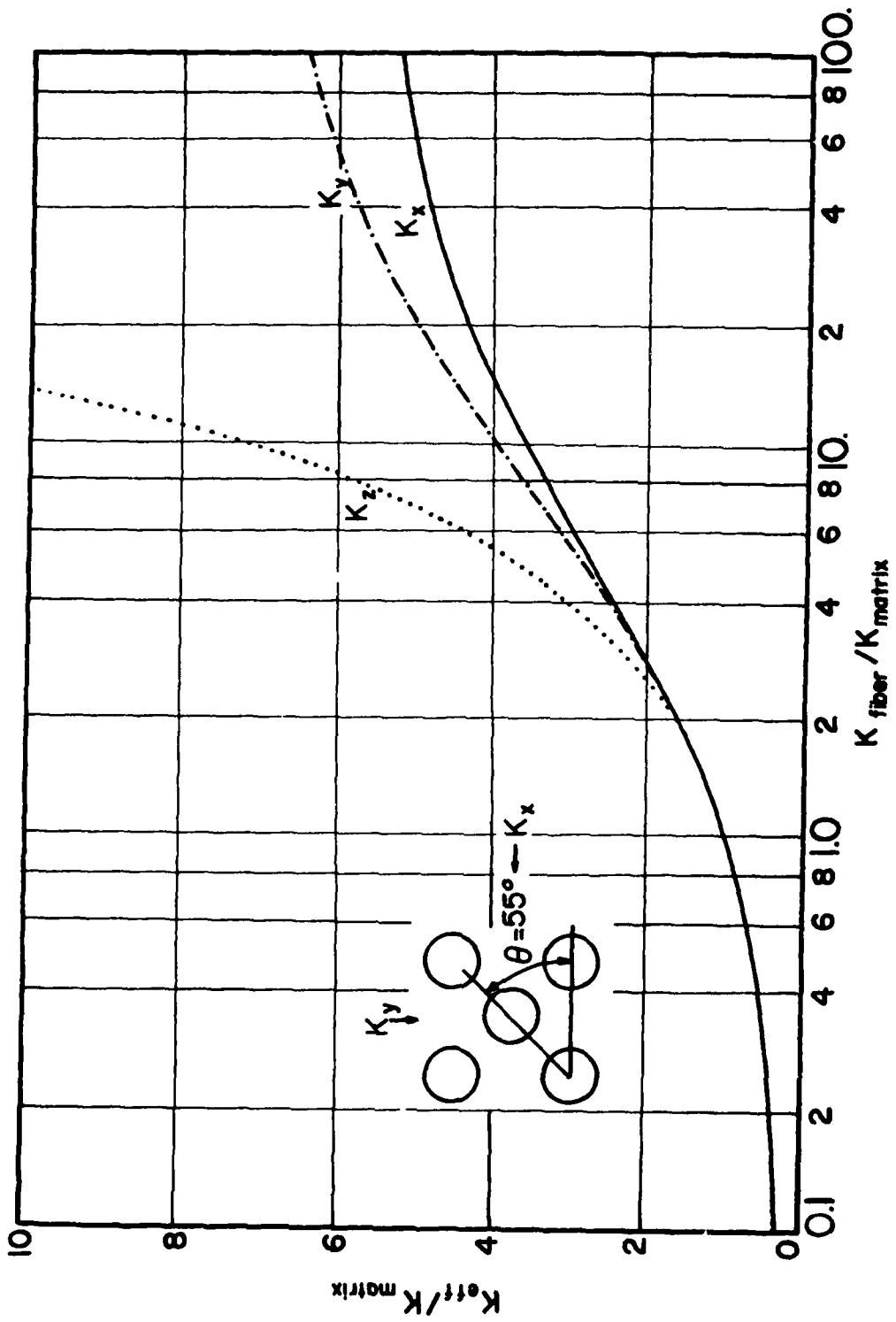Figure A-26 Parallel Fiber (Staggered Array) Volume Ratio = .75

93
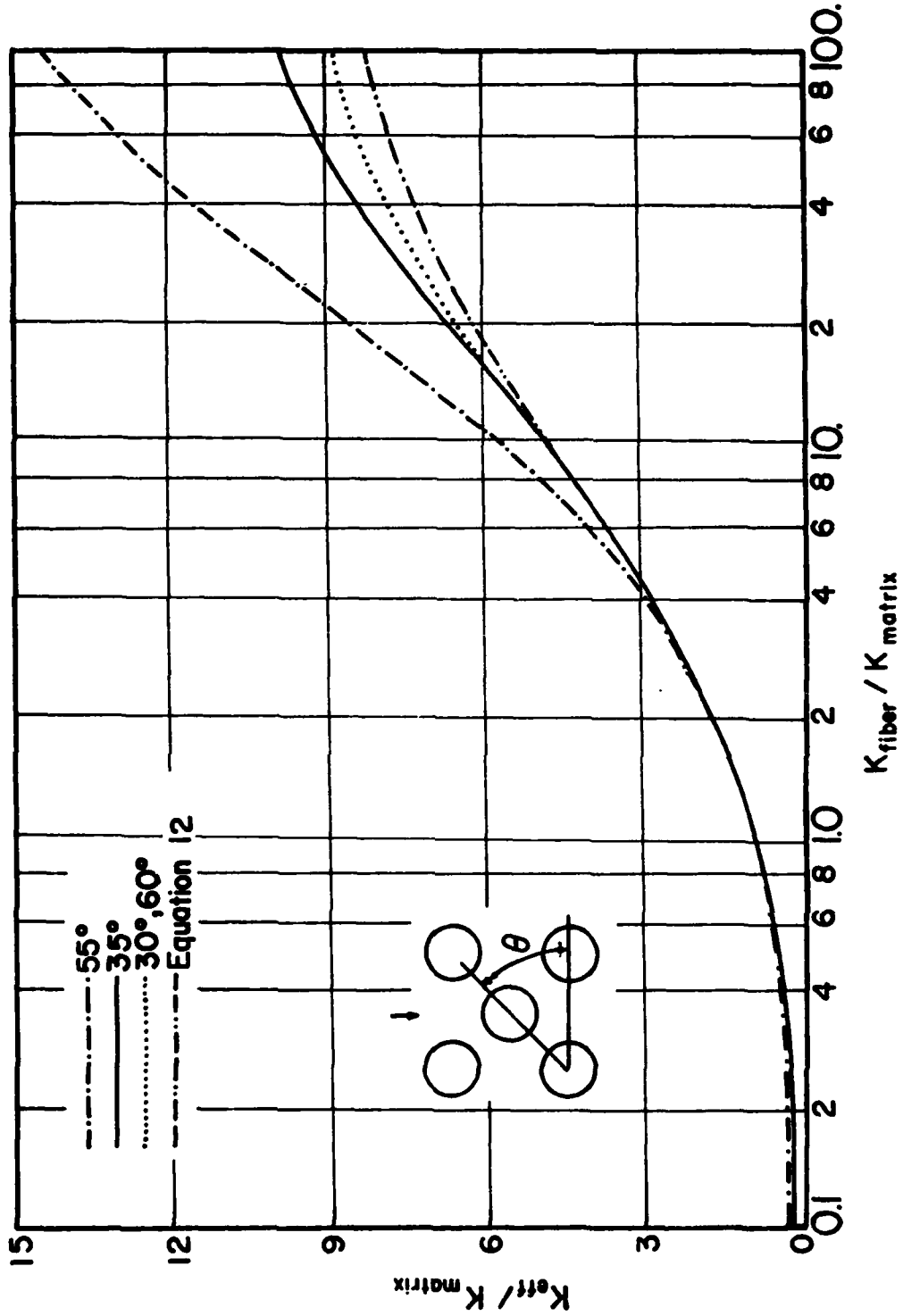
Figure A-27 Parallel Fiber (Staggered Array) Volume Ratio = .80
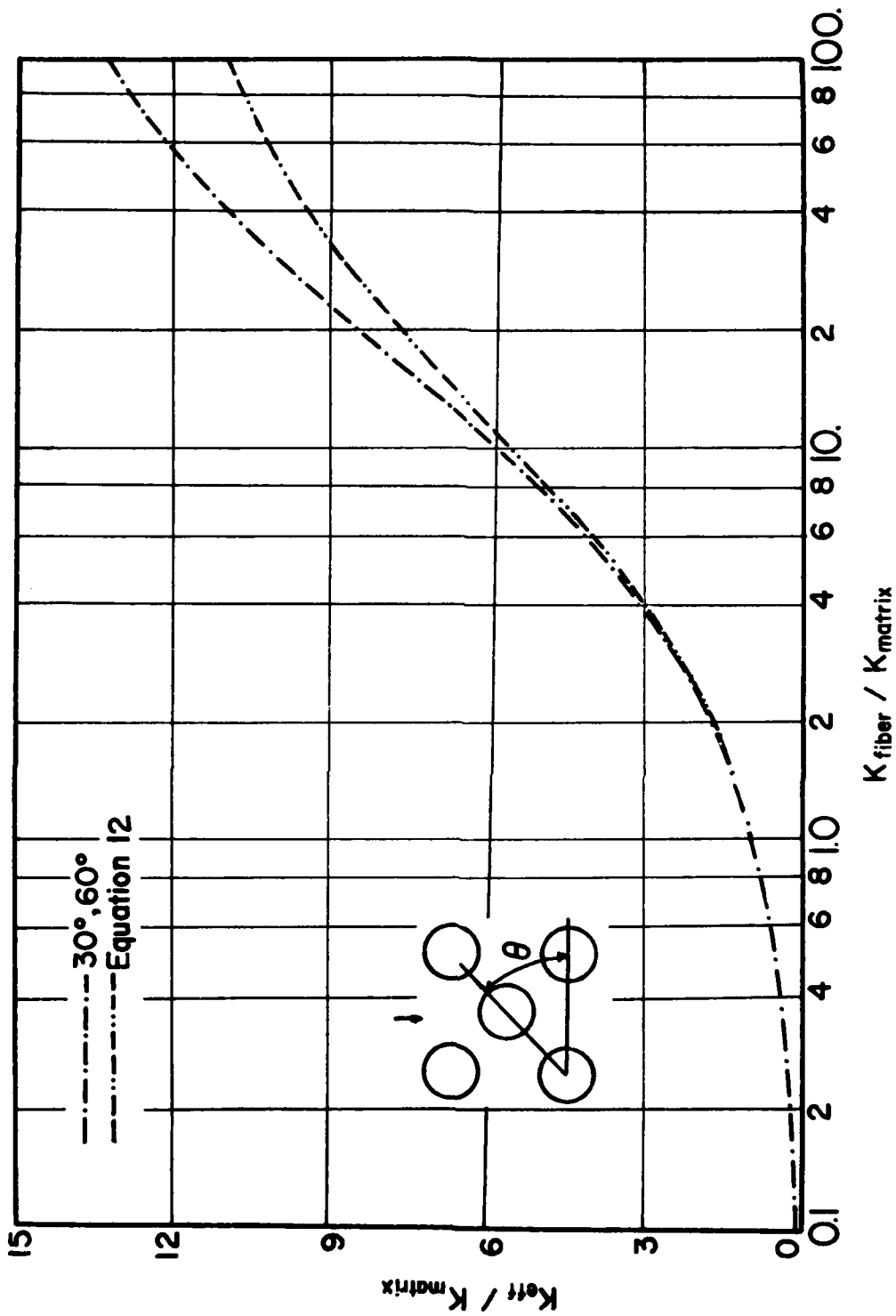
Figure A-28   Parallel Fiber (Staggered Array) Volume Ratio = .85
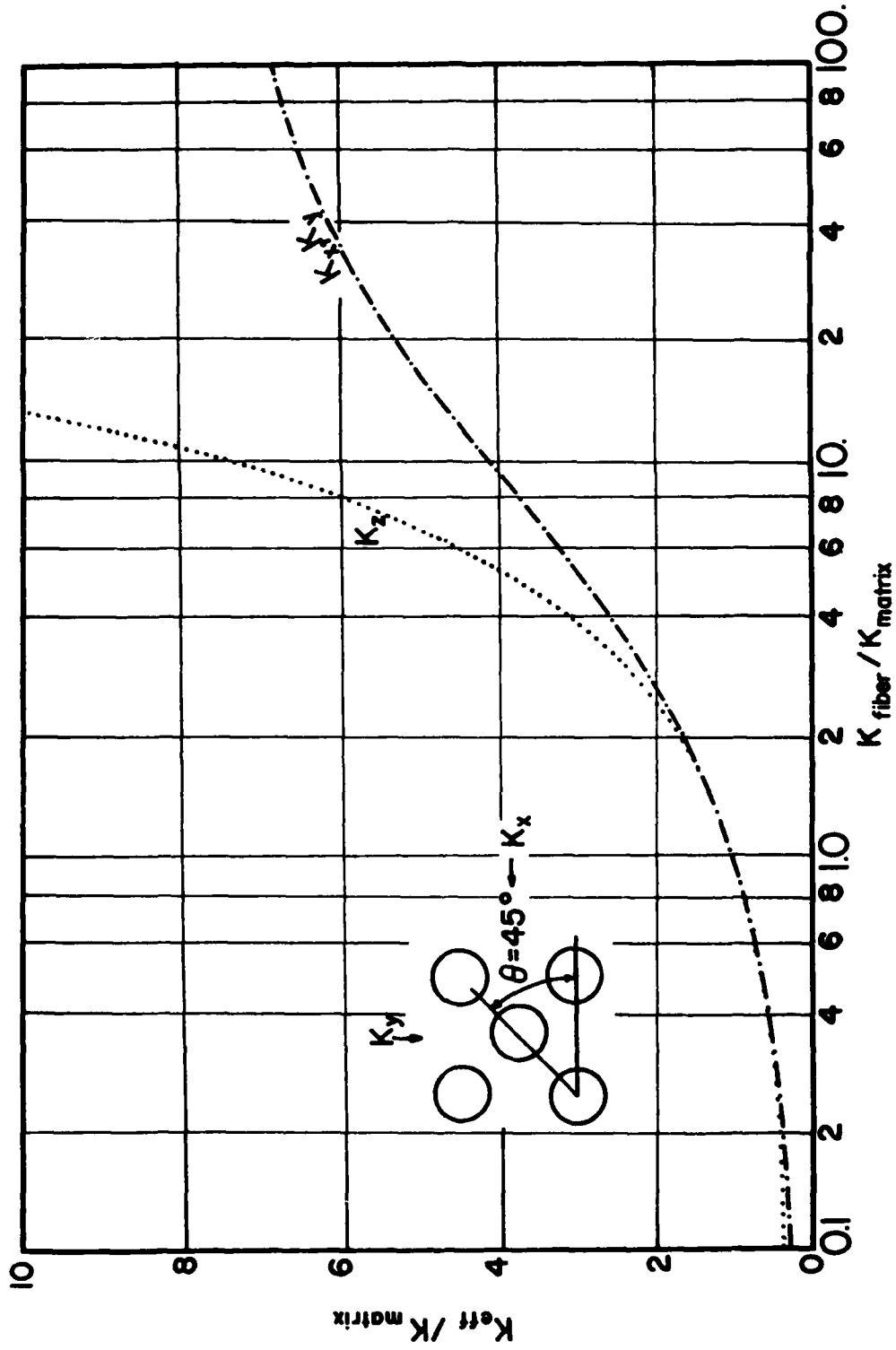
95
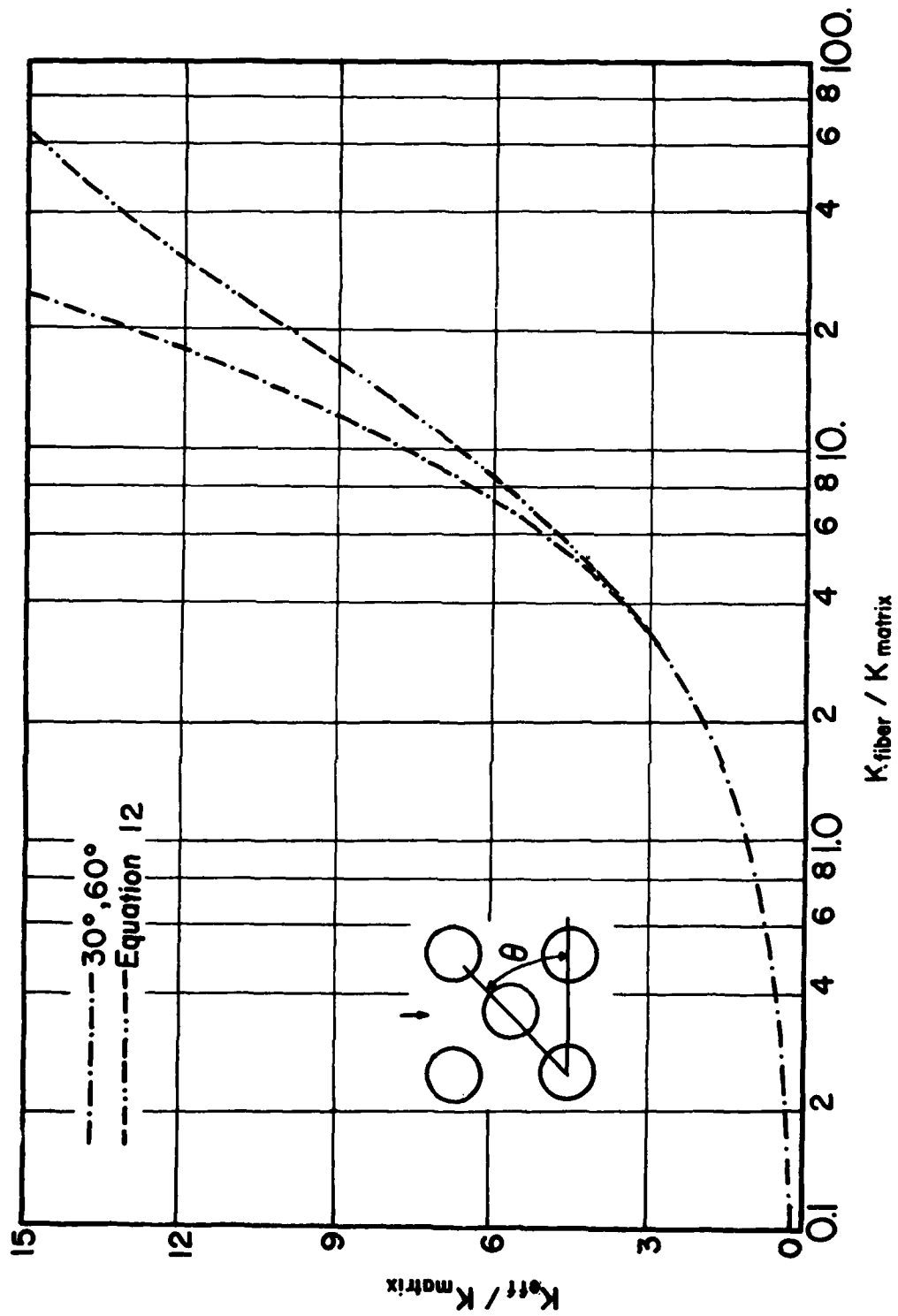
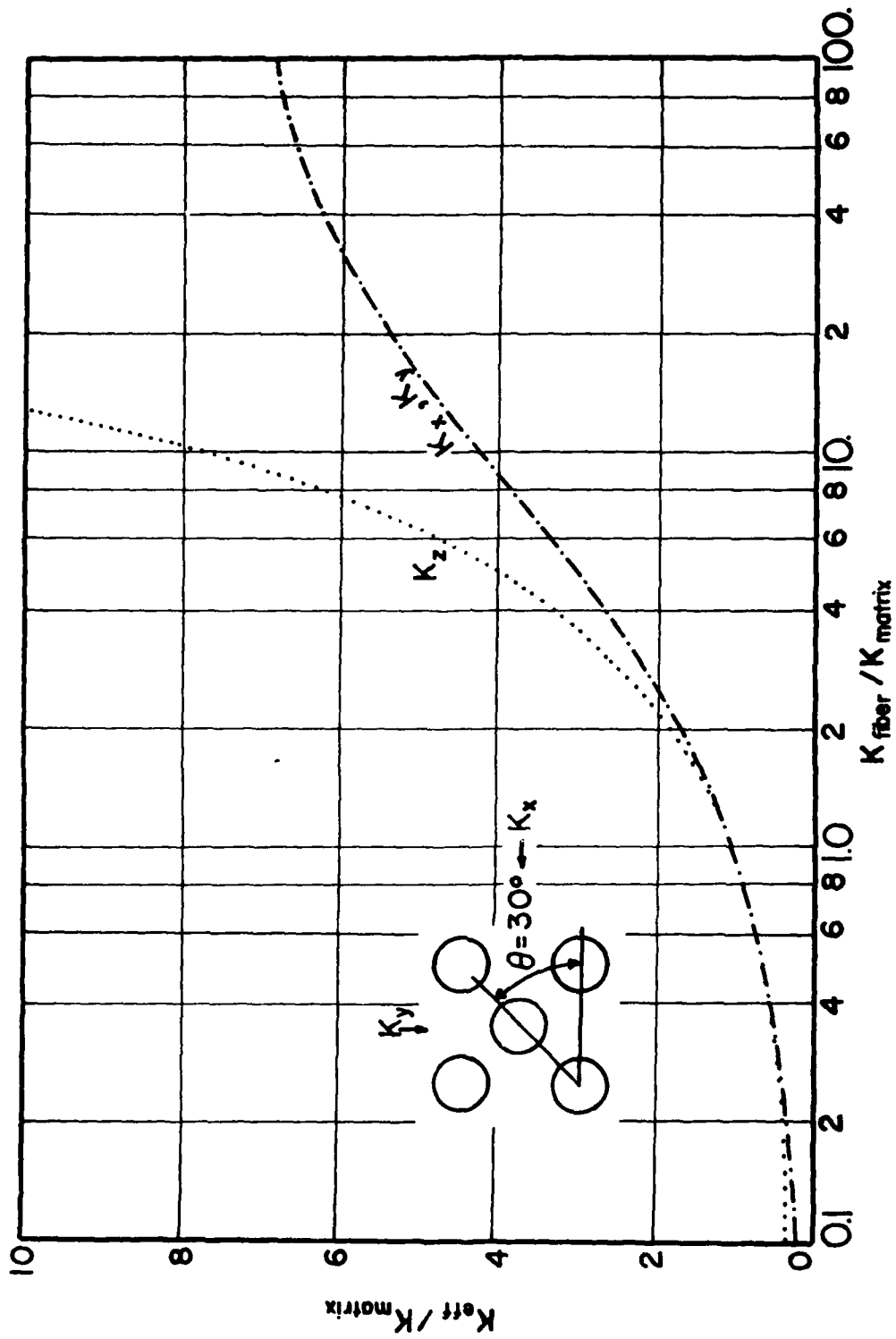Figure A-29 Parallel Fiber (Staggered Array) Volume Ratio = .90

96
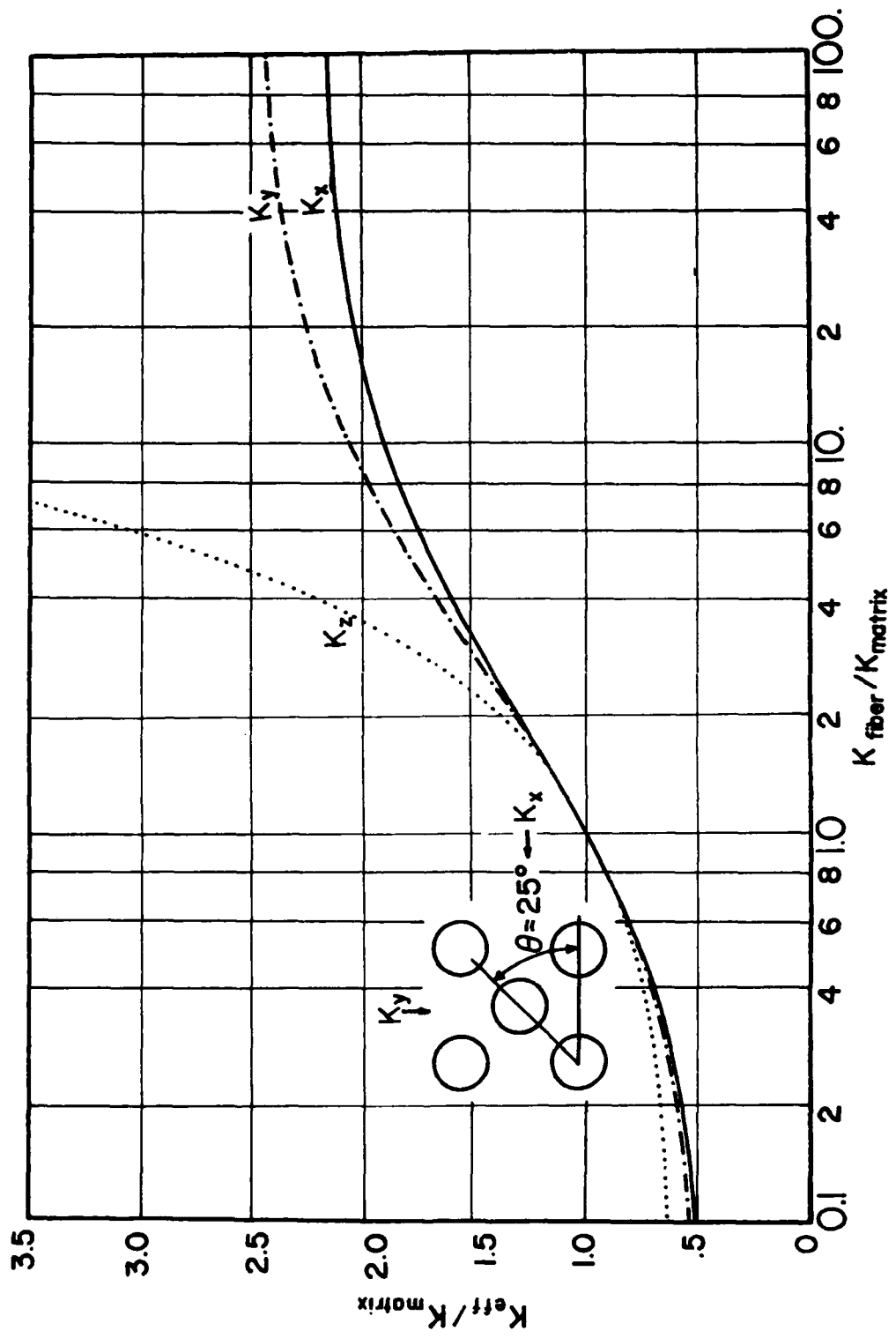
Figure A-30 Parallel Fiber (Staggered Array) Volume Ratio = .40
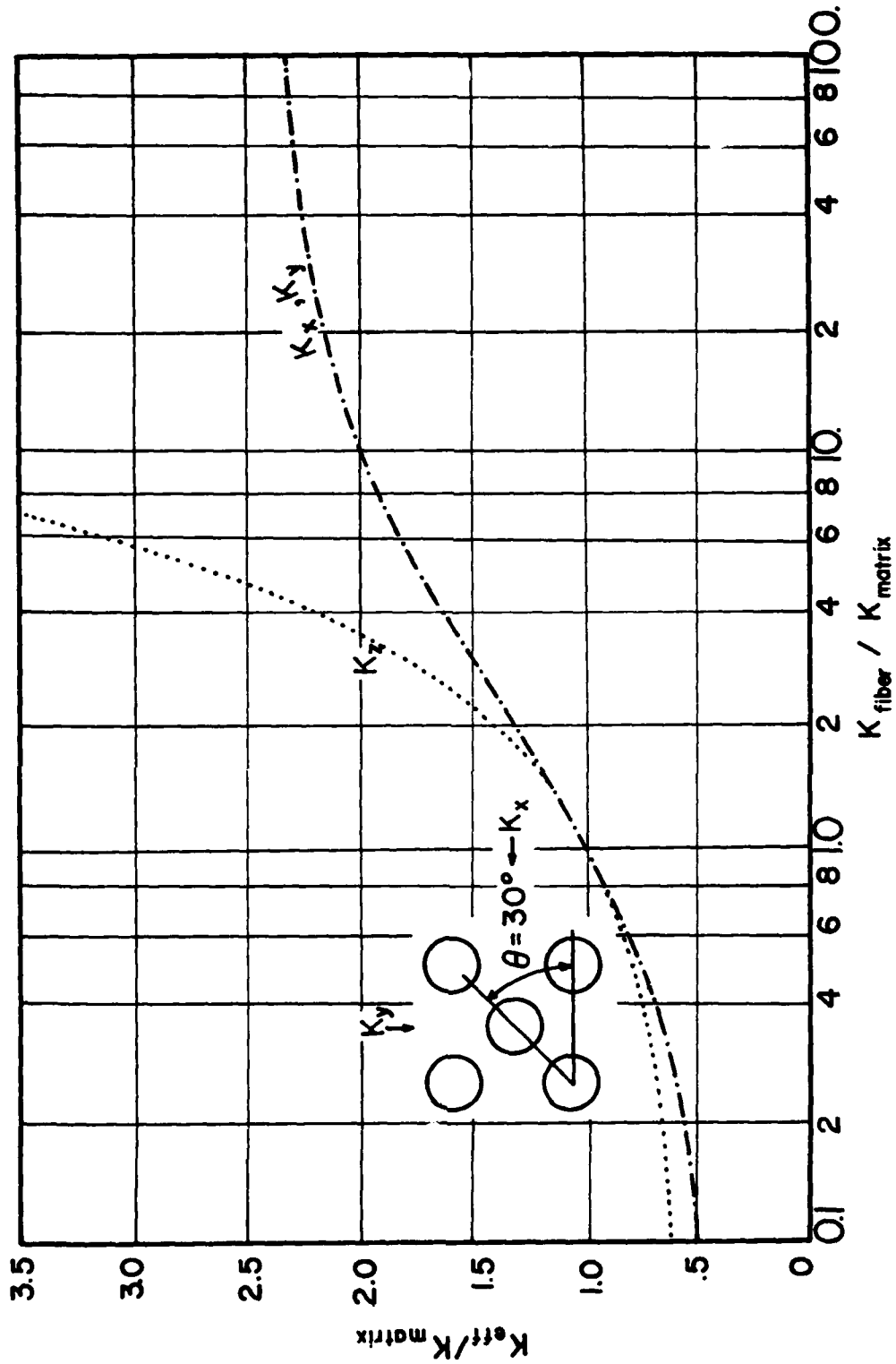
Figure A-31 Parallel Fiber (Staggered Array) Volume Ratio = .40
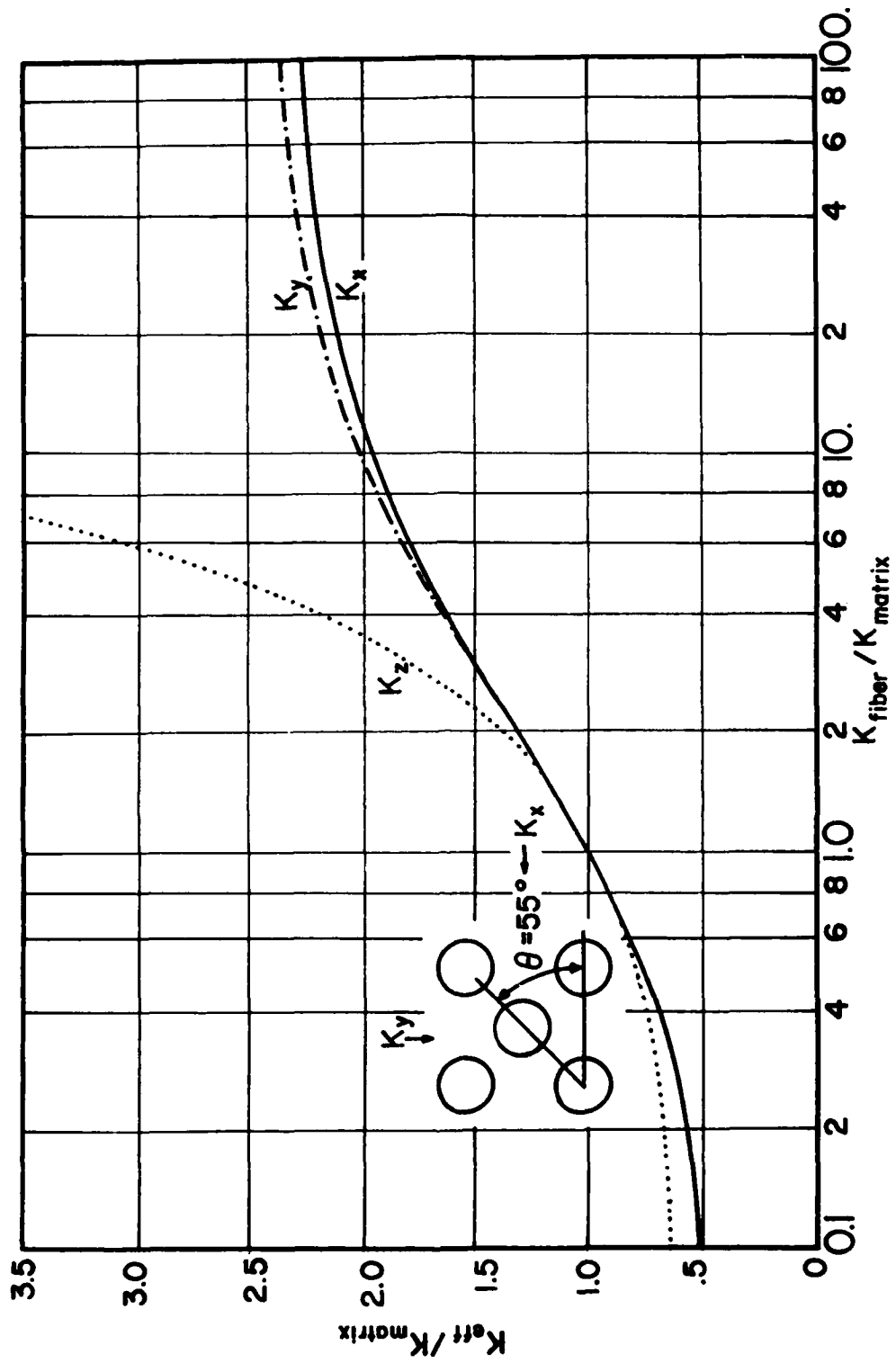
Figure A-32 Parallel Fiber (Staggered Array) Volume Ratio = .40
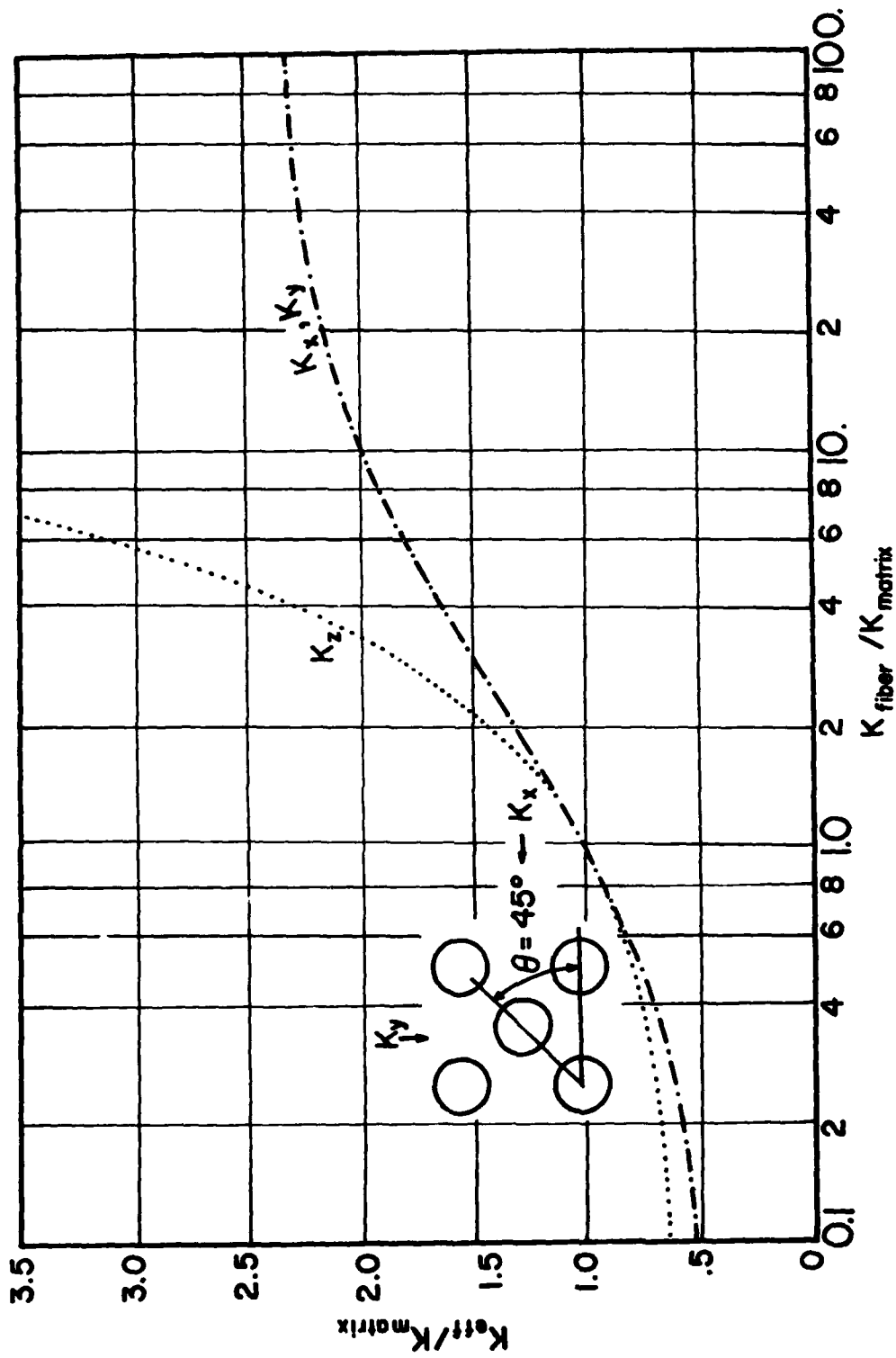
Figure A-33 Parallel Fiber (Staggered Array) Volume Ratio = .40
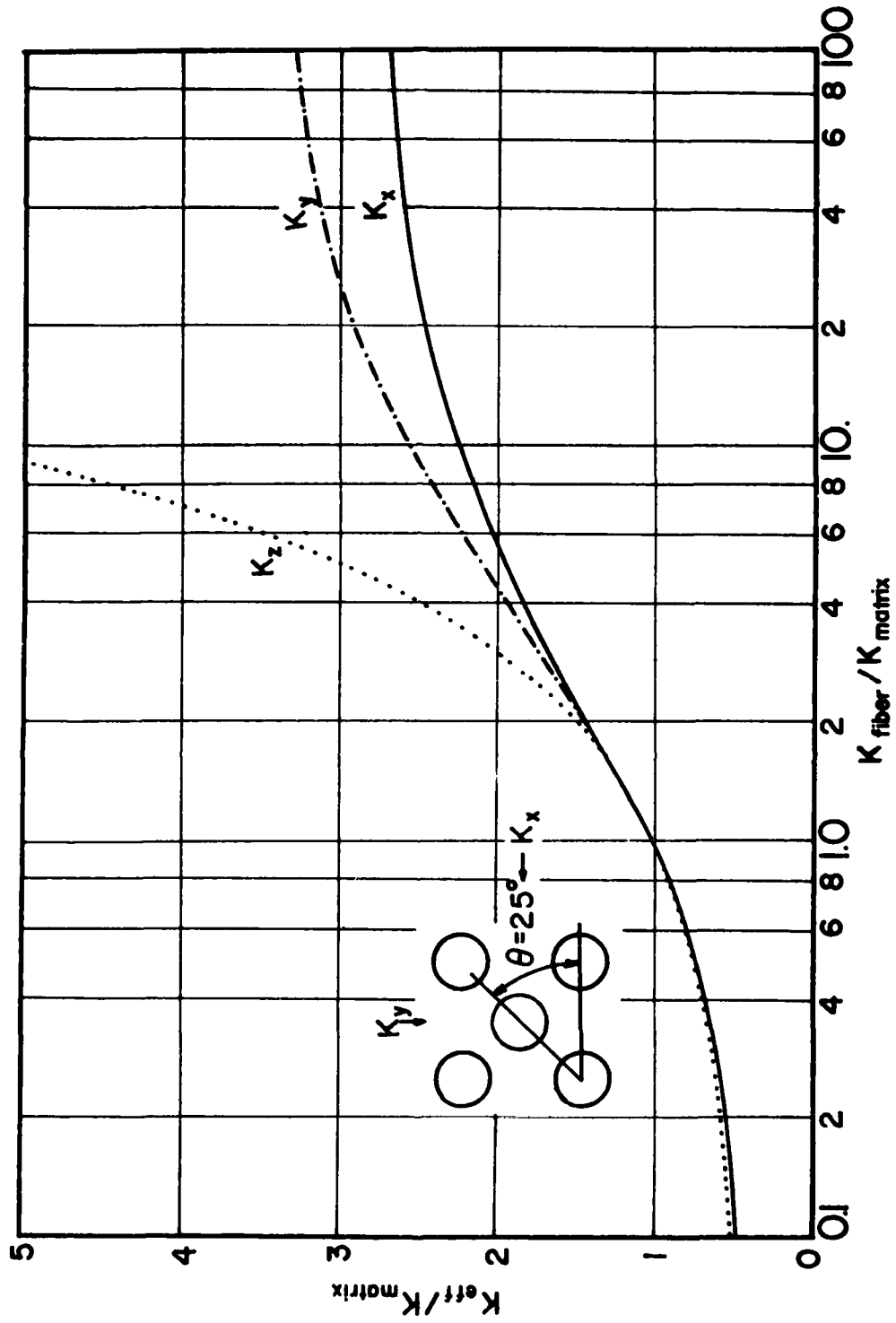
Figure A-34 Parallel Fiber (Staggered Array) Volume Ratio = .50
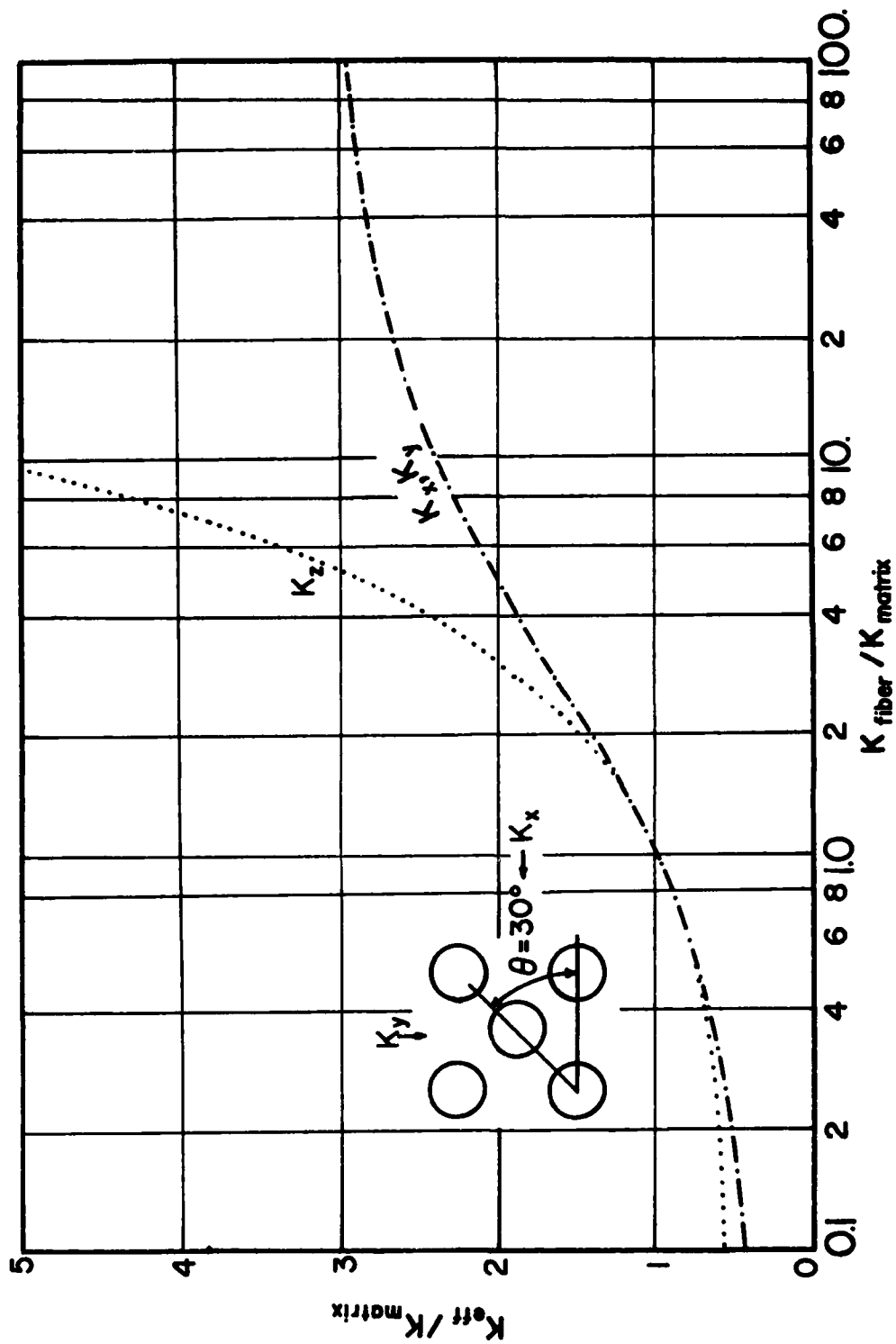
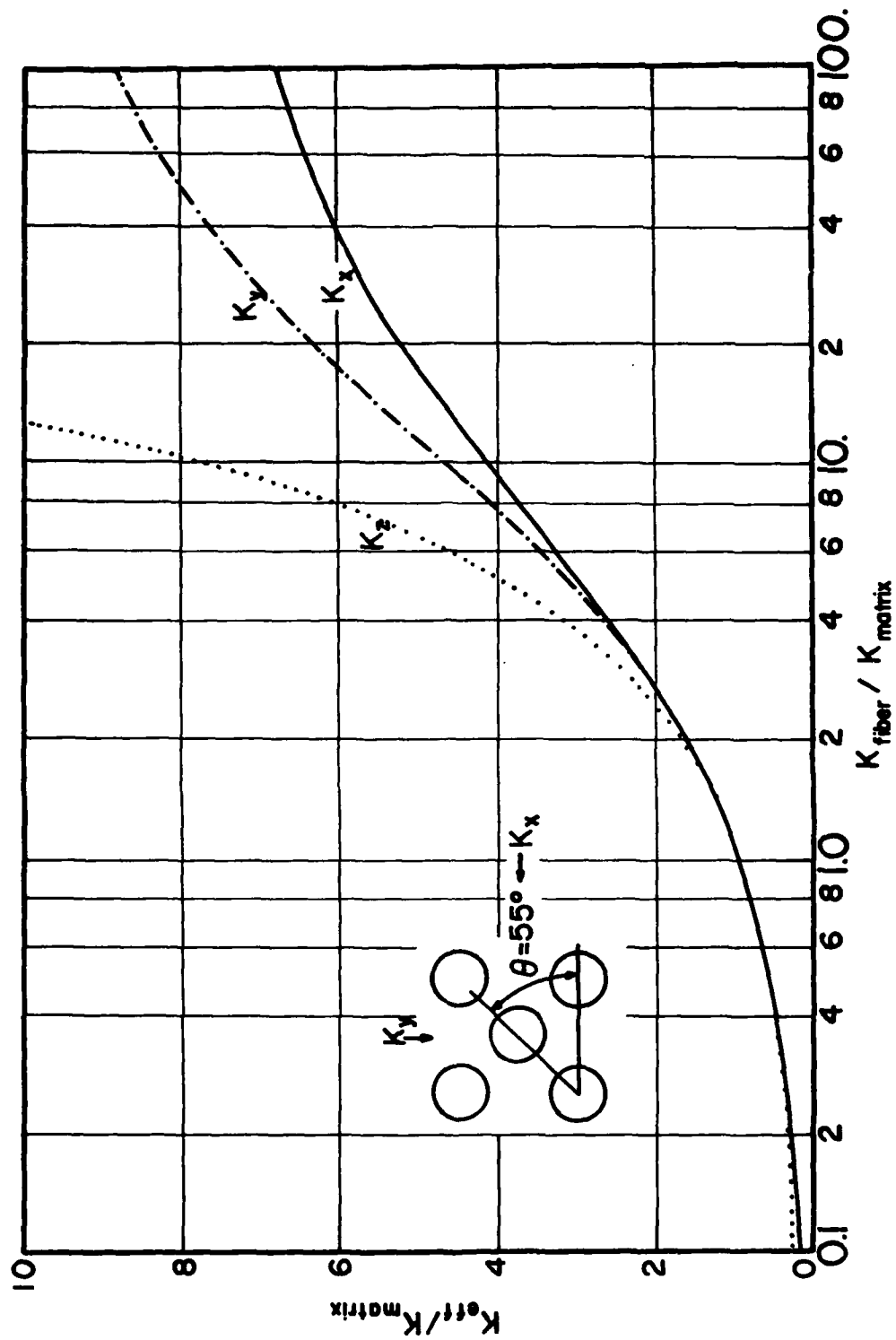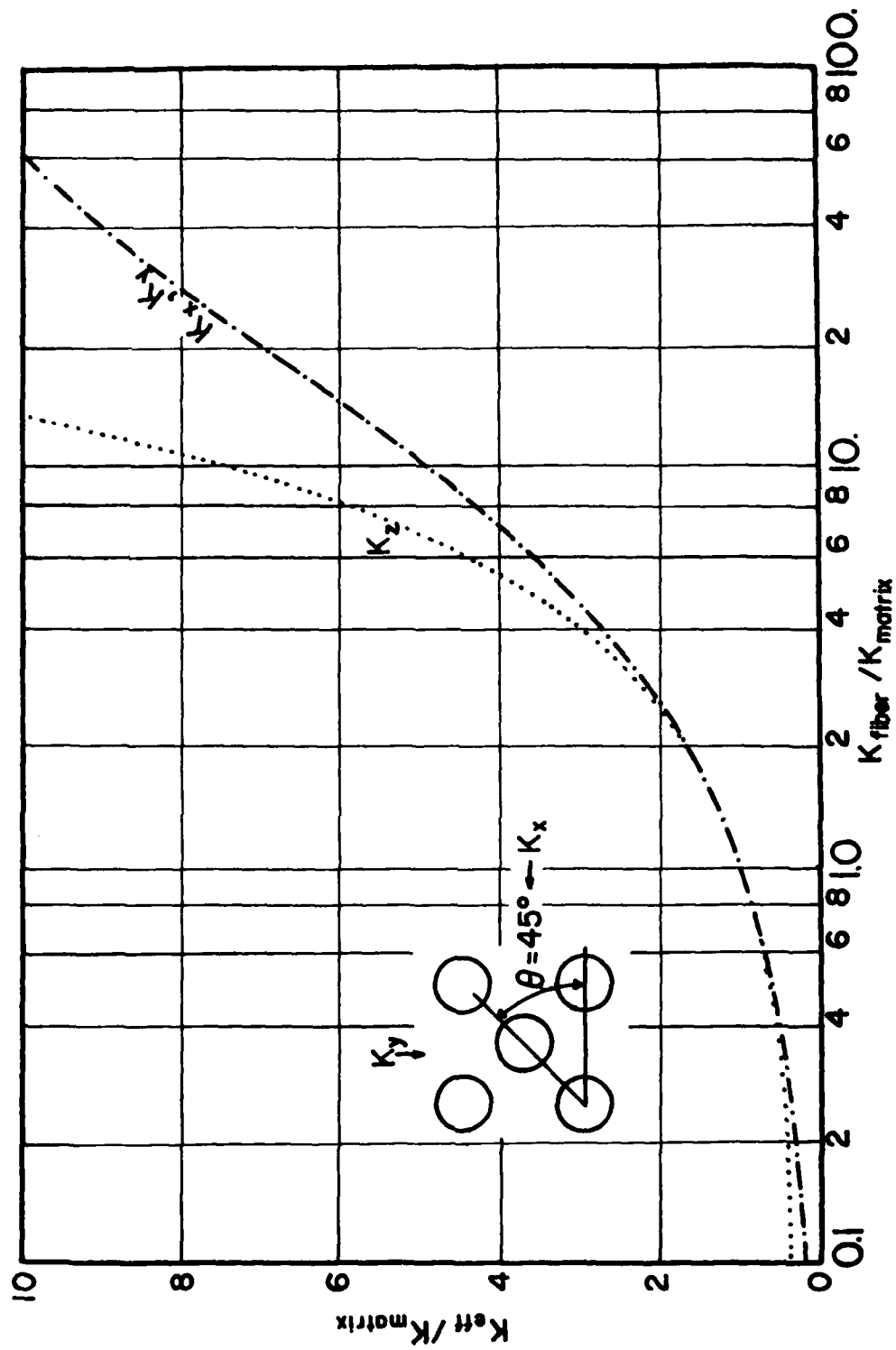Figure A-35 Parallel Fiber (Staggered Array) Volume Ratio = .50

102
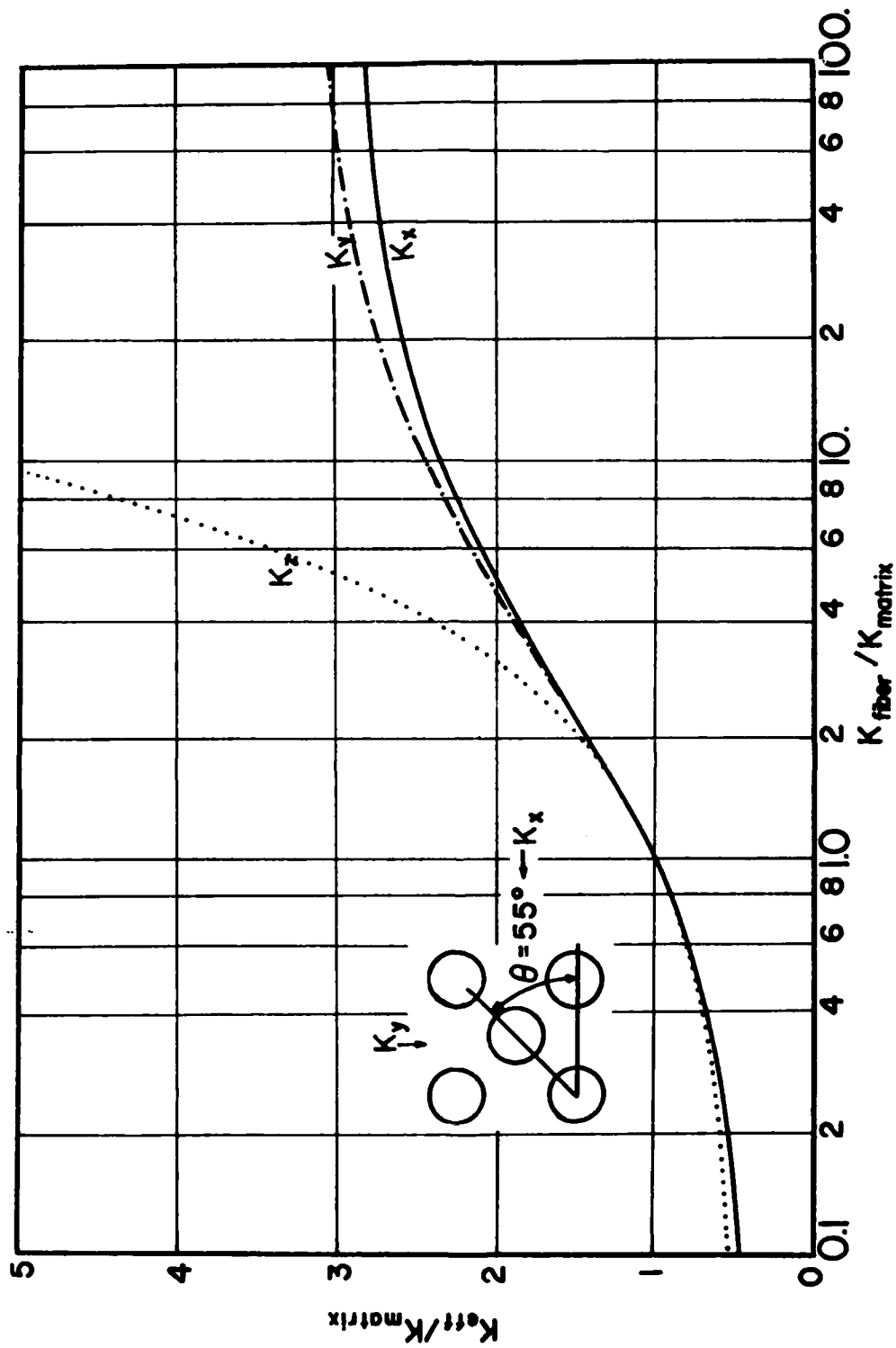
Figure A-36 Parallel Fiber (Staggered Array) Volume Ratio = .50

103
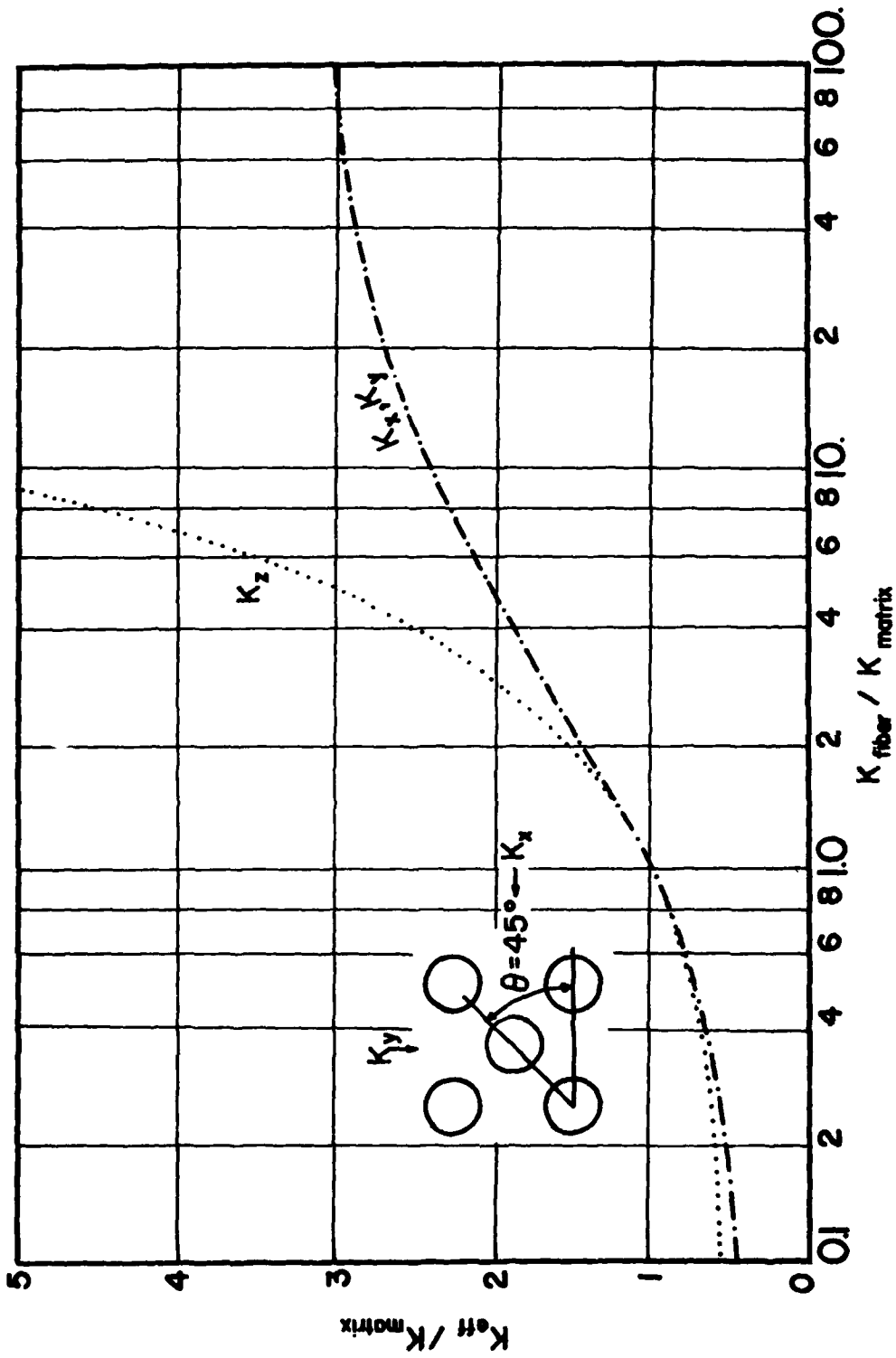
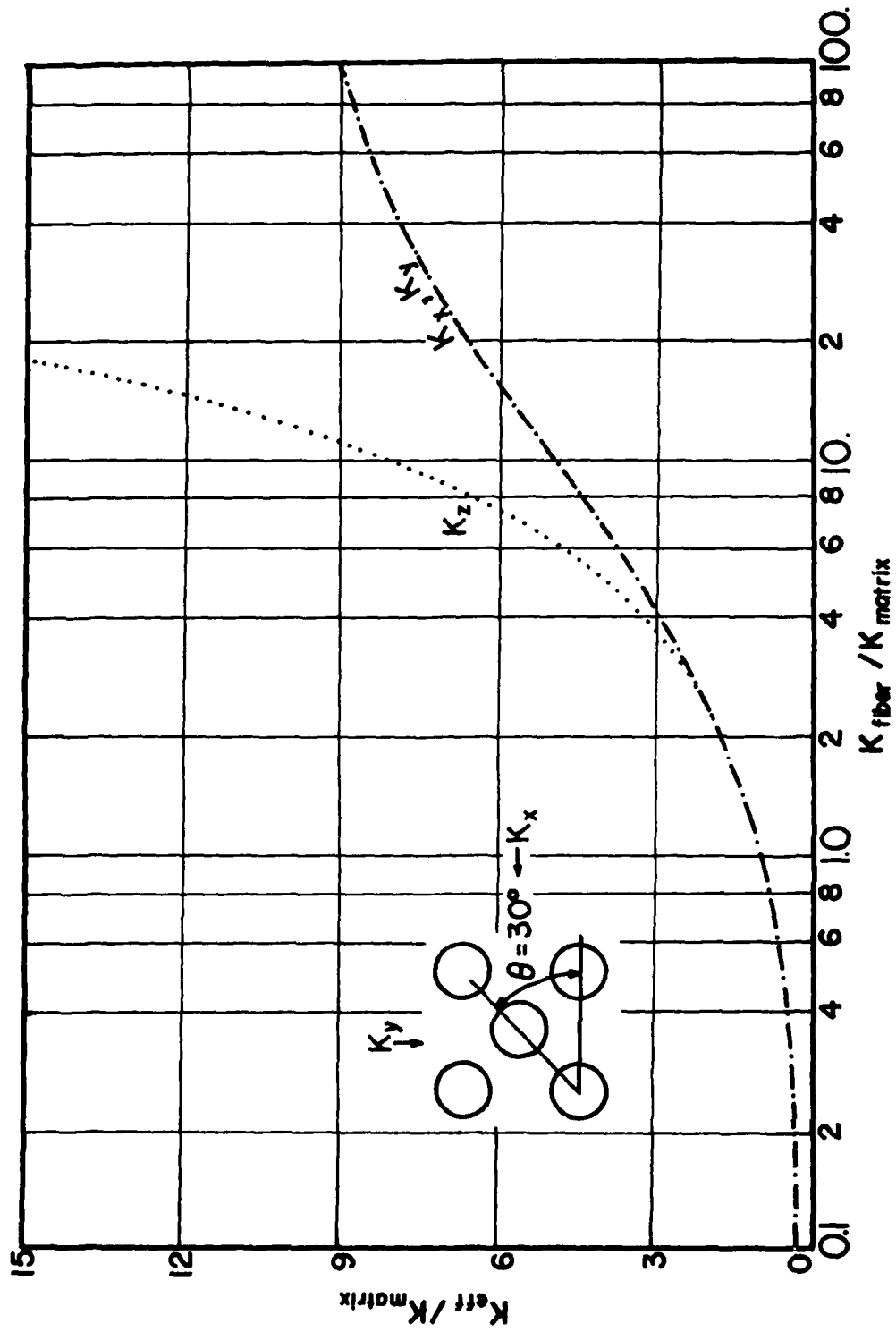Figure A-37 Parallel Fiber (Staggered Array) Volume Ratio = .50

104
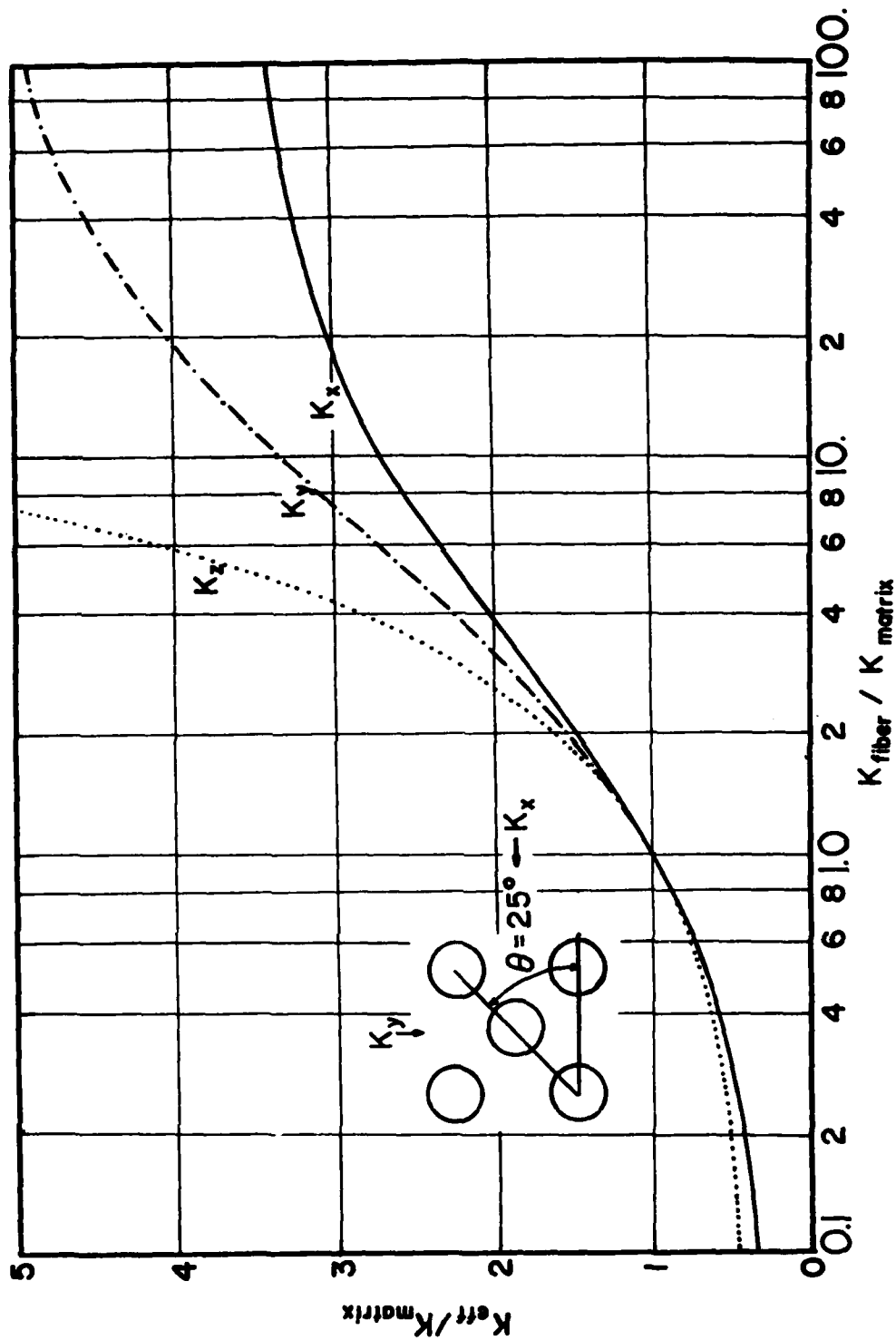
Figure A-38 Parallel Fiber (Staggered Array) Volume Ratio = .60
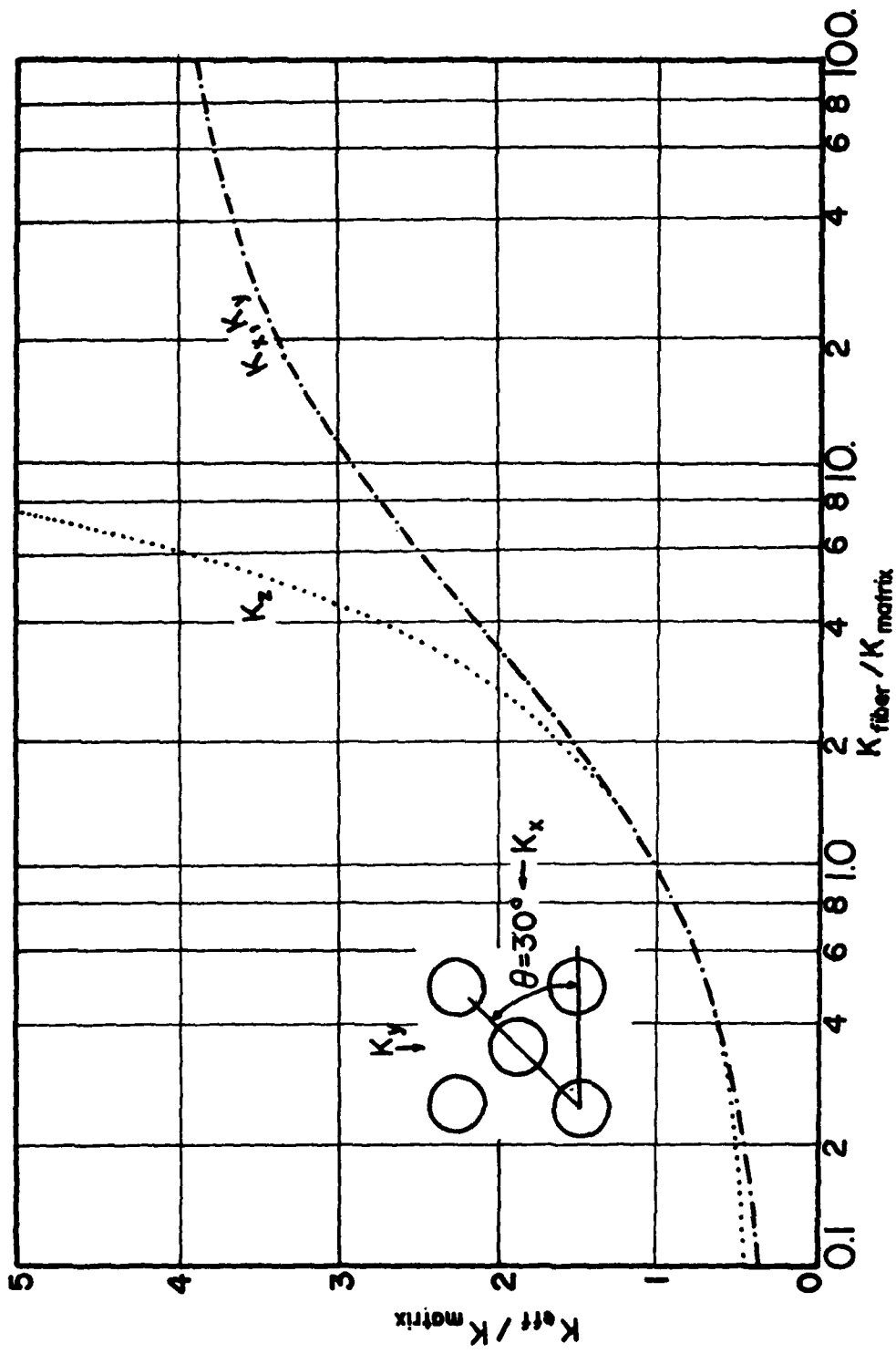
Figure A-39 Parallel Fiber (Staggered Array) Volume Ratio = .60
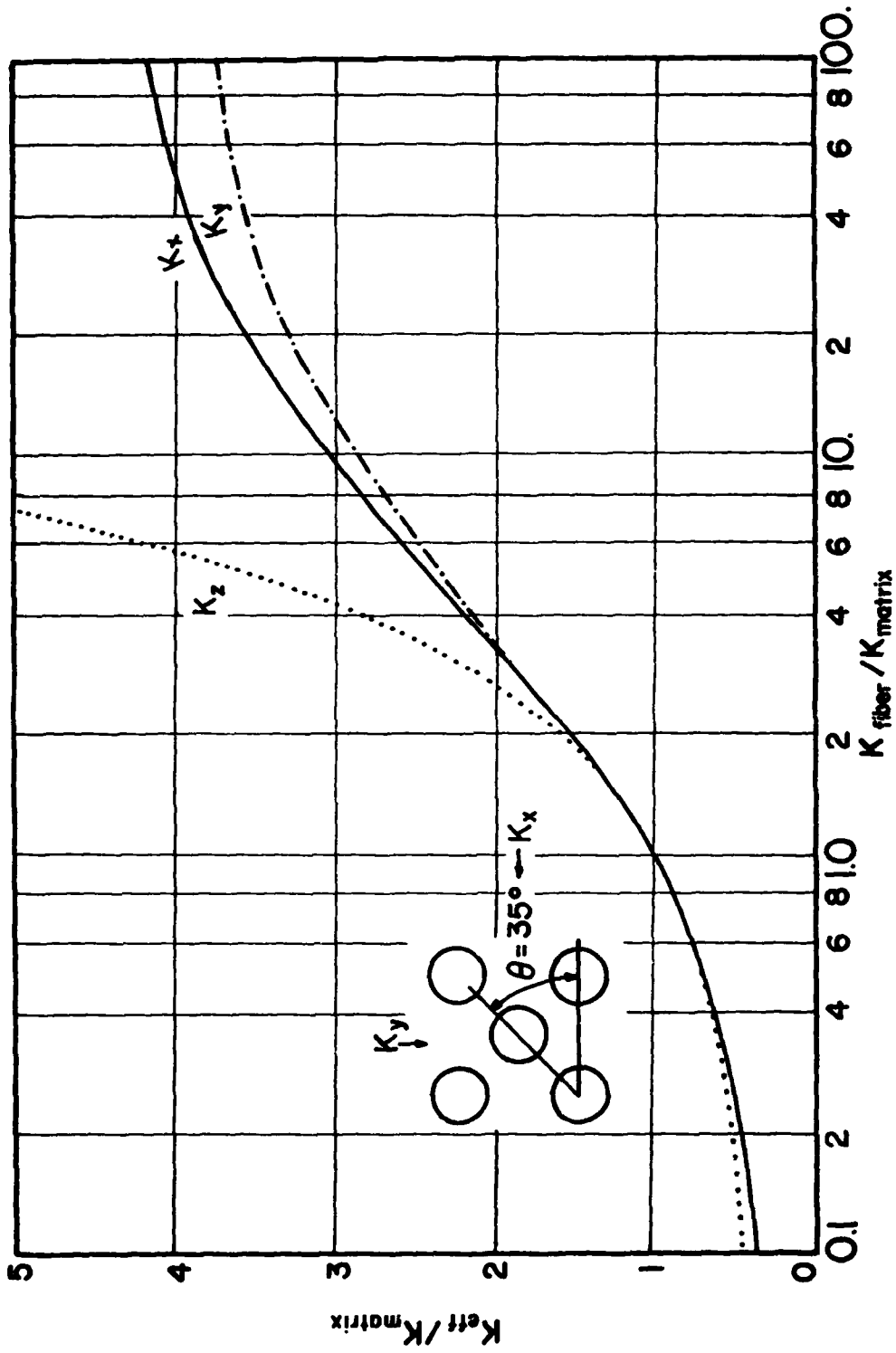
Figure A-40 Parallel Fiber (Staggered Array) Volume Ratio = .60

107
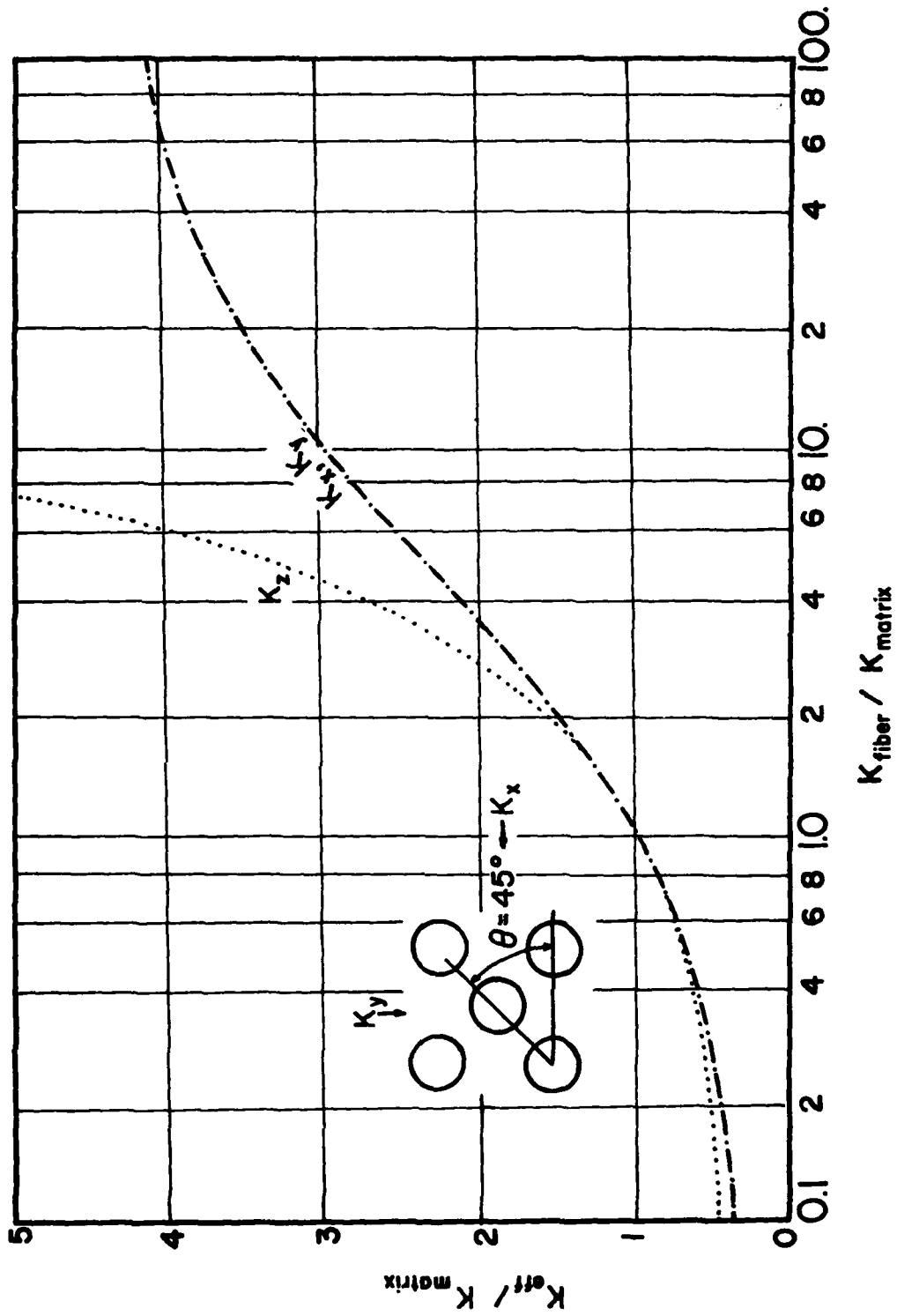
Figure A-41 Parallel Fiber (Staggered Array) Volume Ratio = .60

108
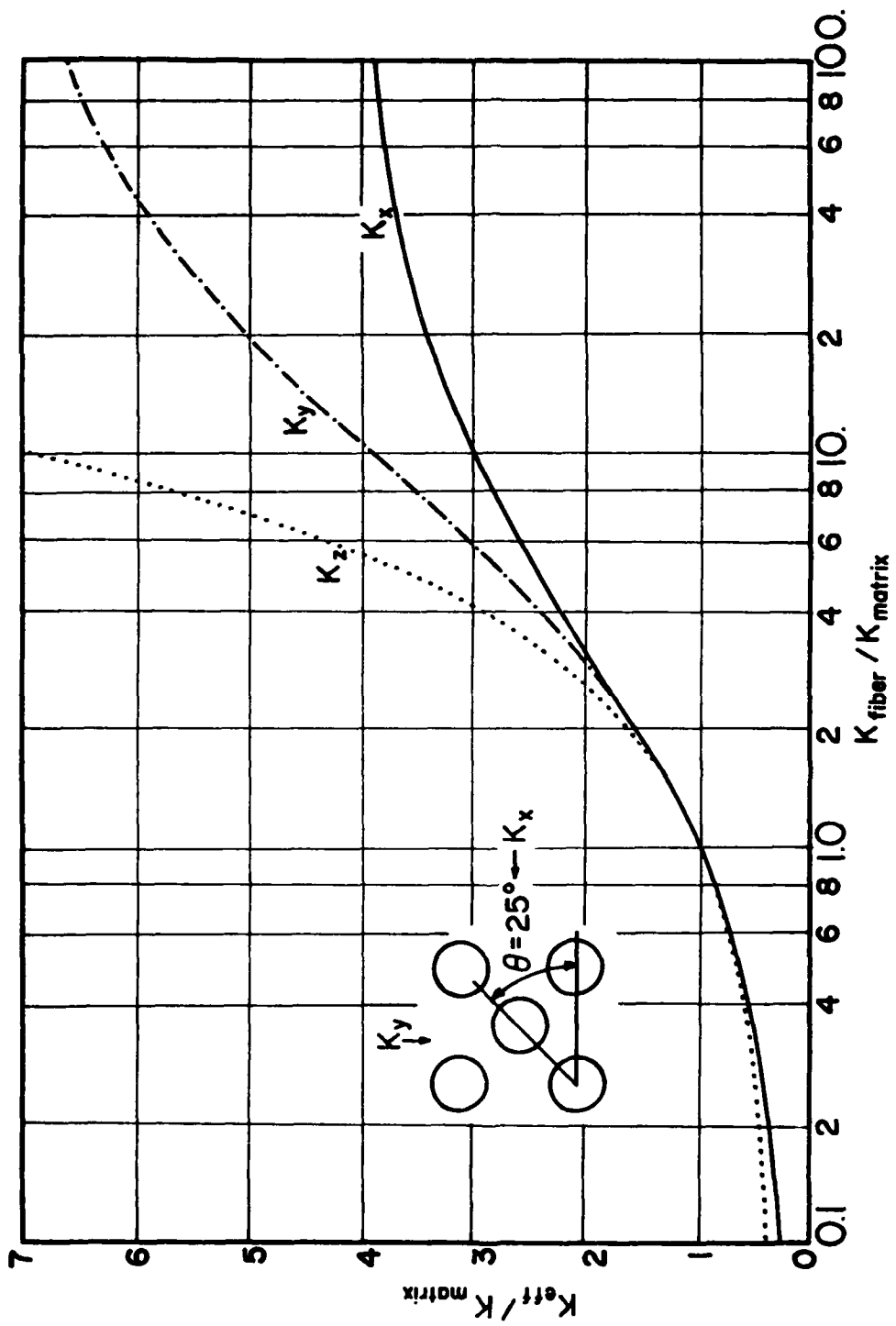
Figure A-42 Parallel Fiber (Staggered Array) Volume Ratio = .65

109
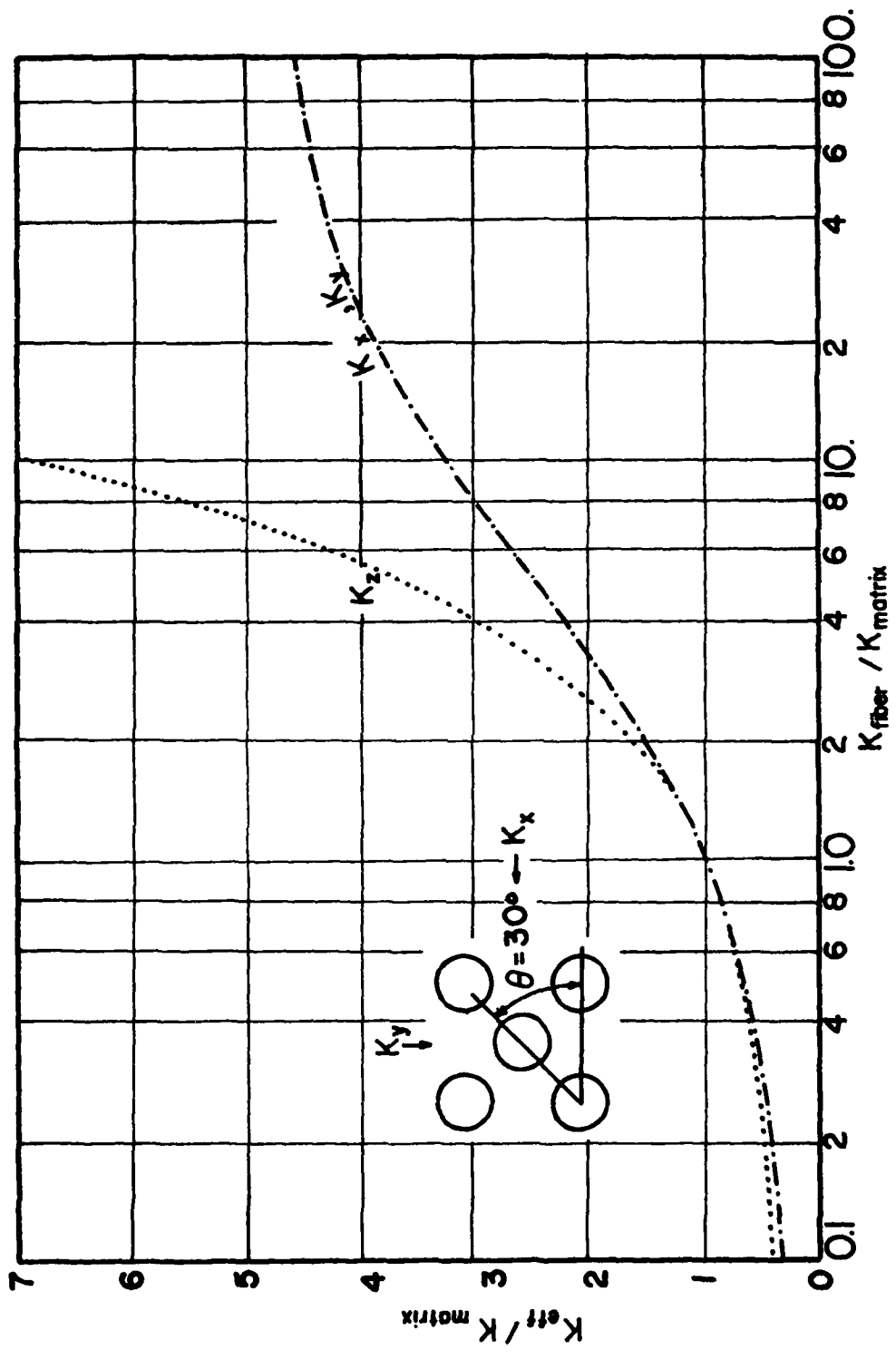
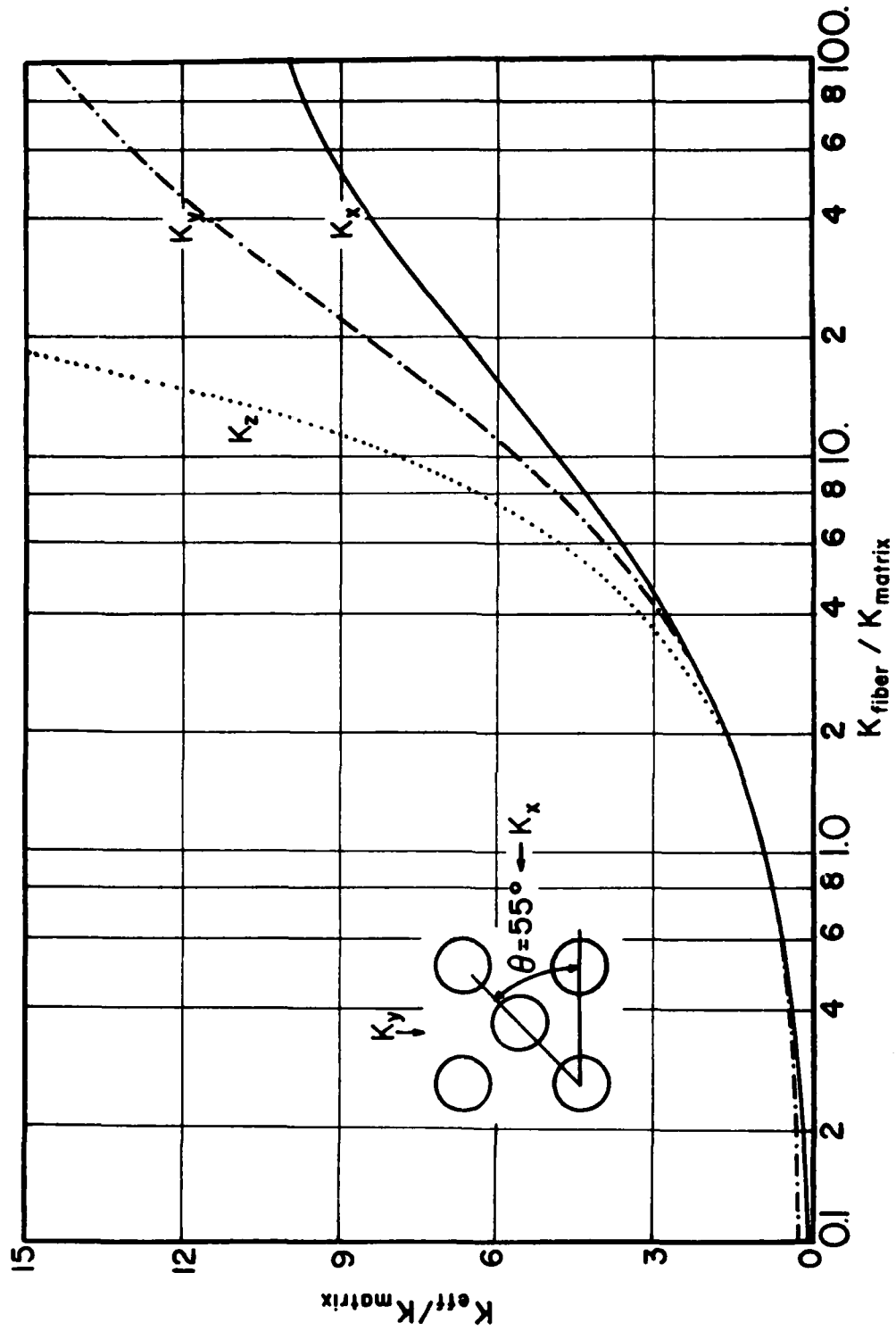Figure A-43 Parallel Fiber (Staggered Array) Volume Ratio = .65

110
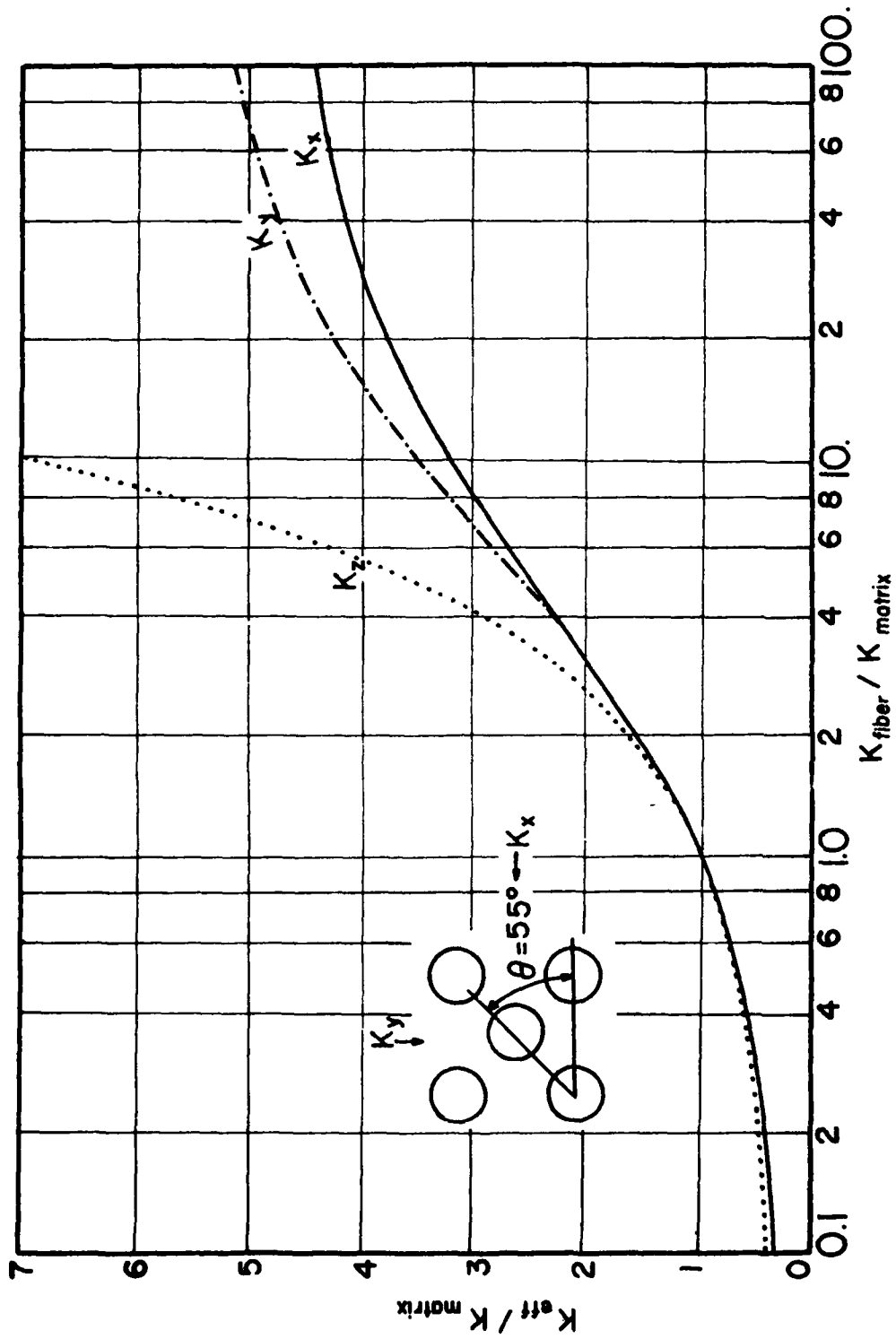
Figure A-44 Parallel Fiber (Staggered Array) Volume Ratio = .65
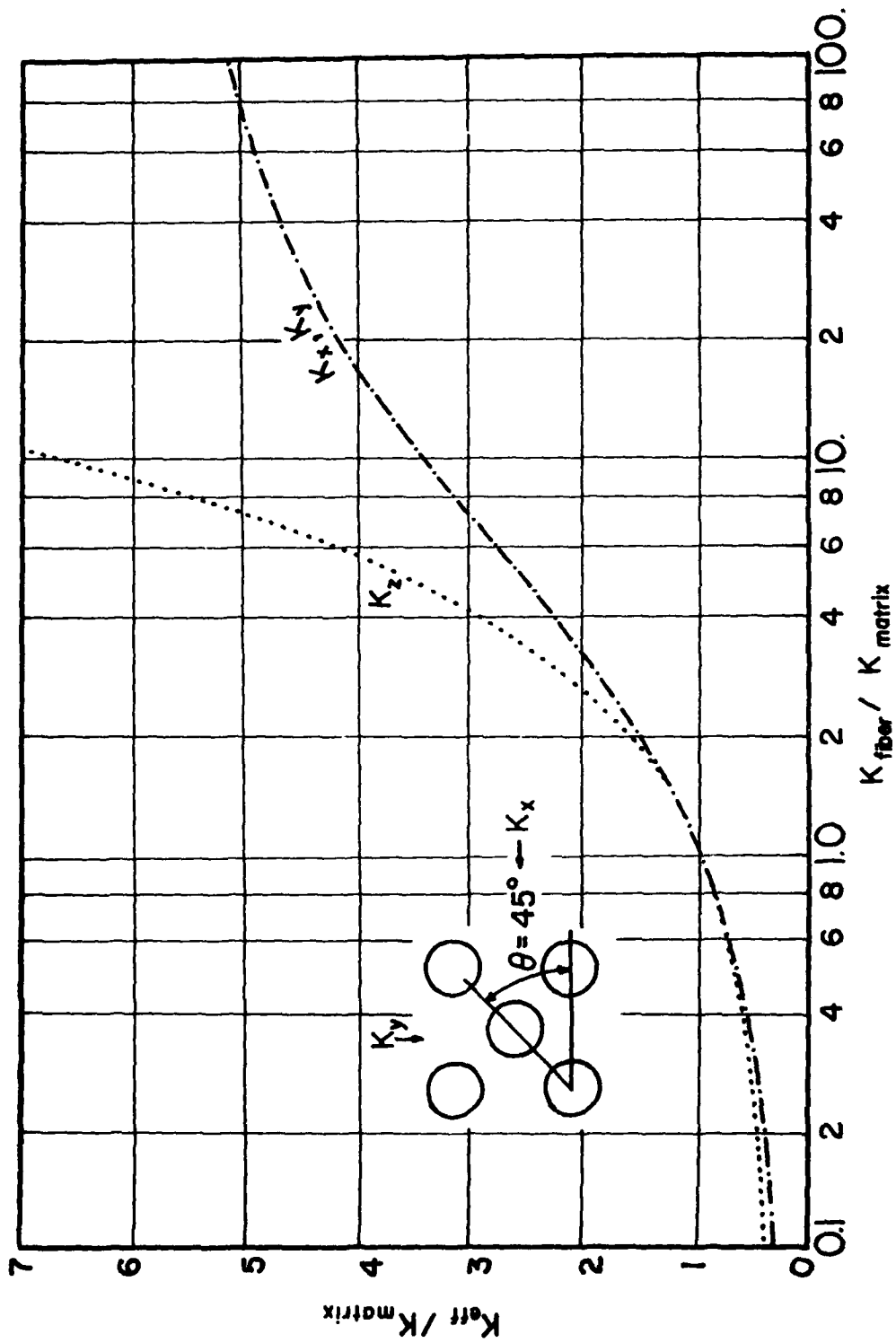
Figure A-45 Parallel Fiber (Staggered Array) Volume Ratio = .65

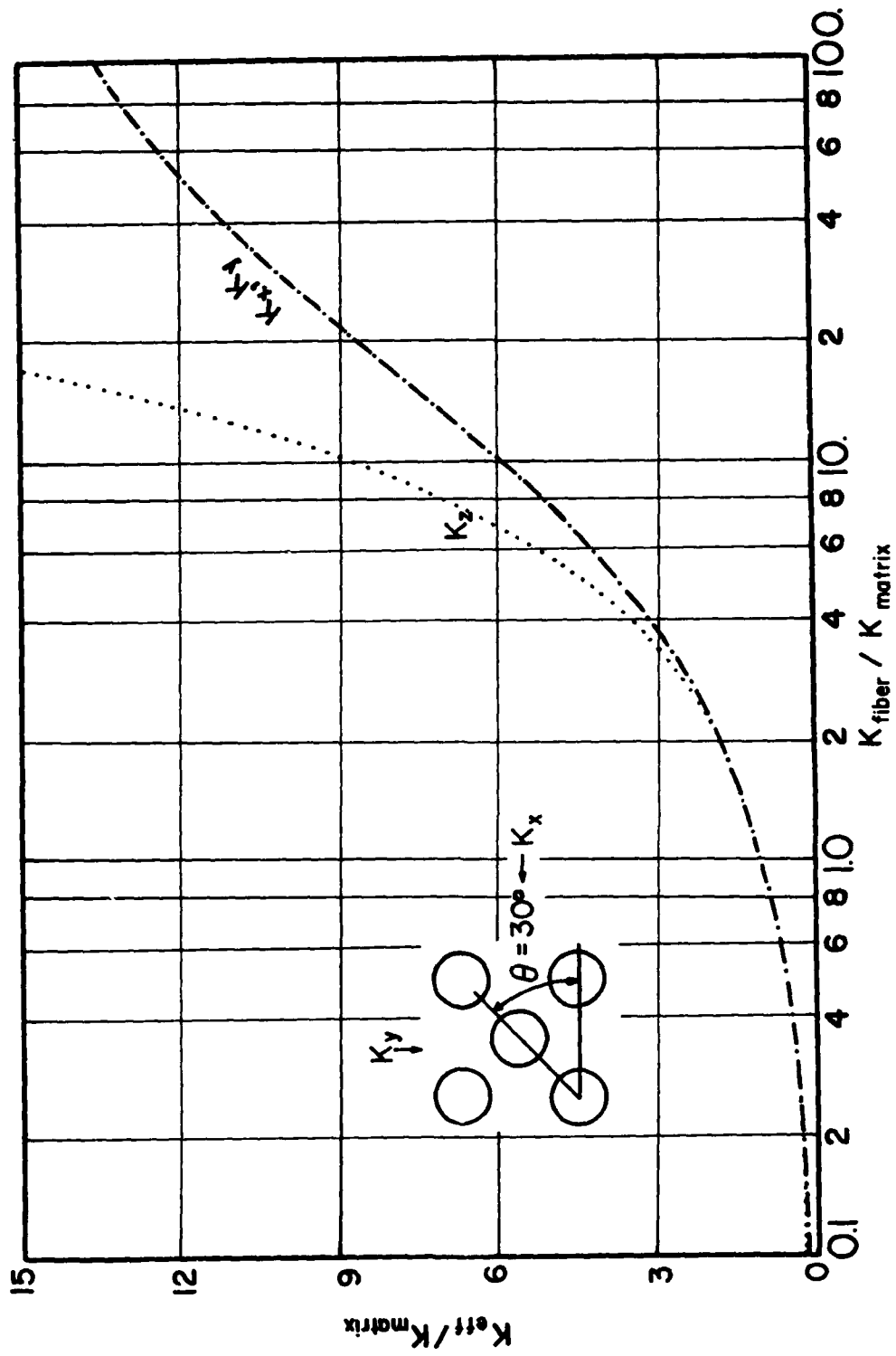Figure A-46 Parallel Fiber (Staggered Array) Volume Ratio = .70

113

Figure A-47 Parallel Fiber (Staggered Array) Volume Ratio = .70

Figure A-48   Parallel Fiber (Staggered Array) Volume Ratio = .70
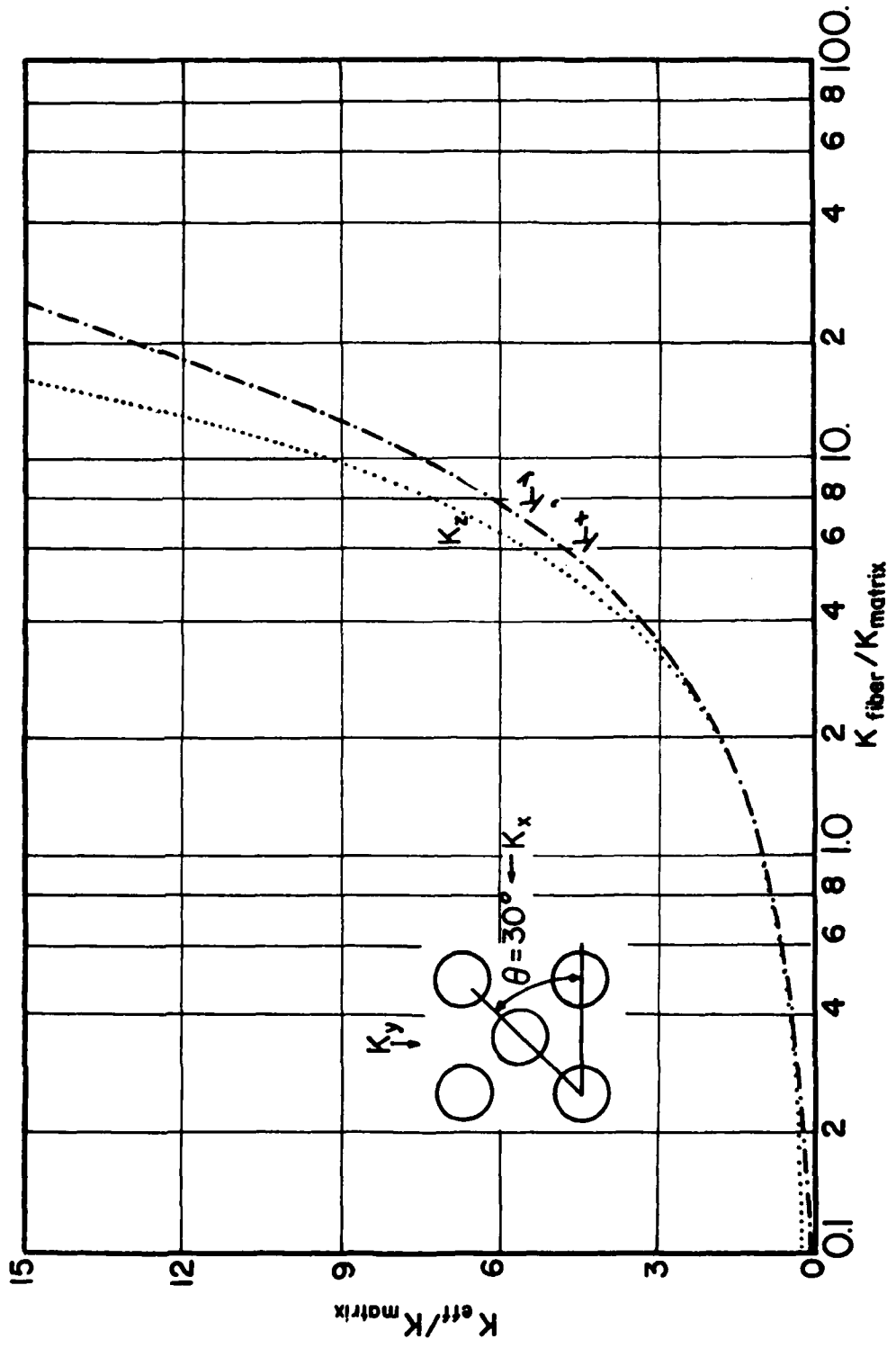
115

Figure A-49 Parallel Fiber (Staggered Array) Volume Ratio = .70

116

Figure A-50 Parallel Fiber (Staggered Array) Volume Ratio = .75

117

Figure A-51 Parallel Fiber (Staggered Array) Volume Ratio = .75

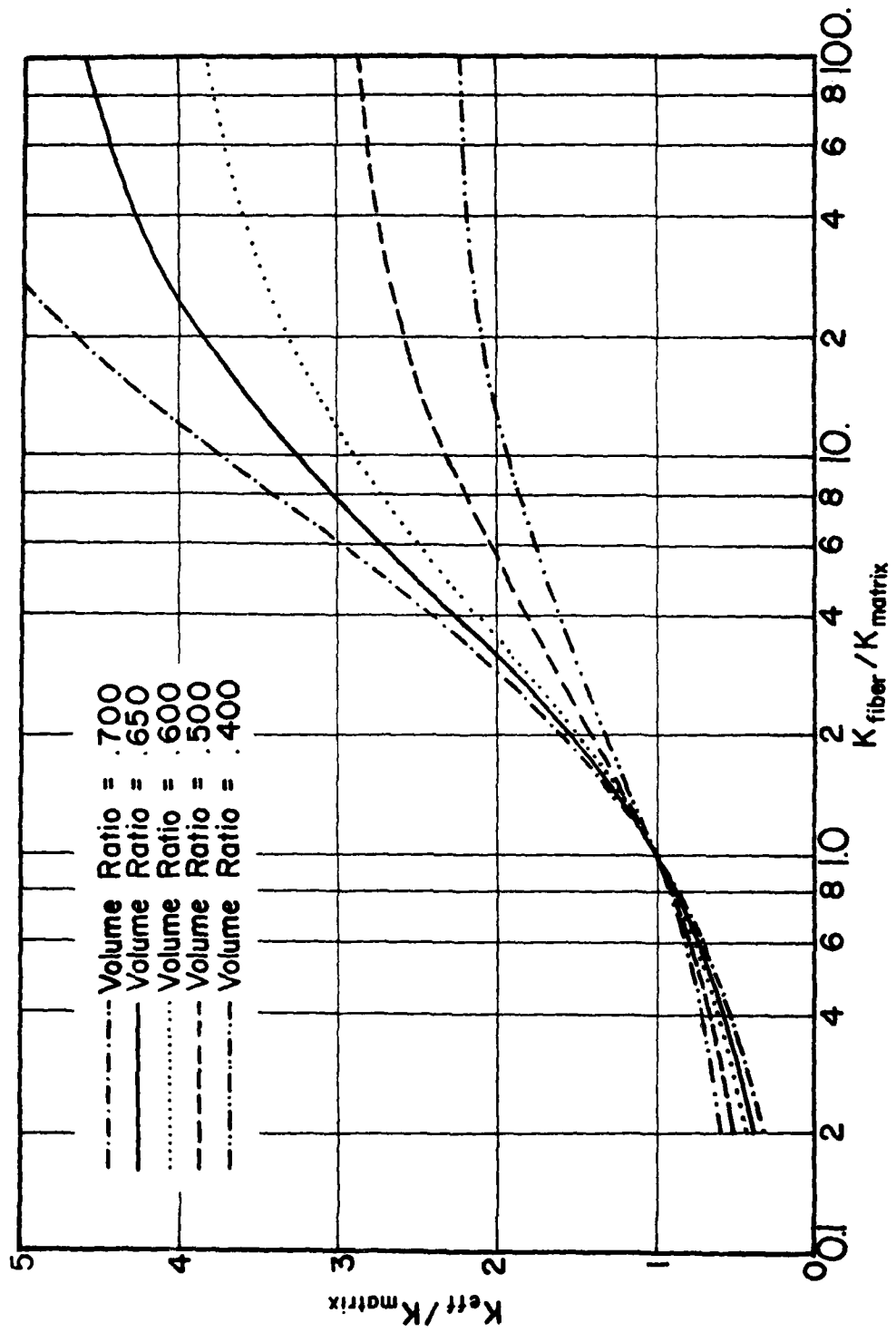Figure A-52 Parallel Fiber (Staggered Array) Volume Ratio = .75

119

Figure A-53   Parallel Fiber (Staggered Array) Volume Ratio = .80

Figure A-54 Parallel Fiber (Staggered Array) Volume Ratio = .80

121

Figure A-55 Parallel Fiber (Staggered Array) Volume Ratio = .85

122

Figure A-56   Parallel Fiber (Staggered Array) Volume Ratio = .90
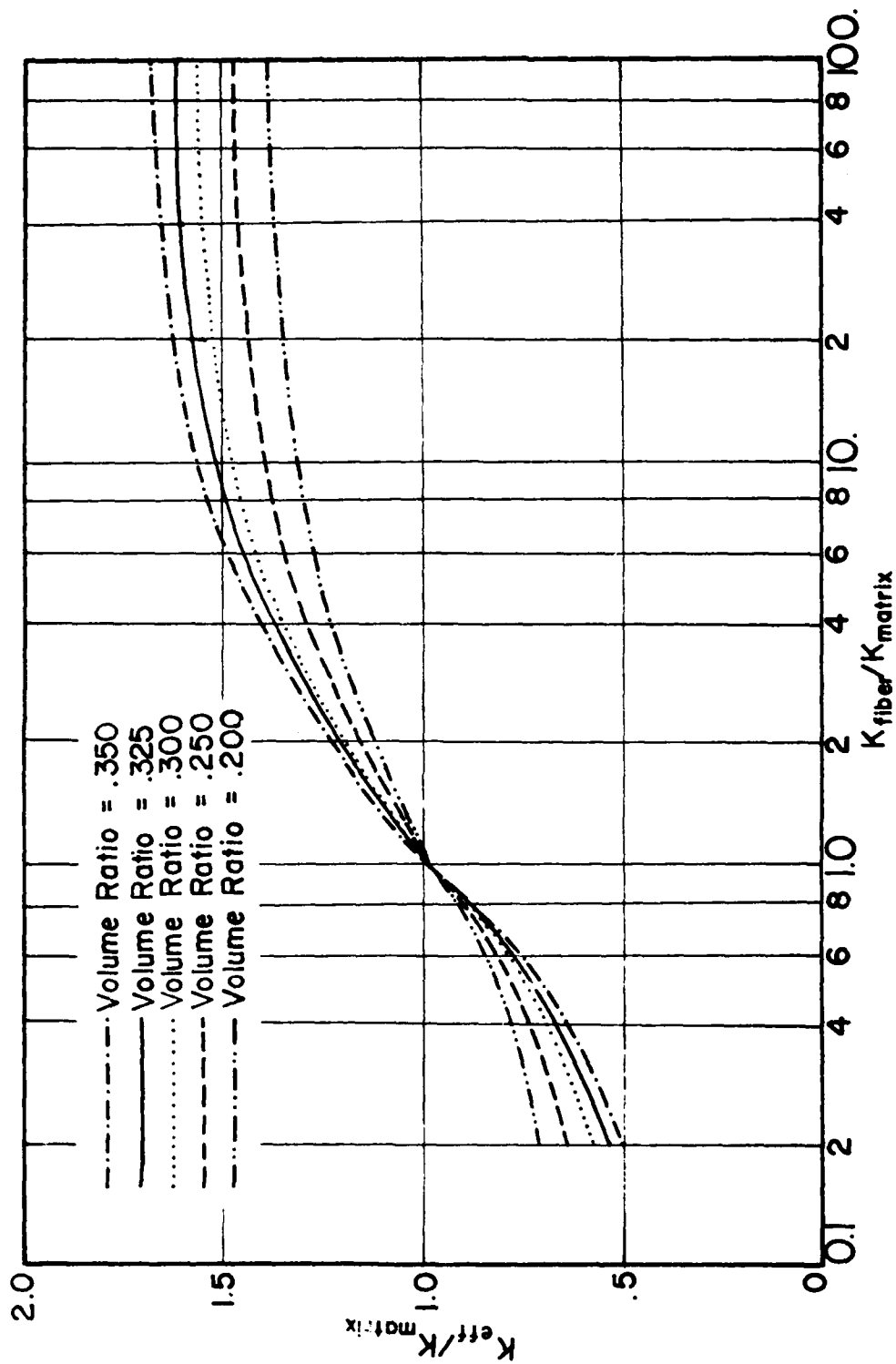
Figure A-57 0° - 90° Array (Transverse - Transverse Array) Aspect Ratio = 1

124

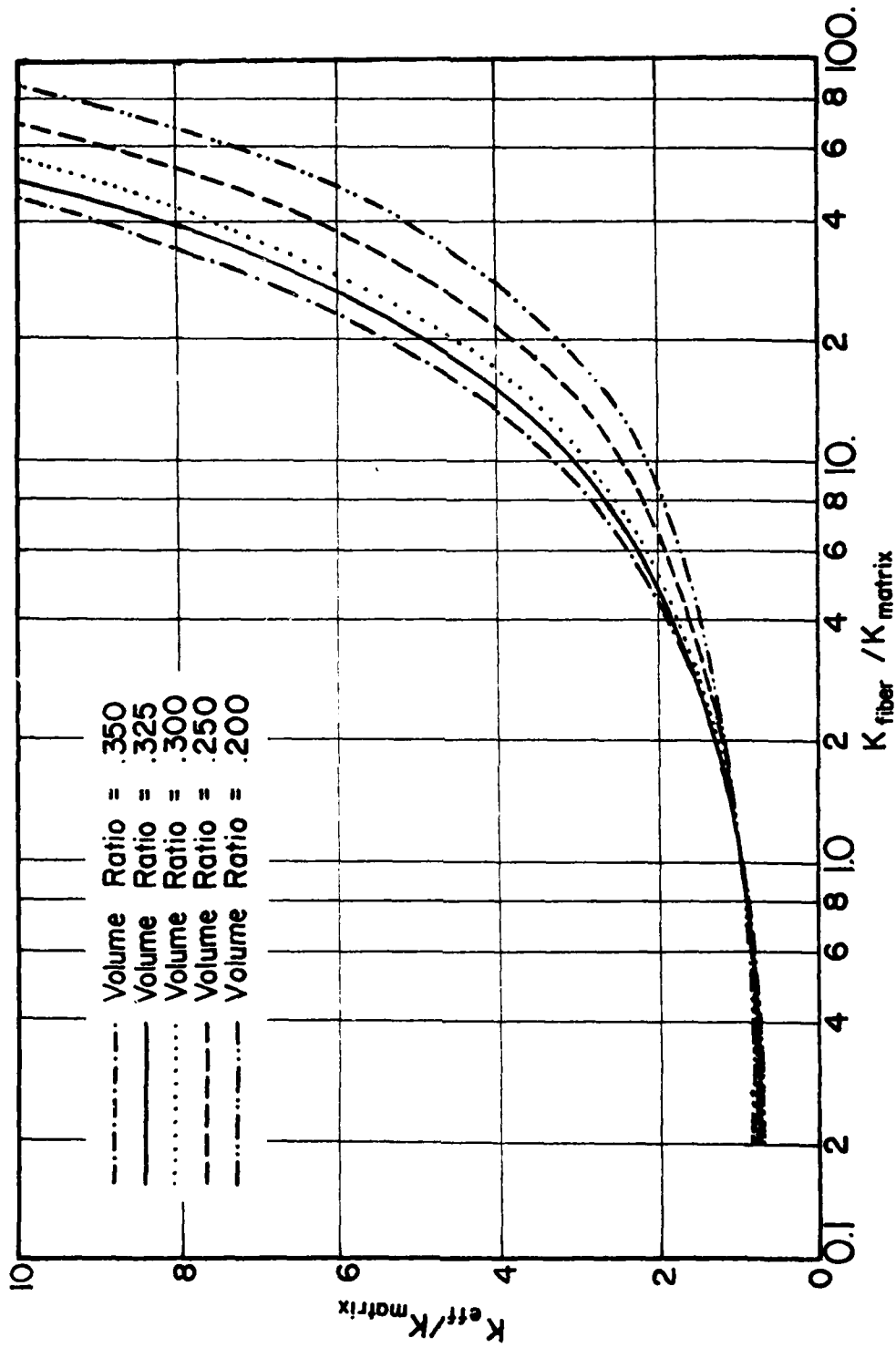Figure A-58 0° - 90° Array (Transverse - Transverse Array) Aspect Ratio = 2

125

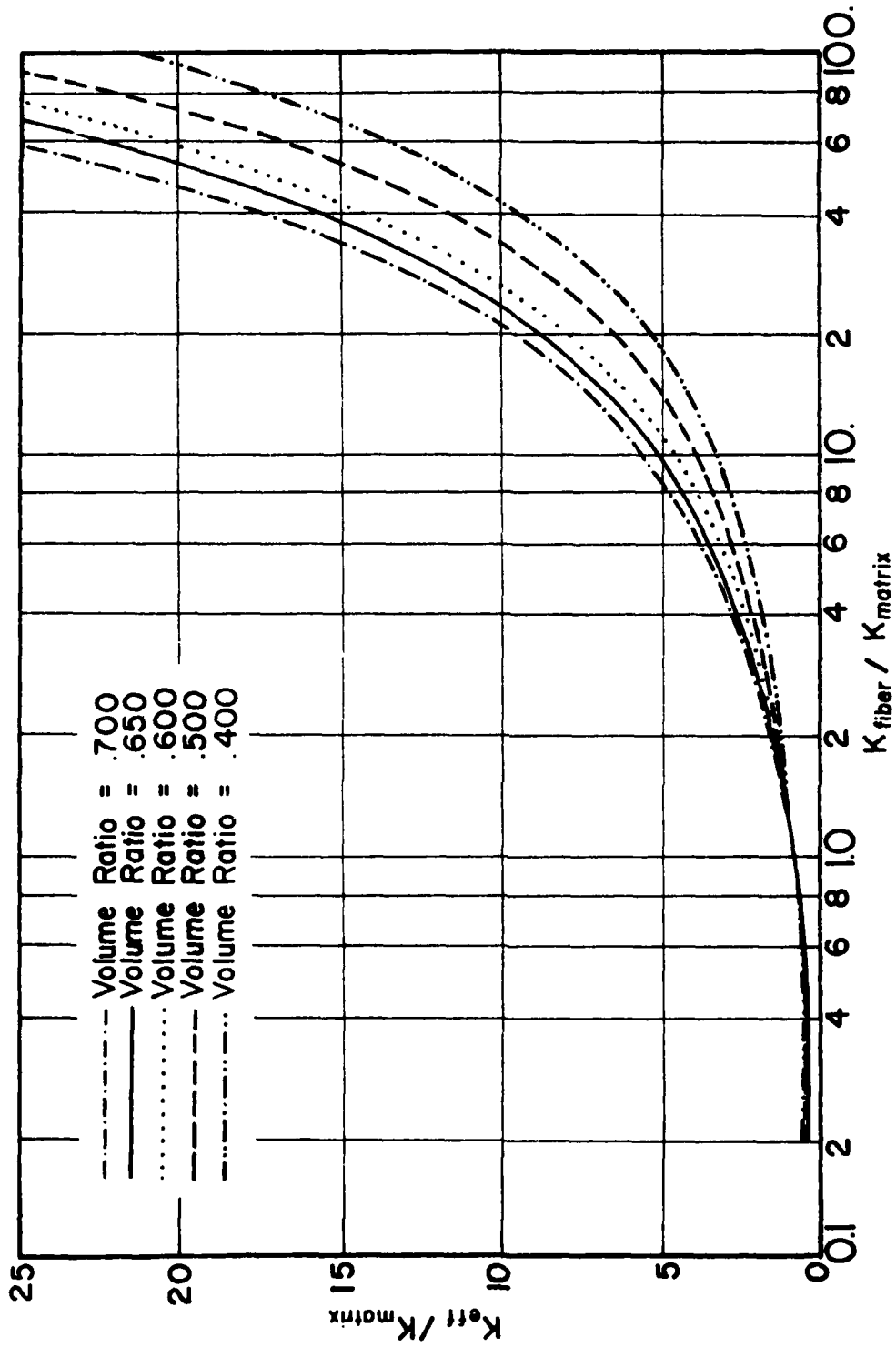Figure A-59 0° - 90° Array (Axial - Transverse Array) Aspect Ratio = 2

126

Figure A-60 0° – 90° Array (Axial – Transverse Array) Aspect Ratio = 1
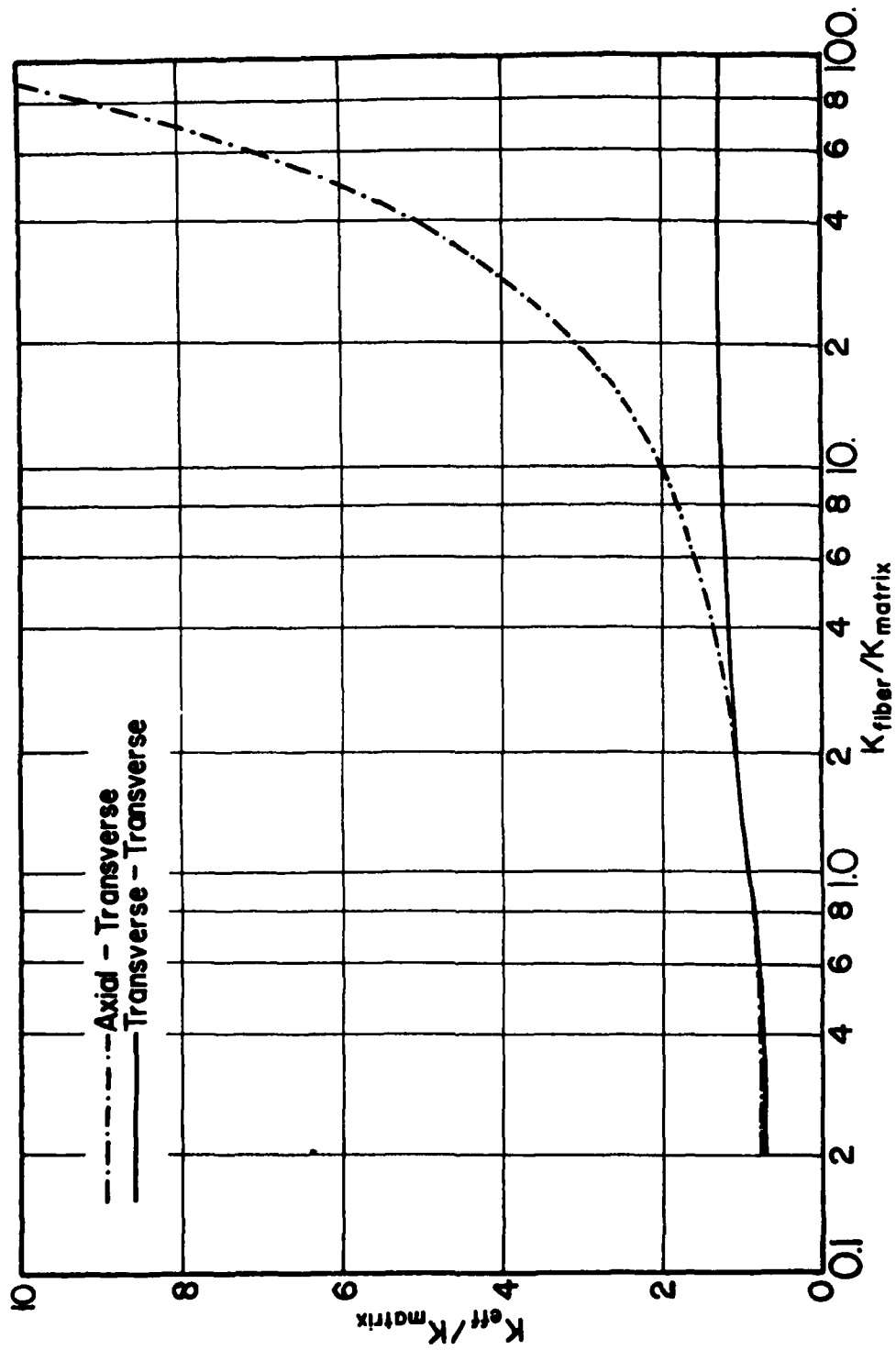
127

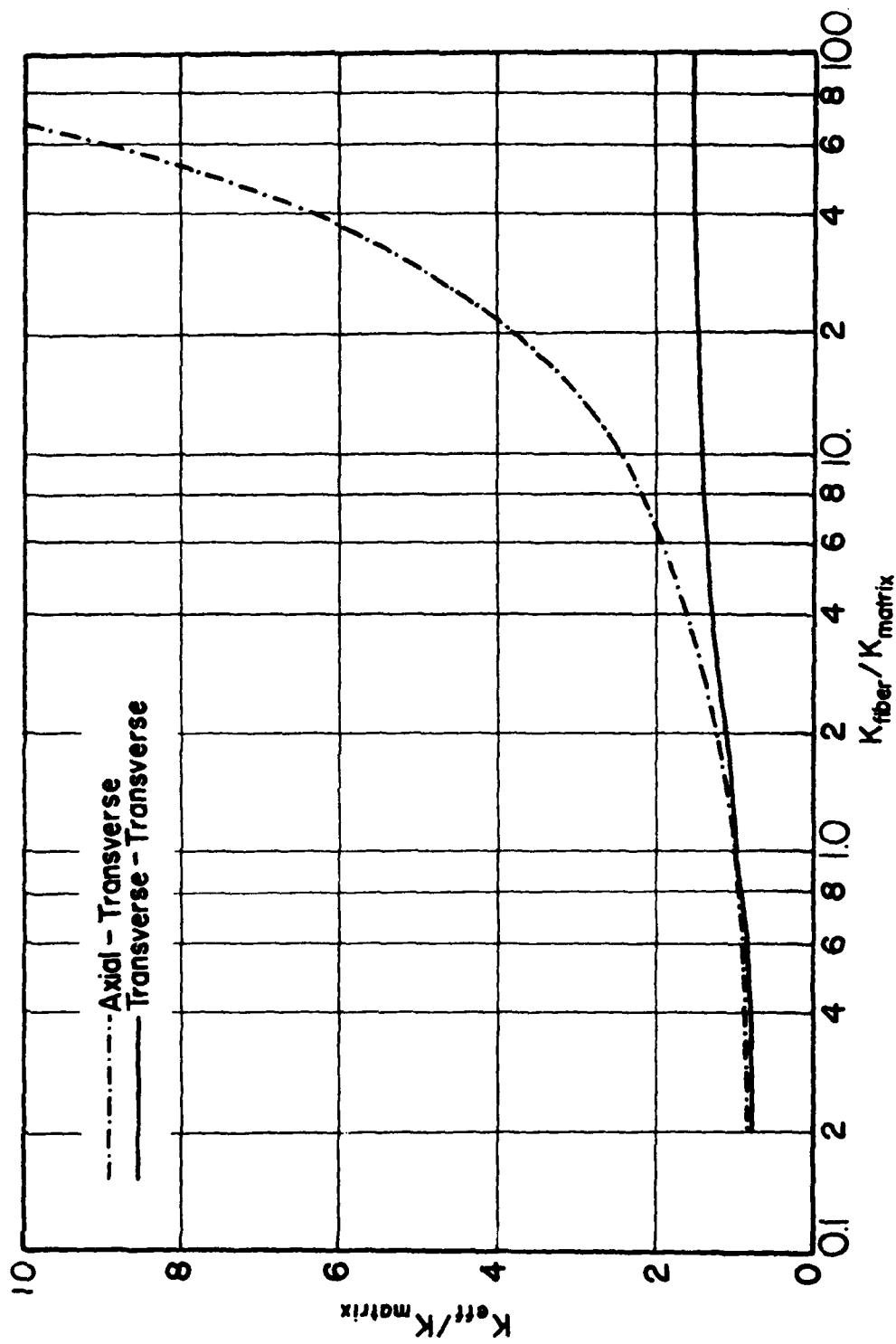Figure A-61 0° - 90° Array - Volume Ratio = .200, Aspect Ratio = 2

Figure A-62 0° - 90° Array - Volume Ratio = .250, Aspect Ratio = 2
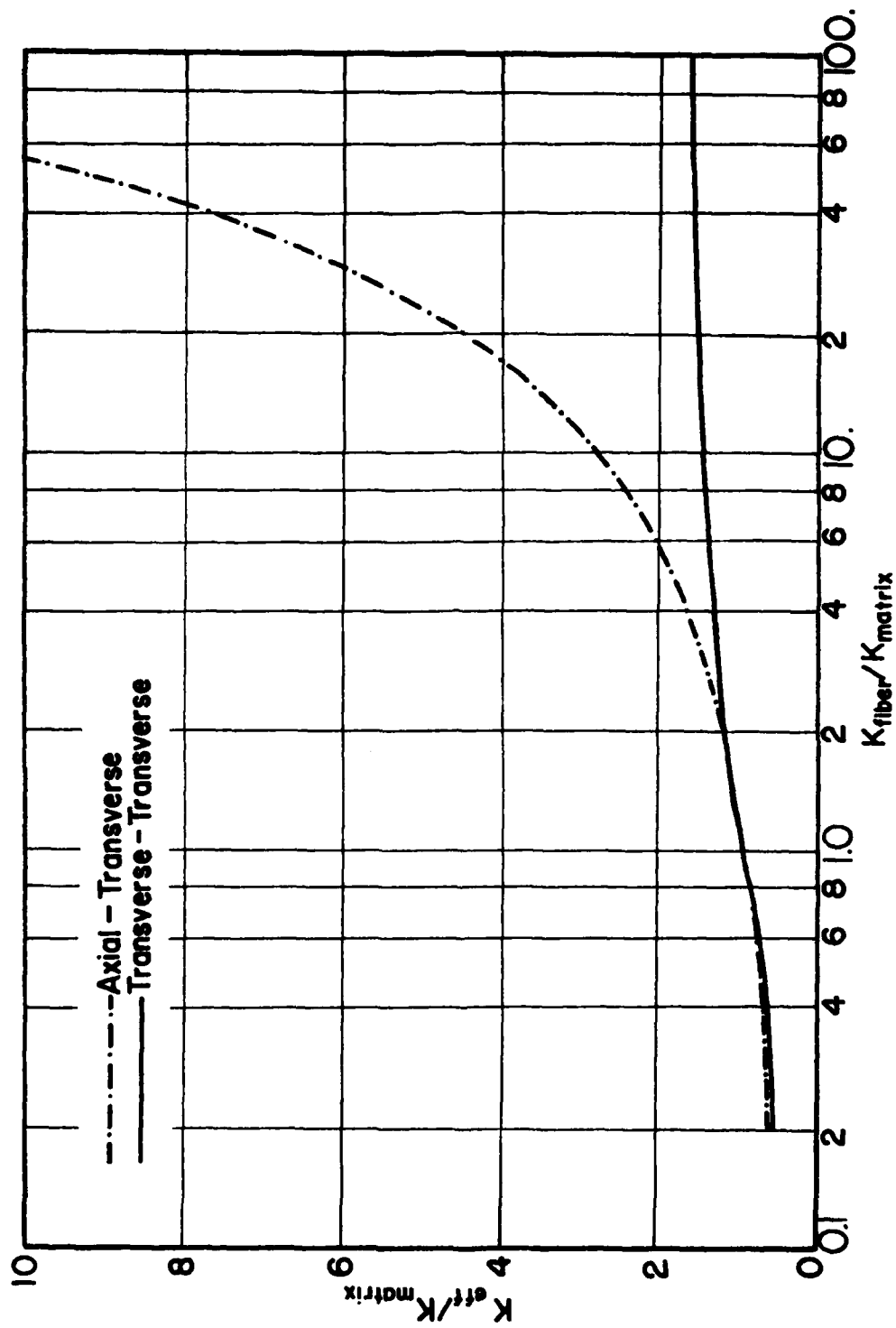
129

Figure A-63 0° - 90° Array - Volume Ratio = .300, Aspect Ratio = 2

130

Figure A-64   0° - 90° Array - Volume Ratio = .325, Aspect Ratio = 2

Figure A-65 0° - 90° Array - Volume Ratio = .350, Aspect Ratio = 2
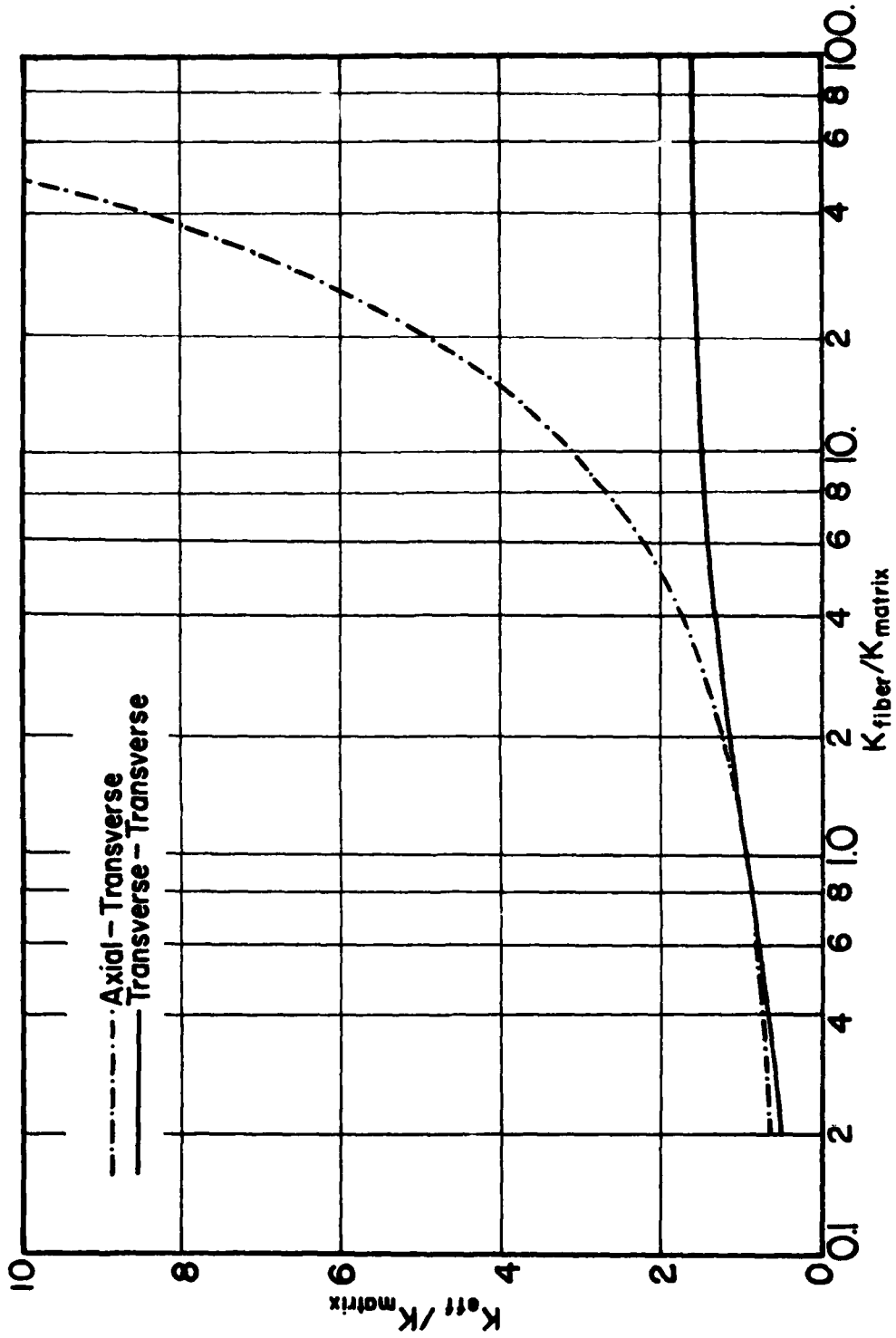
132

Figure A-66 0° - 90° Array - Volume Ratio = .400, Aspect Ratio = 1

133

Figure A-67 0° - 90° Array - Volume Ratio = .500, Aspect Ratio = 1

134

Figure A-68 0° - 90° Array - Volume Ratio = .600, Aspect Ratio = 1

135

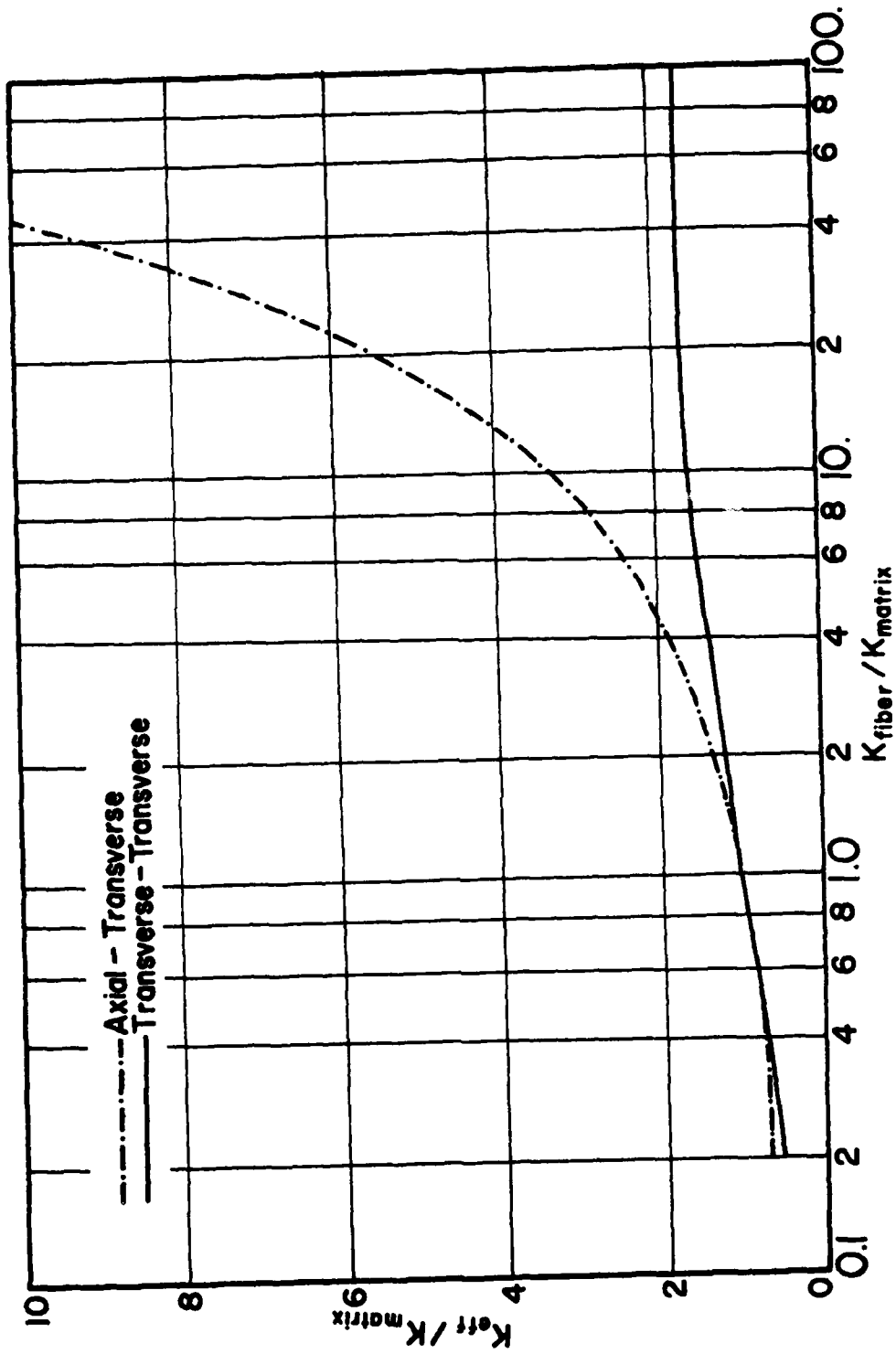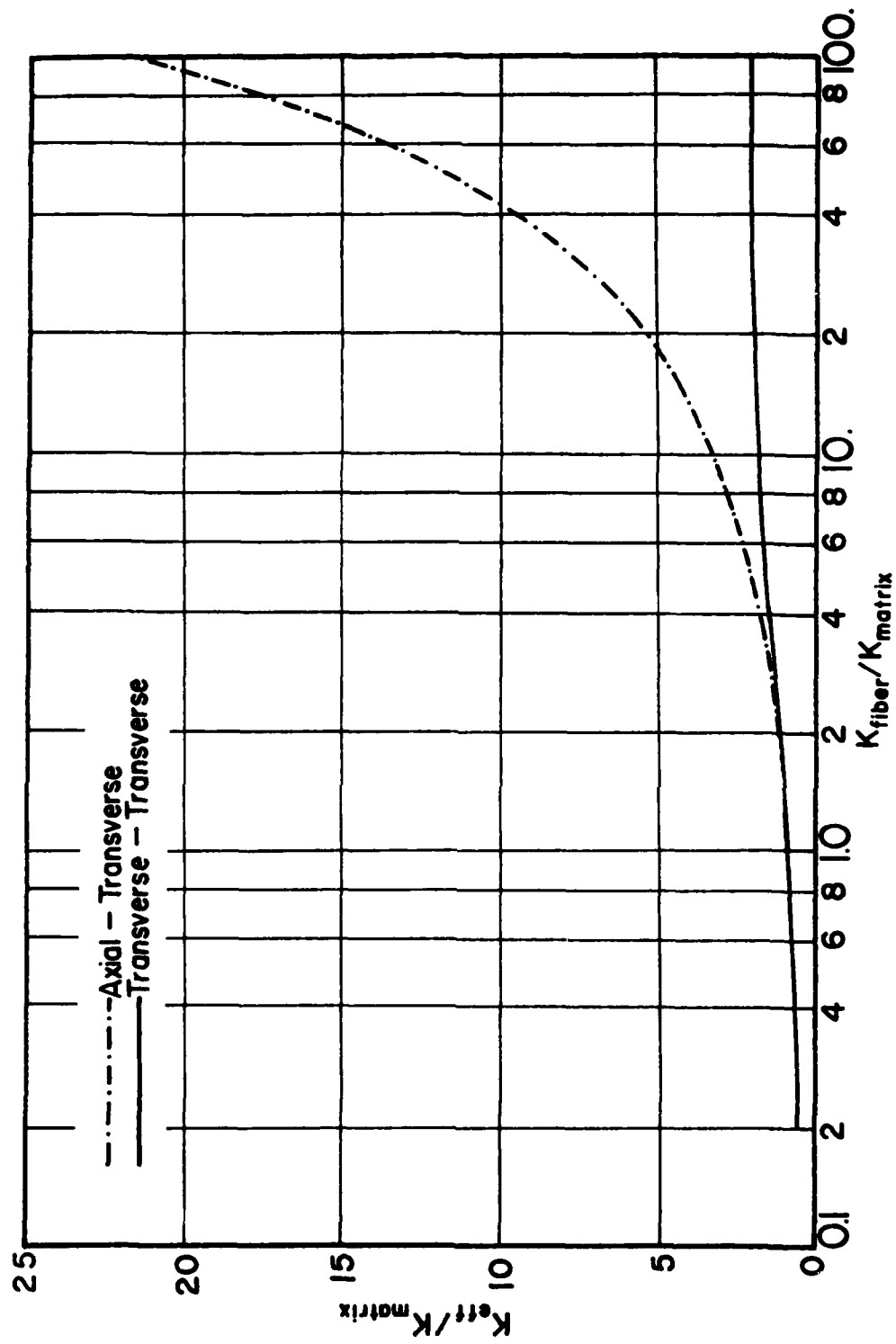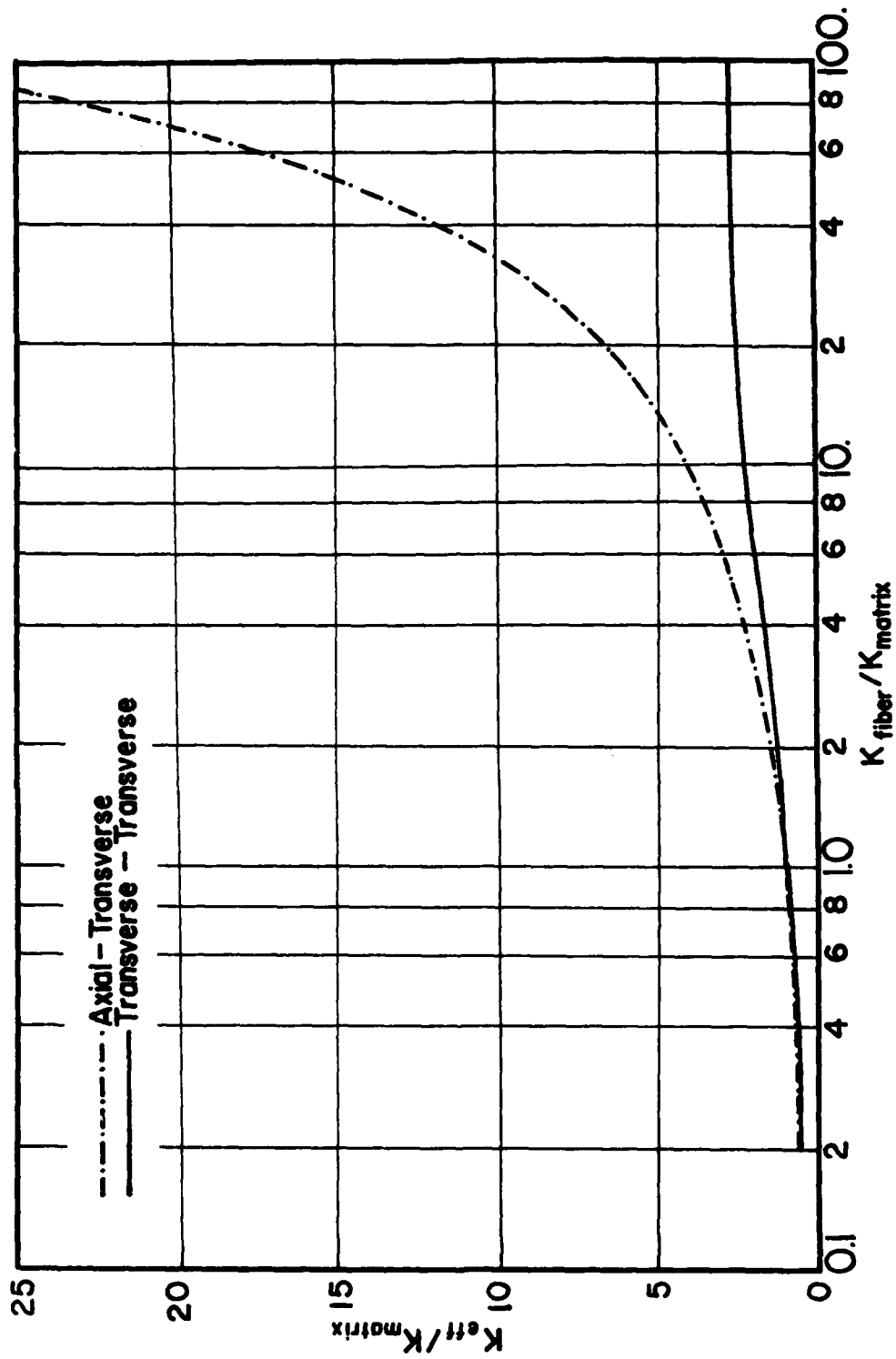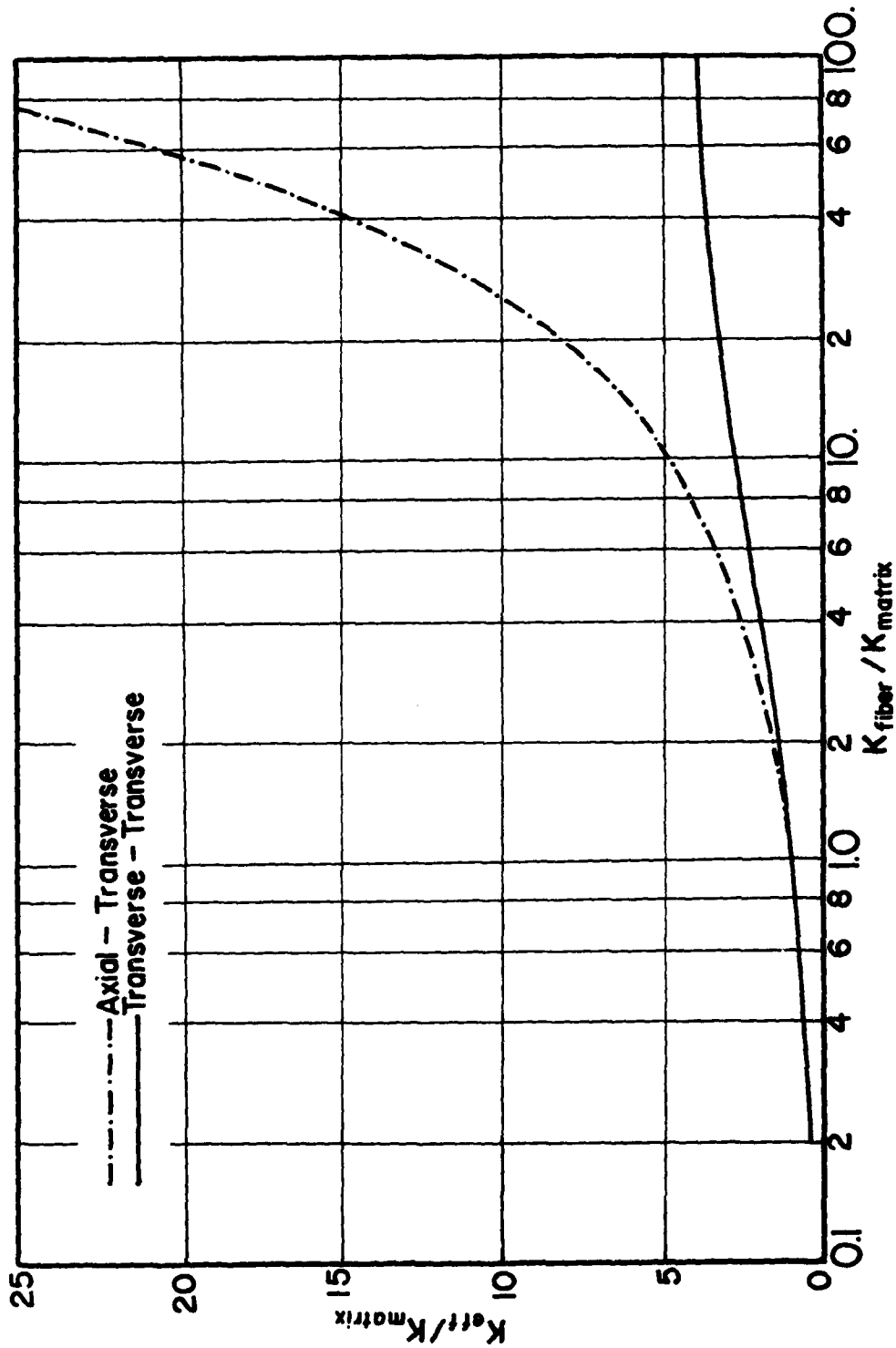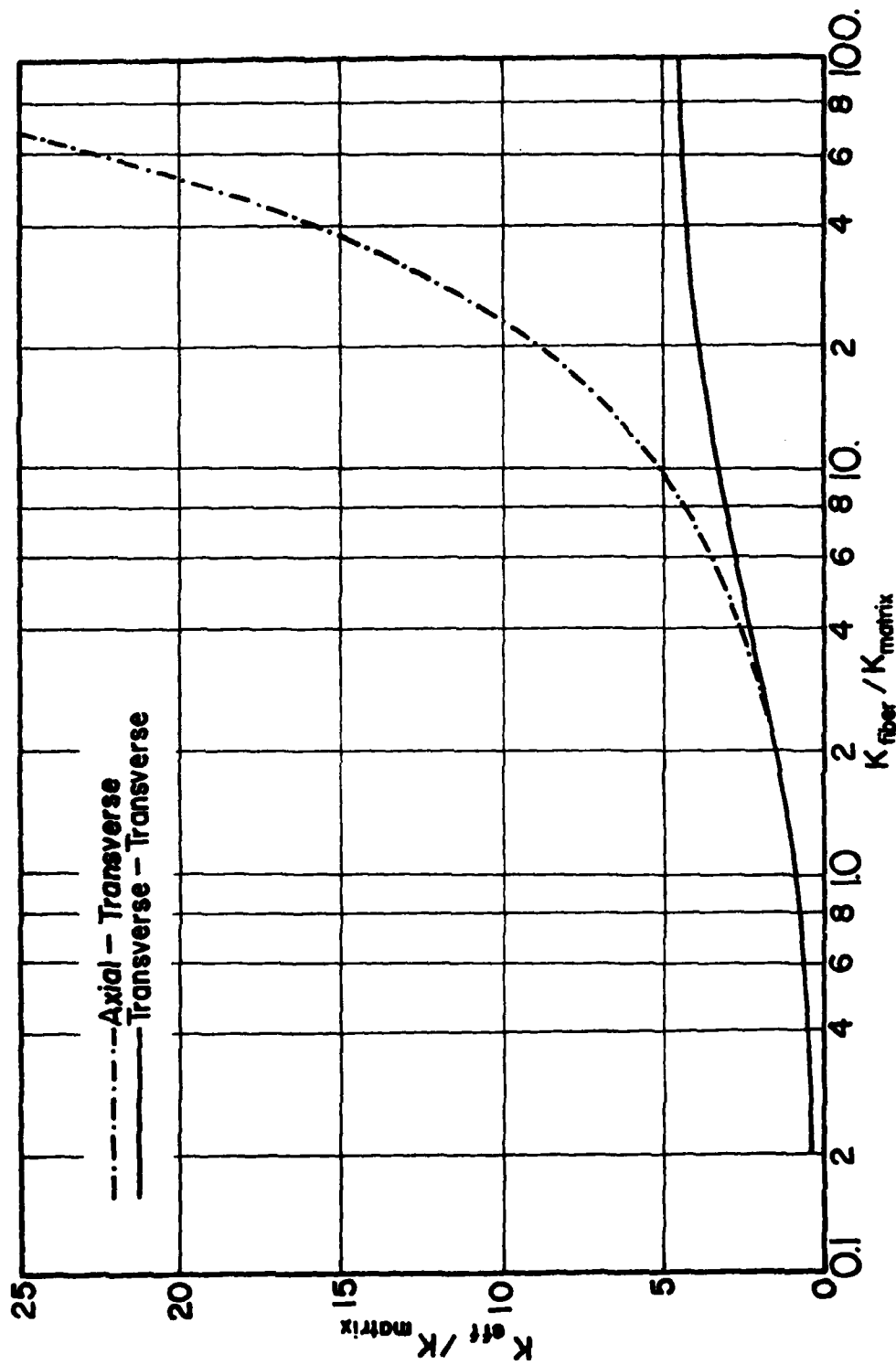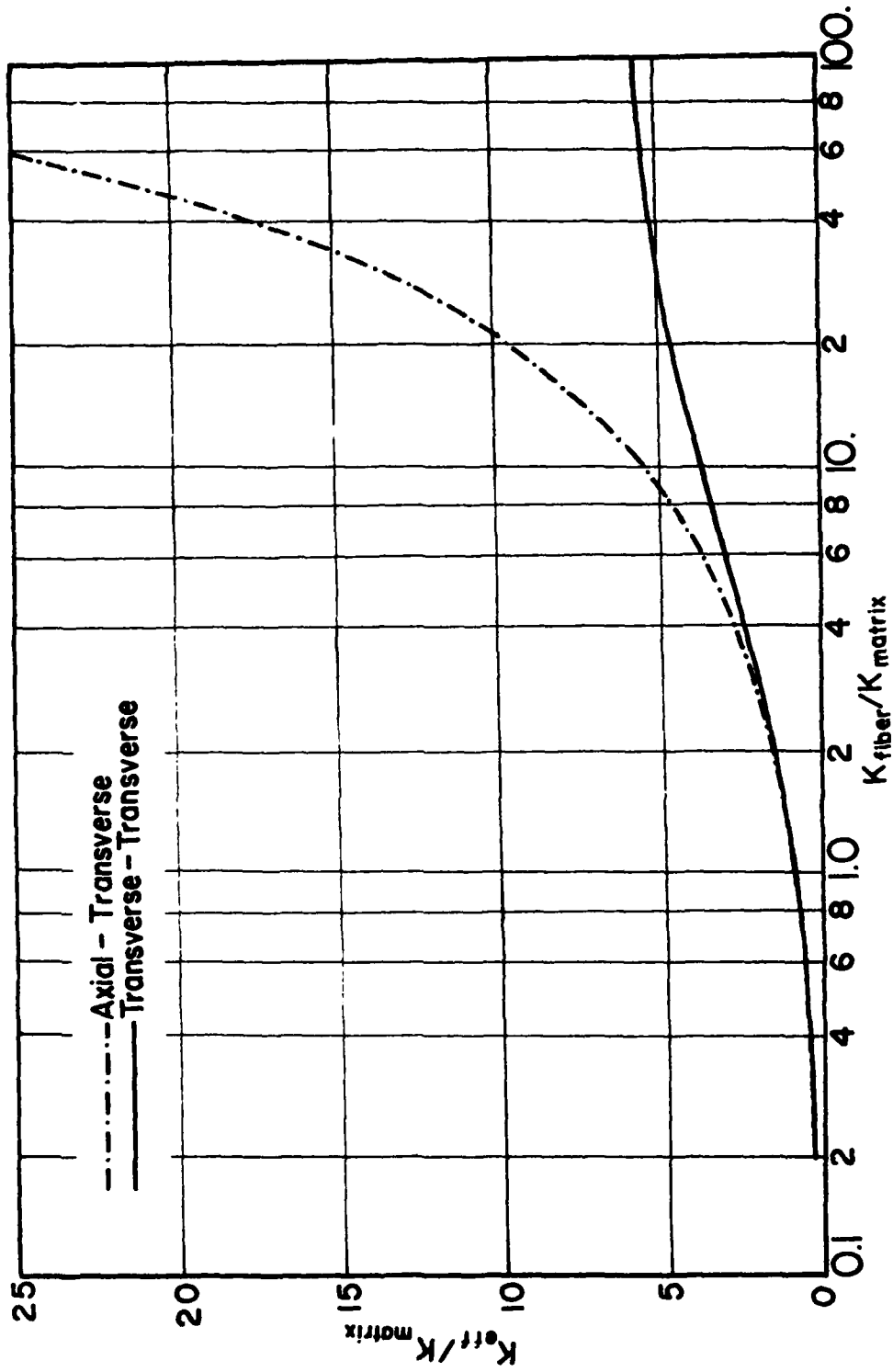Figure A-69 0° - 90° Array - Volume Ratio = .650, Aspect Ratio = 1

136

Figure A-70 0° - 90° Array - Volume Ratio = .700, Aspect Ratio = 1

137

APPENDIX B

PARALLEL FIBER

PROGRAM METHOD

The computer programs which were written to calculate the effective conductivity for both the staggered and retangular arrays follow the methods of Sections 2.2 through 2.4. In the manner discussed, a series of M equations with M unknowns are produced where M is the number of discrete points which are used to satisfy the boundary conditions. These equations are solved for the unknowns which are then put into the appropriate equations to give the effective conductivity for the material under study.

The coefficients are found by the use of the appropriate boundary condition equations. The M equations can then be written using matrix notation in the following manner:

$$[A]_{MxM}(E)_{Mx1} = (C)_{Mx1}$$

Here, A is the M by M coefficient matrix, E is the solution matrix (actually it is just a vector), and C is the matrix (also a vector) containing the constants from the boundary conditions.

The program employs a gauss-elimination technique whereby rows are multiplied through by constants and subtracted in such a way so as to produce an upper triangular matrix. The unknowns can then be found one at a time by starting at the bottom and back-substituting the unknowns into the equations as they are found. Reference 7 gives a very good description of this method.

A standard gauss-elimination procedure is not extremely accurate because of roundoff errors within the computer. This can be greatly improved by a procedure called pivoting where rows are interchanged during the elimination process to put the largest terms in each column on the main diagonal. The programs used here went one step further and included a double pivoting procedure where throughout the elimination the largest terms in the entire array are put in the key positions on the diagonal. This means that columns are interchanged as well as rows. This procedure requires an intricate bookkeeping scheme within the program, but it decreases the effects of roundoff errors still further beyond what the single pivoting can do. The details of these methods will not be discussed here as they are covered in many references (again, Reference 7 is quite good).

Another method used to decrease the effects of roundoff errors in these programs was the use of double precision logic. This doubled the number of digits which were carried throughout the calculations within the computer from 8 to 16 and forced the error to occur in the last of these digits.

In the manner described above, every possible technique has been used to limit the error due to roundoff after each calculation by the computer. However, there is another type of error which is due to the fact that the power series which describe the temperature field are chopped off after a finite number of terms.

139

Theoretically, it is expected that this error in the solution would be reduced when more and more terms in the power series are taken into consideration. This would be true if an infinite number of digits were carried through all the calculations. However, given a fixed number of digits, a point is reached after which the increase in accuracy due to added terms in the series is more than offset by increased error due to roundoff. When several terms are added past this point, the roundoff error increases rapidly to the point where the method becomes unstable and the result becomes meaningless.

The error in the solution is high when a small number of discrete matching points are used due to the chop-off of the power series. It is again high when a large number of points are used due to roundoff, and so there is an optimum number of points that should be used. This optimum number was found to be 15 points for the rectangular array and approximately that number for the staggered array. The locations of these points are discussed in Section II. The number of points for the staggered array varies somewhat due to the intricacies of the matching line.

By using this method of exactly satisfying the boundary conditions at discrete points, it was hoped that they are closely satisfied at the points between the discrete points. As an example of the accuracy obtained, consider the rectangular array. Along the top edge the temperature value deviated from 1 by only $\pm$ 0.0001, at most, and the resulting heat flux distribution along the right side was at most $\pm$ 0.01 percent of the average heat flux along the top and bottom edges. For the staggered array the deviation from exact symmetry was on the order of $\pm$ 0.01 percent of the values for both the temperature and dT/dy symmetry.

At higher values of β (fiber conductivity/matric conductivity) the error in the effective conductivity becomes greater. In addition, the error is increased at higher values of the volume ratio. At the highest possible volume ratios and a β of 100, the value of K_{eff}/K_{matrix} is accurate to three significant figures. Further, this increases to more than six significant figures for the lower values of β and volume ratio. This conclusion is arrived at by comparing the data with that from a routine which uses finite difference methods (discussed in Section III) and by studying the effects of changes in the number of matching points. This conclusion was further strengthened by comparing certain data between the staggered and rectangular arrays which happened to be coincident. Even though the two methods of solution are distinctly different, the very good agreement between results for certain geometries added confidence to the results of both methods. These various relationships are discussed in Section II.

REFERENCES

1. Ashton, J.E., Halpin, J.C., and Petie, P.H., _Primer on Composite Materials: Analysis_, Technomatic Publishing Co., Stamford, Conn. (1969).

2. Wingert, W., Rockwell International--Los Angeles Division, Personal Communication (Feb. 1979).

3. Arpaci, V.S., _Conduction Heat Transfer_, Addison-Wesley Pub. Co., Reading, Massachusetts.

4. Myers, G.E., _Analytical Methods in Conduction Heat Transfer_, McGraw-Hill, New York (1971).

5. Carslaw, H.S. and Jaeger, _Conduction of Heat in Solids_, Oxford: Clarendon Press (1959).

6. Schneider, P.J., _Conduction Heat Transfer_, McGraw-Hill, New York (1957).

7. Gerald, C.F., _Applied Numerical Analysis, Second Edition_, Addison-Wesley Publishing Company, Philippines (1978).

8. Tsou, F.K., Chou, P.C., and Singh, I., "Apparent Tensorial Conductivity of Layered Composites," _AIAA Journal_, Vol. 12, No. 12 (Dec. 1974).

9. Hashin, Z., Shtrikman, S., _Journal of Applied Physics_, Vol. 33, pp. 3125 (1962).

10. Hale, D.K., "The Physical Properties of Composite Materials," _Journal of Materials Science_, Vol. 11, pp. 2105 (1976).

11. Beran, M.J., and Silnutzer, N.R., "Effective Electrical, Thermal, and Magnetic Properties of Fiber Reinforced Materials," _Journal of Composite Materials_, Vol. 5 (April 1971).

12. Elsayed, M.A., and McCoy, J.J., "Effect of Fiber Positioning on the Effective Physical Properties of Composite Materials," _Journal of Composite Materials_, Vol. 7 (October 1973).

13. Springer, G.S., and Tsai, S.W., "Thermal Conductivities of Unidirectional Materials," _Journal of Composite Materials_, Vol. 1 (1967).

14. Behrens, E., "Thermal Conductivities of Composite Materials," _Journal of Composite Materials_, Vol. 2 (January 1968).

15. Amoz, M.B., "Heat Conduction Theory for Composite Materials," _Journal of Applied Mathematics and Physics_ (_ZAMP_), Vol. 27 (1976).